Integrated 4D tectono-stratigraphic evolution of the northern Peloponnese margin and the Gulf of Corinth, Greece

Master thesis in Basin and Reservoir Studies

Martine Johanne Birkemo Krabbendam

Department of Earth Science

University of Bergen

June 2019

Abstract

The Corinth Rift is located in Greece and is a classic area to study the evolution of a rift basin in its early stage. The rift is rapidly extending, active and the syn-rift depositional sequences are well preserved and exposed due to uplift of the northern Peloponnese margin, south of the Gulf of Corinth. Most of the extension today is occurring in the Gulf of Corinth and the deposition is subaqueous, the older part of the rift is exposed on the northern Peloponnese margin. The novel part of this study is that it correlates the onshore northern Peloponnese margin and the offshore Gulf of Corinth area into one model, building a framework for the tectono-stratigraphic evolution of the Corinth Rift. This correlation integrates existing spatial geological onshore data (i.e. mapped stratigraphic boundaries, tectonic structures, sedimentology and directional data), together with onshore satellite sourced digital elevation models and offshore data from seismic surveying, in three cross-sections at key areas of the Corinth Rift basin.

The tectono-stratigraphic evolution of the Corinth Rift is described by three syn-rift stages. This is supported by the restoration of the cross-sections correlating the onshore and offshore data from the western, central and eastern areas of the Corinth Rift. The cross-sections are reconstructed in Move Midland Valley. Syn-rift stage 1 (approximately 5 to 2.2-1.8 Ma) is characterized by: the initiation of faulting induced on pre-existing relief of the Hellenide fold-and thrust belt, its restriction to the northern Peloponnese margin, and the lack of deposition in the Gulf of Corinth at this stage. Syn-rift stage 2 (approximately 2.2-1.8 to 0.7 Ma) represents a 9-19 km northwards shift in fault activity. The deposition of Gilbert-type deltas in the western and central areas (Vouraikos and Kryoneri deltas) are correlated basinward to Seismic Unit 1 in the Gulf of Corinth area. Syn-rift stage 3 (approximately 0.7 Ma to present day) is the last stage of the tectono-stratigraphic evolution. This stage illustrates the development of the Corinth Rift towards an asymmetric basin due to focused displacement along fewer, larger, N-dipping faults on the southern margin of the Gulf of Corinth. Additionally, the present day Diakopto delta in the western area is correlated to Seismic Unit 2, the marine terraces in the central area are correlated to the marine units in Seismic Unit 2, and in the Corinth Canal the marine deposits are correlated to Seismic Unit 2. Based on the reconstruction of the three cross-sections variations in extension along rift axis are observed, and the top basement indicate inherited relief.

Acknowledgments

This thesis is part of a Master degree in Basin and Reservoir Studies at the Department of Earth Science at the University of Bergen. I would like to acknowledge several people that have been important for me and my research project.

First I want to express my sincerest gratitude to my supervisor Martin Muravchik, my co-supervisors Casey W. Nixon, Robert Gawthorpe and Gijs A. Henstra for their guidance, helpful and interesting discussions. In addition I would like to thank Jhon Meyer Muñoz Barrera for help regarding Move Midland Valley.

I thank my fellow geology students at the University of Bergen for five remarkable years. A special thanks my friends at “Hovedkvarteret” and “Grotten”.

Last but not least, I would like to thank Dick, Johanne and Manuel for their patience, support and encouragement, as well as proof reading and for the good advice.

Martine Johanne Birkemo Krabbendam Bergen, 3rd of June 2019

Table of Contents

1. Introduction

1.1 Background and rationale

This M.Sc. thesis study focuses on the Corinth Rift, an area subjected mainly to N-S extension northwest in the Aegean region (Fig.1.1) (e.g. Roberts and Michetti, 2004; Ford et al., 2013). This continental rift is one of the most active on Earth and has previously been studied both at the northern Peloponnese margin and subsurface Gulf of Corinth (e.g. McKenzie, 1978; Ori, 1989; Collier and Dart, 1991; Rohais et al., 2007b; Bell et al., 2008; 2009; Taylor et al., 2011; Ford et al., 2013; Charalampakis et al., 2014; Nixon et al., 2016; Gawthorpe et al., 2018). The rifting in this area initiated in latest Miocene/Early Pliocene, approximately 5 Ma and it is currently active (e.g. McKenzie, 1978; Keraudren and Sorel, 1987; Ori, 1989; Doutsos and Piper, 1990; Billiris et al., 1991; Roberts, 1996; Goldsworthy and Jackson, 2001; Leeder et al., 2008; Gawthorpe et al., 2018). The rift cuts the pre-existing NNW-SSE-trending Hellenide fold-and thrust belt and it is thought that the pre-existing relief and drainage patterns are inherited by the early rifting (e.g. Ford et al., 2013; 2017). The early rift initiation was located south of the Gulf of Corinth, at the northern Peloponnese margin, but present day seismic activity and extension is focused below the modern Gulf of Corinth. Several authors have discussed the evidence of a northwards migration of the locus of rifting and fault activity (e.g. Doutsos et al., 1988; Armijo et al., 1996; Rigo et al., 1996; Goldsworthy and Jackson, 2001; Bernard et al., 2006; Rohais et al., 2007a; Bell et al., 2008; Ford et al., 2013; 2017; Lambotte et al., 2014; Demoulin et al., 2015; Nixon et al., 2016; Gawthorpe et al., 2018).

The Corinth Rift is considered a very good example for studying early rift history because it is possible to study the active processes as the rifting is ongoing and the structures are not inverted. The syn-rift sequence, which includes strata deposited during active rifting, is relatively well preserved and due to uplift of the northern Peloponnese area, some of these deposits are exposed (e.g. Ford et al., 2013; 2017; Gawthorpe et al., 2017; 2018). The Corinth Rift is therefore a great area to study the evolution of structural and sedimentary processes (Ori, 1989; Collier and Dart, 1991; Rohais et al., 2007b; Bell et al., 2008; 2009; Ford et al., 2013; Nixon et al., 2016).

This study has correlated the onshore northern Peloponnese margin to the offshore Gulf of Corinth to discuss the regional tectono-stratigraphic evolution of the area. The region has been divided into three key parts. Cross-sections have been created based on existing geological data of the onshore area and seismic surveying from the offshore area. The cross-sections were reconstructed by using the software Move Midland Valley. This study is important to better constrain the evolution of the Corinth Rift and also how rift systems are developing. The understanding of extensional basins are valuable as they can preserve records of past climate change, may contain reserves of hydrocarbons, water and minerals, and active faulting may be a cause of natural hazards (e.g. Gawthorpe and Leeder, 2000).

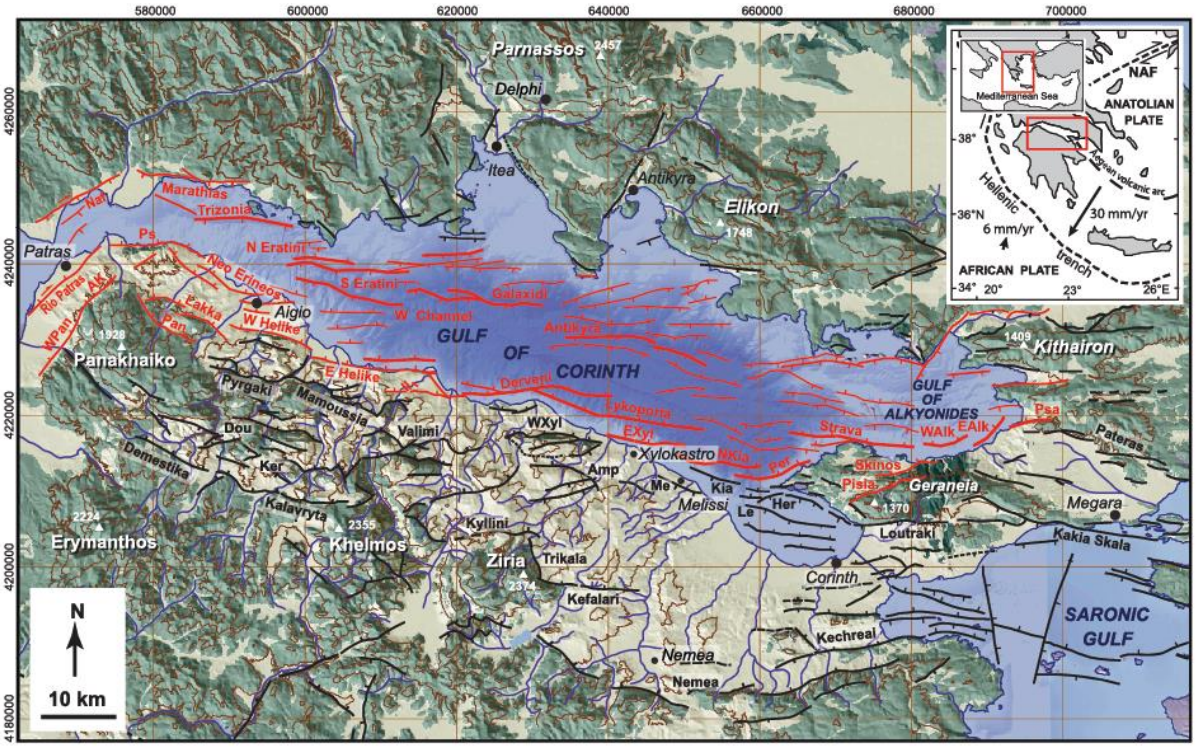

Figure 1.1. The Corinth Rift with active faults (active post 0.8 Ma) indicated in red color and currently inactive faults indicated in black color. The green color represents the pre-rift Hellenide basement, while the beige color represents the Plio-Pleistocene syn-rift sediments. Inset show the location of the Corinth Rift. Abbreviations of fault names in bold: AK, Ano Kastritsi fault; Amp, Amphithea fault; Dou, Doumena fault: EAlk, East Alkynoides fault; EXyl, East Wylokastro fault; Her: Heraion fault; Ker, Kerpini fault; Kia, Kiato fault; Le, Lechion fault; Me, Melissi fault; Naf, Nafpaktos fault; NKia, North Kiato fault; Pan, Panachaikon fault; WXyl, West Xylokastro fault. From Gawthorpe et al. (2018). The faults subsurface Gulf of Corinth are from Nixon et al. (2016) and the faults at the northern Peloponnese margin are from Rohais et al. (2007a); Ford et al. (2013); (2017); Gawthorpe et al. (2018).

1.2 Aims and objective

The aim of this M.Sc. study was to correlate the evolution northern Peloponnese margin to the evolution of the Gulf of Corinth. This was achieved by integrating field-generated structural and sedimentary data from the northern Peloponnese margin with seismic data gathered from the Gulf of Corinth.

The objectives for this study were:

i. Construct cross-sections at the northern Peloponnese margin and subsurface Gulf of Corinth
ii. Restore the cross-sections that were constructed
iii. Correlate the cross-sections of the northern Peloponnese margin to the corresponding sections subsurface Gulf of Corinth
iv. Interpret the tectono-stratigraphic evolution of the Corinth Rift
v. Compare the Corinth Rift to other rift systems and discuss the controlling factors and driving mechanisms of the evolution

1.3 Thesis outline

After this introduction, chapter 2 will give a short description of the evolution and stratigraphic patterns of rift basins. Chapter 3 focuses on the geological framework of the northern Peloponnese margin and the Gulf of Corinth, which includes a description of the tectonic framework and the structural and stratigraphic setting. Chapter 4 explains the methodology, while chapter 5 presents the present-day sections and chapter 6 describes the main steps in the restoration process. Chapter 7 will discuss the tectono-stratigraphic evolution and the controlling factors and driving mechanisms of the evolution before conclusions and suggestions for further work in the last chapter.

2. Theoretical background

This chapter gives a short description of the main processes of extensional rift systems, such as rift initiation and main ideas behind the structural development, as well as the important interaction between sediment supply and accommodation.

2.1 Evolution of Rift Basins

Continental rifts are regions of extensional deformation where the lithosphere has been exposed to deviatoric tension large enough to be broken (e.g. McKenzie, 1978; Ziegler, 1992; Ravnås and Steel, 1998). Pre-existing structures, strength and rheology of the lithosphere influence the location and distribution of strain (e.g. Kearey et al., 2009).

The mechanism of the initiation of rifting is divided into two groups, passive and active rifting (Sengör and Burke, 1978). Passive rifting is when the rifting initiates due to deviatoric tensions large enough to cause the lithosphere to break which causes thinning of the lithosphere and upwelling of the asthenosphere (McKenzie, 1978). Two types of passive rifting are recognized. One type is characterized by drag on the base of the lithosphere due to convection currents in the underlying upper mantle, the other type is characterized by stresses caused by plate boundary forces. The active rifting explains rifting due to an area in the underlying upper mantle that has low density, is anomalously hot (Bott, 1995) and rises, weakening the lithosphere and causing uplift, thinning and breakup of the lithosphere (e.g. Allen and Allen, 2013). The initiation of the Corinth Rift was mainly due to a subduction of the African plate beneath the Eurasian plate and an interaction with the westward movement of the Anatolian plate (e.g. McKenzie, 1978; Le Pichon and Angelier, 1979; 1981; Jolivet et al., 1994).

Initial rifting is generally characterized by several isolated fault segments consisting of normal faults distributed over a large area with small and shallow depocenters due to low subsidence rate. Larger depocenters will form as fault tips propagate towards each other and in the end the fault tips links (Fig. 2.1) (Cowie et al., 2000; Gawthorpe and Leeder, 2000). This is also what have happened in the Corinth Rift, where the isolated fault segments have linked through time creating a border fault system at the southern margin of the Gulf of Corinth (Nixon et al., 2016).

Cowie et al. (2005) proposed a model of rift evolution based on the study of the northern North Sea rift. The evolution is described by initiation of the rift (stage 1) with faulting distributed over a large area characteristic by small faults which are dipping towards and away from the rift axis (Fig. 2.2.a). The thermal gradient is weak at this stage. In stage 2 the faults that are dipping towards the rift axis accumulate more displacement than the faults dipping away from the rift axis (Fig. 2.2.b). The thermal gradient increases towards the rift axis. The last step, stage 3, is characterized by active faults dipping towards the rift axis and the faults dipping away from the rift axis are less active or inactive (Fig. 2.2.c). The thermal gradient is focused at the rift axis (Cowie et al., 2005). This shows that during rift initiation a wide range of faults over a distributed area are active and that a dip towards the rift axis is preferred as well as a shift of larger displacement over time on faults closer to the rift axis causing rift narrowing (Fig. 2.2) (Cowie et al., 2005). The Corinth Rift have experienced localization of the strain on fewer larger faults, but differs from this model as it has not experience rift narrowing (Nixon et al., 2016).

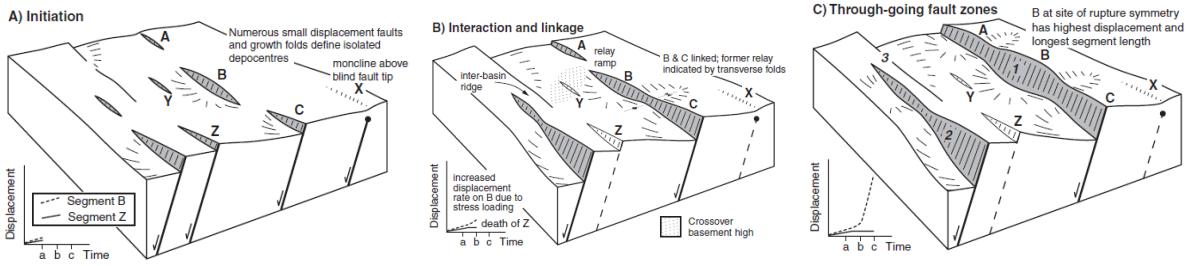

Figure 2.1. Schematic evolution of a normal fault array a) Fault initiation stage with several isolated faults distributed over an area b) Second stage in the evolution and the faults begin to interact c) Last stage in the evolution characterized by fault linkage. Slightly modified from Gawthorpe and Leeder (2000).

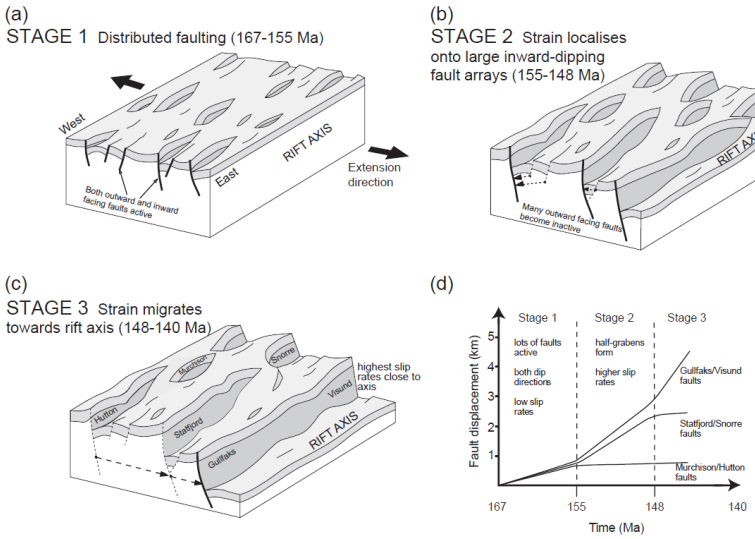

Figure 2.2. Schematic migration of faults a) The initial stage characterized by faults dipping towards and away from the rift axis b) Second stage characterized by larger displacement along the faults dipping towards the fault axis compared to the faults dipping away from fault axis c) Last stage characterized by the largest displacement on the faults closest to the rift axis. From Cowie et al. (2005).

2.2 Stratigraphic patterns typical of Rift Basins

The sedimentary record is a complex interplay between tectonic and climatic processes. The tectonic processes could be active faulting, and climatic processes affect the type of sediment, the source of sediment and the sediment supply. Both processes influence the global eustatic sea-level (Gawthorpe and Leeder, 2000). The depositional architecture of rift basins is a function of variations in the rates of sediment supply in combination with variations in rates of accommodation. The sediment supply is controlled by climate, the distance the basin has to the main hinterland area, the size of the drainage catchment, the half-graben morphology and the pre-rift substrate (Ravnås and Steel, 1998).

The creation of the accommodation is a function of global eustatic sea-level and tectonic subsidence and uplift. If the global sea level rises, more accommodation is created and if it falls the accommodation will be less. Structural processes controlling the accommodation are fault activity, as vertical displacement along active faults causes hangingwall subsidence and often footwall uplift (Ravnås and Steel, 1998, and references therein). Rift basins are generally divided into four types based on the relation between sediment supply and accommodation. These are overfilled, balanced, underfilled and starved sedimentary basins (Ravnås and Steel, 1998). These types are characterized by different types of deposits, the overfilled and balanced sediment infill is represented by the three-fold sandstone-mudstone-sandstone motif; the underfilled type is characterized by the two-fold conglomerate-sandstone-mudstone motif; and the sediment-starved basin is represented by the one-fold mudstone motif. When the basin is overfilled the sediment supply is higher than the accommodation, when the basin is balanced the sediment supply is equal to the accommodation, and when the basin is underfilled, or starved, the accommodation is higher than sediment supply (Ravnås and Steel, 1998). The Corinth Rift has through history been sediment overfilled, underfilled and starved, and today the basin is sediment underfilled and starved (Gawthorpe et al., 2018).

The drainage pattern in rifts are controlled by pre-existing drainage pattern or by fault growth. If the drainage pattern inherited the flows are more erosive and are able to flow across the developing faults. If the drainage pattern is not inherited the flows will follow elevation, relay ramps and usually flow around fault tips (Gawthorpe and Leeder, 2000; Cowie et al., 2006). The Corinth rift is thought to have inherited pre-existing topography with pre-existing

drainage pattern in the early rift history (Ford et al., 2013; 2017). The drainage pattern that develop in rift systems are oriented parallel or perpendicular to the rift axis, also known as axial drainage systems and transverse drainage systems, respectively (Ravnås and Steel, 1998; Gawthorpe and Leeder, 2000).

3. Geological Setting

The aim of this chapter is to give an overview of the geological setting of the study area. The chapter gives an introduction to the geological area and the tectonic framework before further describing the structural and stratigraphic setting through time.

3.1 Introduction

The northern Peloponnese margin and the Gulf of Corinth is located northwest in the Aegean region and the area is dominated by N-S extension and normal faulting (Fig. 1.1). The rift structure is trending ESE-WNW and cuts the former NNW-SSE trending Hellenic Mountain belt which is also the main sediment source to the rift (Doutsos and Poulimenos, 1992; Armijo et al., 1996; Skourtsos and Kranis, 2009; Ford et al., 2017; Gawthorpe et al., 2018). The Gulf of Corinth is 105 km long and it is 0.5 km wide at the narrowest point located to the west and 30 km at its broadest point located to the east (Armijo et al., 1996; Ford et al., 2013).

The history of the N-S extension is divided into two rift phases on a regional scale by Gawthorpe et al. (2018). Rift phase 1 is estimated to have lasted from 5.0-3.6 Ma to 2.2-1.8 Ma and rift phase 2 initiated 2.2-1.8 Ma and is ongoing (Gawthorpe et al., 2017; 2018). From rift phase 1 to the initiation of rift phase 2 there was a 15-30 km migration of the fault activity towards the north. The deformation became focused on fewer faults and the extension rates accelerated and today most of the active faults are subsurface Gulf of Corinth. Geodetically measured extension rates can reach up to 15 mm $year^{-1}$, with maximum Holocene uplift rate of 2-3 mm $year^{-1}$ (Clarke et al., 1997; Avallone et al., 2004; Pirazzoli et al., 2004; Bernard et al., 2006; Ford et al., 2013; Gawthorpe et al., 2018).

3.2 Tectonic framework

The main driving forces to the extensional regime in the Aegean region are the Hellenic subduction zone where the African plate is being subducted beneath the Eurasian plate and the interaction with the westward movement of the Anatolian plate (Fig. 3.1) (McKenzie, 1978; Le Pichon and Angelier, 1979; 1981; Jolivet et al., 1994). The extensional deformation that occurs in Greece is interpreted to be the result of the combination of back-arc extension due to the roll-back of the subducting African plate, gravitational collapse of the over-thickened crust of the former Hellenic Mountain belt and the westward propagation of the dextral north Anatolian fault (Fig. 3.1) (Le Pichon and Angelier, 1979; 1981; Jolivet et al., 1994; 2013; Armijo et al., 1996; Jolivet, 2001; Zelt et al., 2004; Rohais et al., 2007a; 2007b; Bell et al., 2009; Ford et al., 2013).

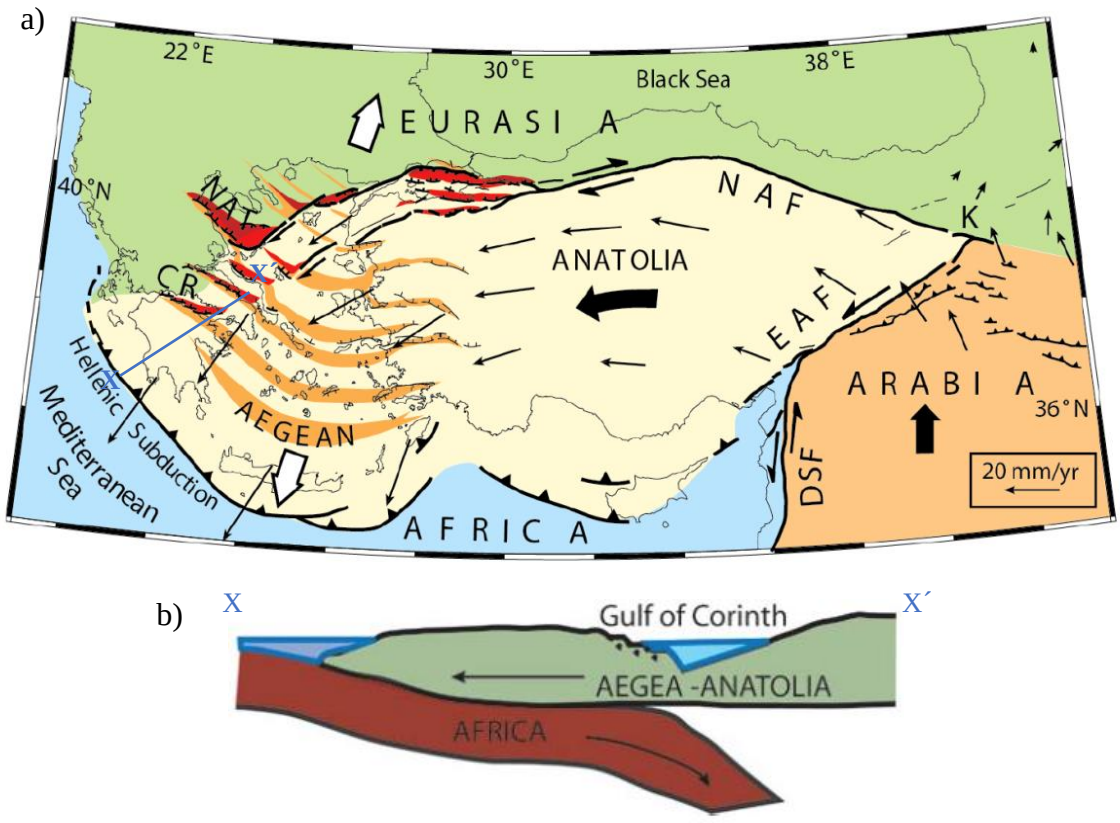

Figure 3.1. a) Greece is located on the Aegean microplate and is bounded by the Hellenic subduction zone to the south, the North Anatolian fault to the west and the Anatolia microplate to the east b) Cross-section of the rift, the Peloponnese and the African plate being subducted beneath the Aegean-Anatolian plate. Location of the cross-section is shown in a). Abbreviations: CR: Corinth rift; NAT: North Aegean Trough; NAF: North Anatolian Fault; K: Karliova Triple Junction; EAF: East Anatolian Fault; DSF: Dead Sea Fault. Modified from Armijo et al. (1999) and Turner et al. (2010).

3.3 Structural setting

Recent studies have defined rift phase 1 and 2 which explain the regional evolution of the rift on a basin scale (Gawthorpe et al., 2017; 2018).

3.3.1 Rift Phase 1

Rift phase 1 is estimated to have initiated 5.0-3.6 Ma and lasted until 2.2-1.8 Ma. It was located south of the present Gulf of Corinth and is now preserved at the northern Peloponnese margin (Gawthorpe et al., 2017; 2018). The geometry of the rift was similar to a graben structure because faulting occurred at both the southern and northern margin with N-and S-dipping faults respectively (Fig. 3.2). These north and south fault blocks were approximately 3-8 km wide and the rifting zone was about 20-30 km wide (Gawthorpe et al., 2018). The rift had most likely no connection to the ocean, except for some sporadic connection to the southeast (Gawthorpe et al., 2018). Before 3.6 Ma the depositional environment was shallow lacustrine, but at approximately 3.6 Ma the depositional environment changed to a deeper water environment with hemipelagic and turbiditic deposits (Gawthorpe et al., 2018). The subsidence rate was higher than the sedimentation rate which caused the basin to be sediment starved and underfilled and the lake that formed is known as Lake Corinth (Fig. 3.2) (Gawthorpe et al., 2018).

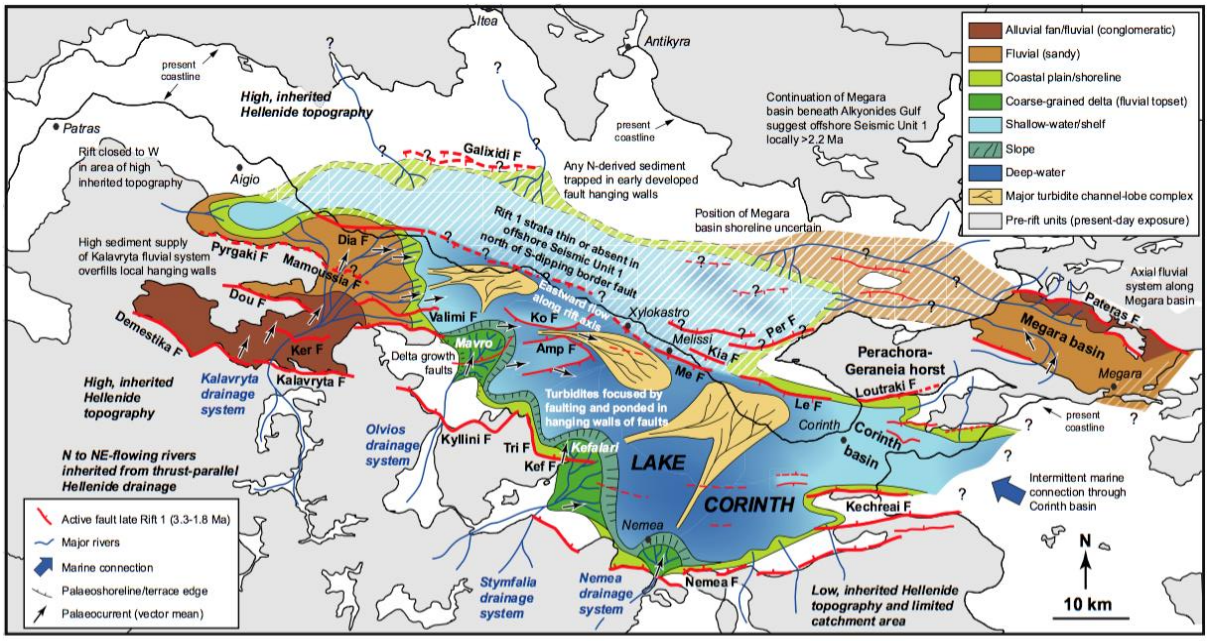

Figure 3.2. The Late rift phase 1 (Late Pliocene/Early Pleistocene). The active N- and S- dipping faults (red) define the border of the rift. The rift is closed to the west and the strata are thin or absent subsurface Gulf of Corinth indicated with the striped blue area. Modified from Gawthorpe et al. (2018).

3.3.2 Rift Phase 2

Rift phase 2 is estimated to have initiated 2.2-1.8 Ma and is still ongoing in the Gulf of Corinth. It is suggested that the faulting started in the east and migrated westward (2007a; Rohais et al., 2007b; Ford et al., 2013; Gawthorpe et al., 2017; 2018). During the initiation of the second rift phase, Lake Corinth was destroyed as a result of the 15-30 km northwards migration of fault activity and uplift of the area (Ori, 1989; Gawthorpe et al., 2018). The rate of Holocene uplift at the southern footwall block has its maximum (~2 mm year^{-1}) at the center of the rift and decreases towards the west and east (Fig. 3.3) (Pirazzoli et al., 2004; Turner et al., 2010; Charalampakis et al., 2014; Gawthorpe et al., 2018). The rift was bounded by N- and S-dipping faults, but between 0.6 and 0.3 Ma the rift developed a dominant southern border fault as the S-dipping faults on the northern margin became less active and some inactive (Fig. 3.4) (Bell et al., 2008; 2009; Nixon et al., 2016). Since approximately 0.6 Ma the Gulf of Corinth has been open to the sea during interglacial highstands which caused land barriers to be broken in the west and/or in the east (Fig. 3.4) (Nixon et al., 2016). When the Rion Strait sill in the west was flooded the environment in the rift was marine. When sea level dropped the Rion Strait sill could work as a barrier to marine waters and the environment of the rift became lacustrine (Perissoratis et al., 2000; Nixon et al., 2016). This change in alternating marine and lacustrine environment can be observed in the seismic package and is marked by an unconformity found subsurface Gulf of Corinth (Perissoratis et al., 2000; Gawthorpe et al., 2018). The age for the unconformity has been discussed in previous work, but a core of the deposits has been recently studied and the age is estimated to be 0.78 Ma (McNeill et al., 2019).

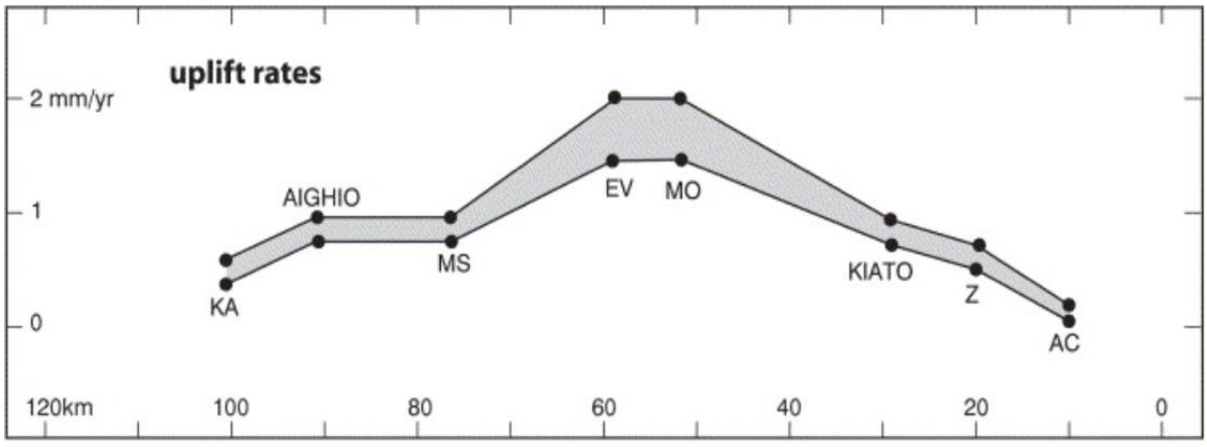

Figure 3.3. Uplift rates along the Gulf of Corinth. Abbreviations: AC, Ancient Corinth; Z, Zevgolatio; EV, Evrostini; MS, Megalo Spilaio; KA, Kamares. From Pirazzoli et al. (2004).

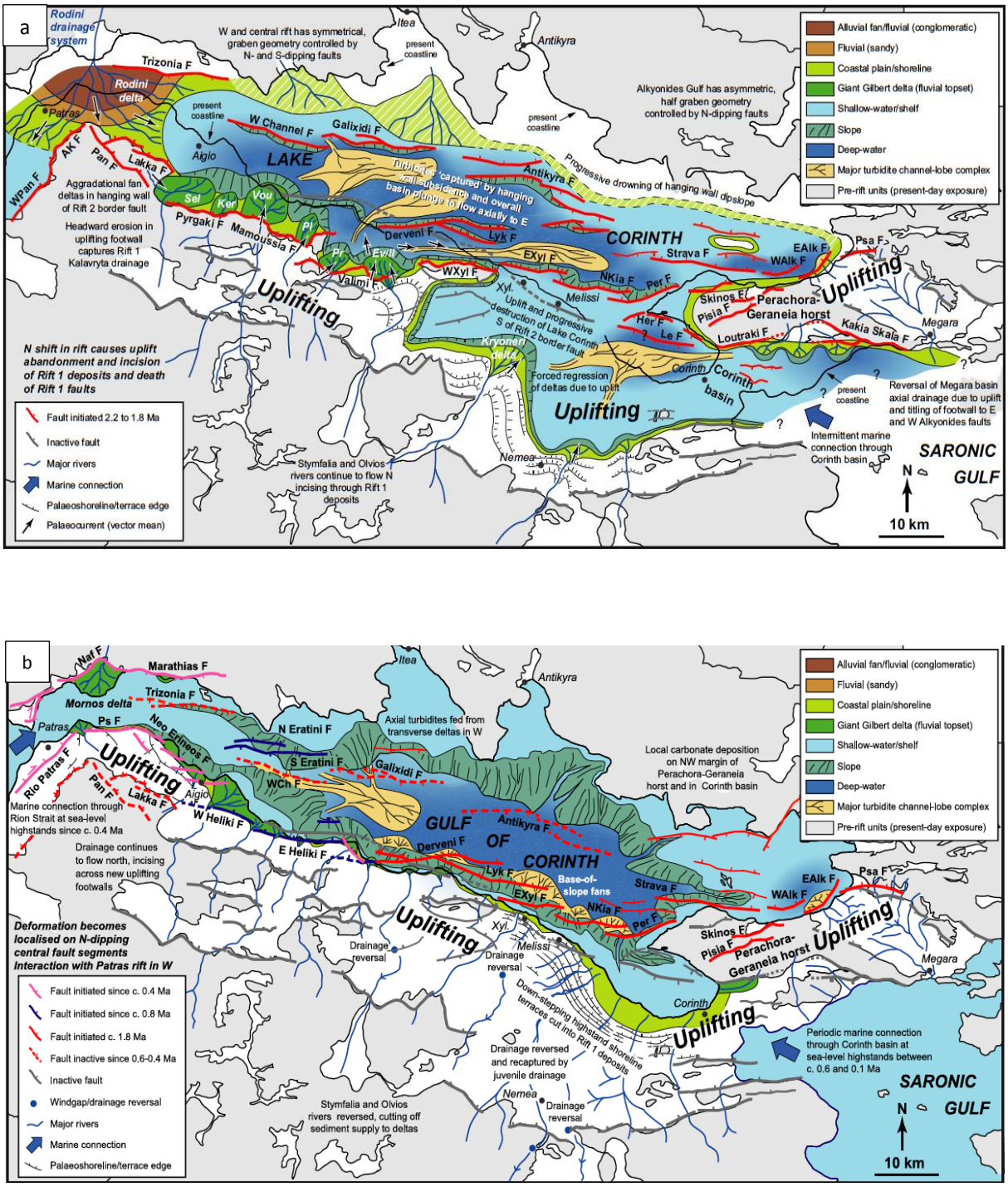

Figure 3.4. a) Early rift phase 2, Early to Middle Pleistocene. Both N-and S-dipping faults are active and the southern margin is progressively uplifted causing forced regression and destruction of Lake Corinth. There is no connection to the Ionian sea to the west. b) Late rift phase 2, Late Pleistocene. Dominated by N-dipping faults forming a southern border fault system. The southern margin continues to be uplifted. The rift is connected to the Ionian sea in the west. Modified from Gawthorpe et al. (2018).

3.4 Stratigraphic setting

3.4.1 Pre-rift stratigraphy

The pre-rift basement was formed during the formation of the Hellenides fold- and thrust belt which is of Mesozoic age and consists mainly of carbonate, clastic and metamorphic rocks (Doutsos et al., 1988; Le Pourhiet et al., 2003; Rohais et al., 2007b; Skourtsos and Kranis, 2009; Taylor et al., 2011; Ford et al., 2013; Gawthorpe et al., 2018). The pre-rift deposits are of importance since they are the main sediment source for the syn-rift sedimentation (Ori, 1989). An unconformity that represents a time gap of about 15-20 Myr separates the pre-rift basement from the syn-rift deposits (Ford et al., 2013).

3.4.2 The syn-rift stratigraphy of the northern Peloponnese margin

Below is a short description of the deposits characterized for the area near Diakopto, Xylokastro and the Corinth Canal at the Isthmus of Corinth which is studied in this thesis.

Western area (Diakopto area)

The syn-rift deposits at the western area on the northern Peloponnese margin are divided into three main groups: the Lower Group; the Middle Group and the Upper Group (Rohais et al., 2007a; 2007b; Ford et al., 2013). The Lower Group is of Late Pliocene age, between 4 Ma and 2.5-1.8 Ma, and consists of alluvial and fluvial deposits. The Middle Group is age estimated 2.5-1.8 Ma to 0.7-0.45 Ma and consists mainly of lacustrine fan delta deposits. The Upper Group was deposited 0.7-0.45 Ma to present day and the Diakopto delta is the of focus in this project (Fig. 3.5). In the area near Diakopto, the Lower Group deposits are fining towards the north, and furthest north the Ladopotamos Formation is overlain by the Katafugion Formation. The Katafugion Formation has limited areal distribution and the deposits are indicative of a transgression (Ford et al., 2013). The Ladopotamos and Katafugion formations are truncated by the Middle Group Vouraikos delta and the pro-delta Derveni Formation (Fig. 3.5). The Vouraikos delta, as well as most of the deltas deposited in the Corinth Rift, are described as Gilbert-type deltas. These type of deltas are characterized by high-angle delta front slopes, are generally coarse-grained and ideally have a distinct geometry with topset, foresets and bottomset (e.g. Postma and Roep, 1985). In previously studies the Lower, Middle and Upper Groups have been correlated to sediment packages subsea Gulf of Corinth and it is interpreted that the Upper Group is mainly deposited basinward, while there is not much of the Lower Groups deposited in the area now occupied

by the Gulf of Corinth. The Middle and Upper Group are time equivalent to Seismic Unit 1 and Seismic Unit 2 respectively (these units are described below in sub-chapter 3.4.3) (Ford et al., 2013; Nixon et al., 2016).

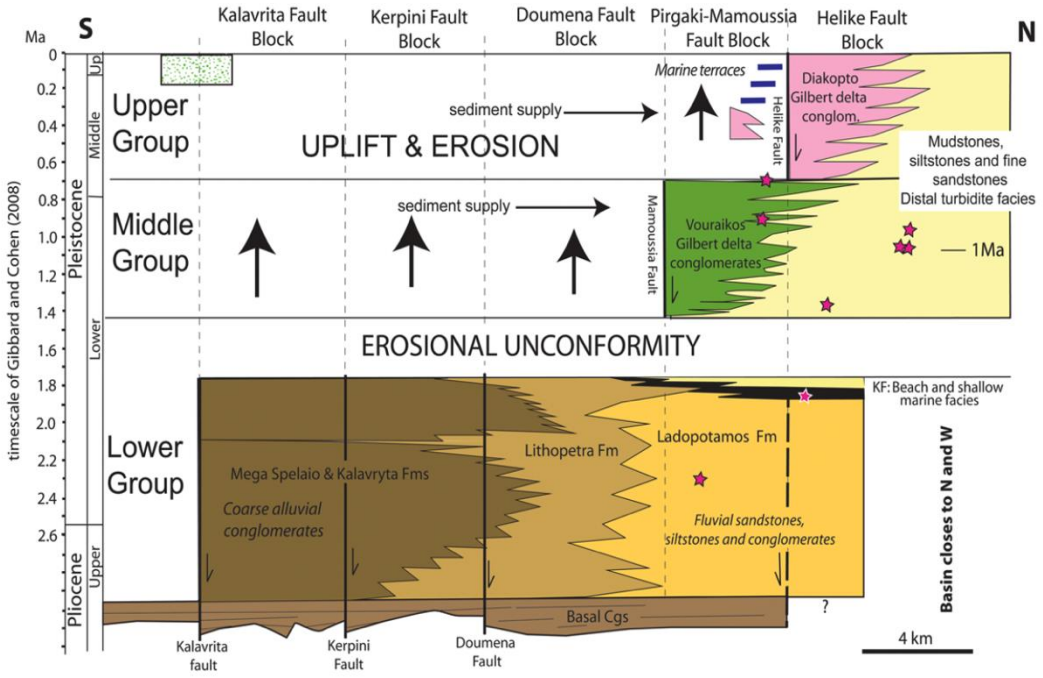

Figure 3.5. Chronostratigraphy of the study area in the western part of the northern Peloponnese margin, close to Diakopto. The stratigraphy is divided into the Lower, Middle and Upper Group. The Lower Group consists mainly of alluvial and fluvial deposits. The Middle Group is defined to the Vouraikos delta and the Derveni Formation (pro-delta deposits) and the Upper Group to the Diakopto delta in this area. The pink stars represents palynological dates and the timescale is of Gibbard and Cohen (2008). KF, Katafugion Formation. Modified from Ford et al. (2017)

Central area (Xylokastro area)

The syn-rift deposits in the central area on the northern Peloponnese margin show an overall deepening upward trend, from fluvial and shallow lacustrine to deep-water lacustrine conditions (Gawthorpe et al., 2017; 2018). The 3 km deepening upward sequence is divided into four syn-rift lithostratigraphic units: Korfiotissa Formation; Ano Pitsa Formation; Pellini Formation and Rethi-Dendro Formation (RDF) which are confined to rift phase 1. Korfiotissa Fm. was deposited in a fluvial to continental depositional setting; Ano Pitsa Fm. was deposited in an environment dominated by fluvial and lake foreshore-shoreface processes; Pellini Fm. consists of deposits characterized by lower slope to pro-delta depositional environment and the Rethi-Dendro Fm. consists of deep water lacustrine deposits (Fig. 3.6) (Gawthorpe et al., 2017; 2018). During rift phase 1 coarse-grained conglomeratic deltas prograded northwards into 300-600 m deep water, and the delta of focus in this study is the Kefalari delta (Gawthorpe et al., 2017; 2018). These deposits can be age correlated to the

Lower Group deposits in the western area (Fig. 3.7). The initiation of the second rift phase and a northwards shift in fault activity resulted in deposition of coarse-grained deltas, such as the Kryoneri delta. This delta is approximately time equivalent to the Middle Group in the west and the Seismic Unit 1 described in sub-chapter 3.4.3 below (e.g. Ford et al., 2013; Gawthorpe et al., 2017; 2018). The palaeo-shoreline migrated further northwards and marine terraces defined as thin deposits that dip <10 degrees seawards were deposited and can now be observed at different elevations (Armijo et al., 1996). They record uplift of the southern rift flank and are correlated to the marine isotope stages (MIS) and are age equivalent to the Upper Group and Seismic Unit 2 (described in sub-chapter 3.4.3 below) (e.g. Armijo et al., 1996; Nixon et al., 2016, and references therein).

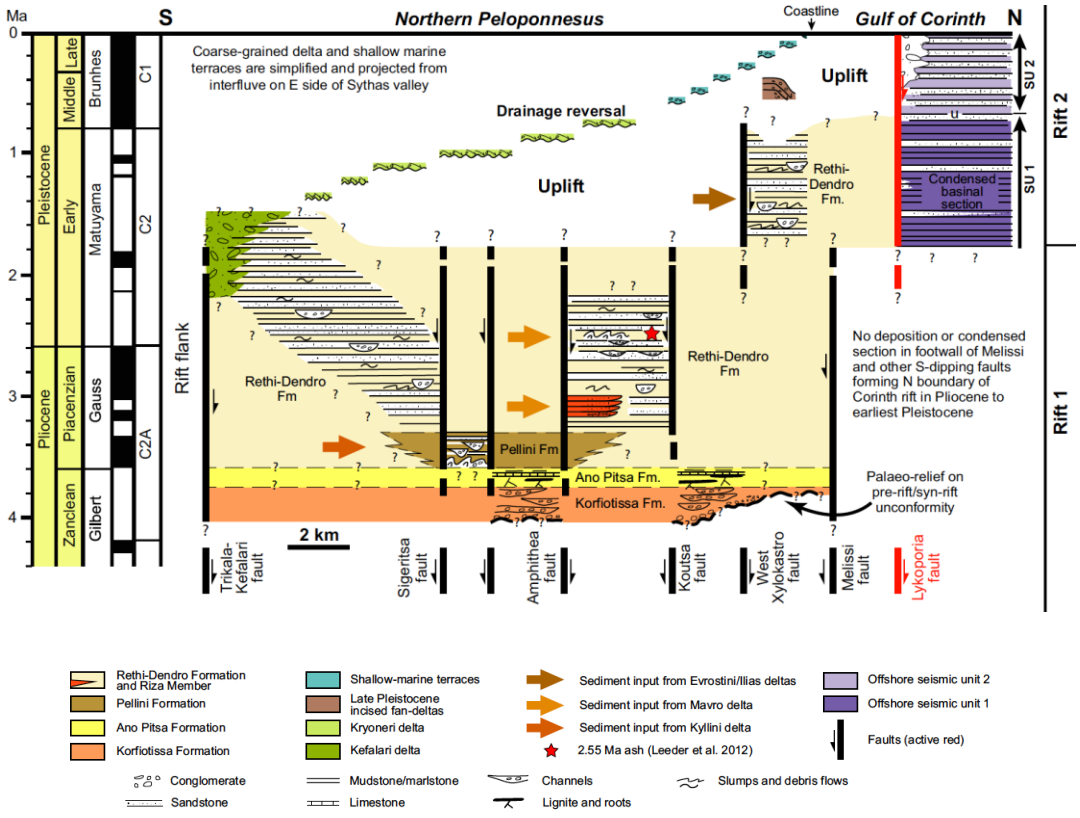

Figure 3.6 Chronostratigraphy of the study area in the central part of the northern Peloponnese margin, close to Xylokastro. The formations important for this study are the Korfiotissa Fm., Ano Pitsa Fm., Rethi-Dendro Fm. and the Kefalari delta, the Kryoneri delta and the marine terraces. These are correlated with the Seismic Units based on Nixon et al. (2016). The age model is proposed ages by Gawthorpe et al. (2018). Slightly modified from Gawthorpe et al. (2018).

Eastern area (Corinth canal at the Corinth Isthmus)

The syn-rift deposits in the eastern area are, by earlier studies, divided into three parts, the Lower Pliocene Group, the Trapeza-Isthmos Group and the fan-delta of Holocene age (Collier and Dart, 1991). The Lower Pliocene Group consists mainly of alluvial/lacustrine to marine deposits and is dated 3.5-4.5 Ma so this group is time equivalent to the Lower Group in the western area (Collier and Dart, 1991; Ford et al., 2013). The Trapeza-Isthmos Group is dated >350 ka to 205 ka and consists mainly of offshore marls, beachface/alluvial sandstones and conglomerates (Collier, 1990). In the northwestern part of the Corinth Canal there are six marine transgressive cycles identified which represent the 100 kyr glacio-eustatic highstands. Two recent master thesis projects (Meling, 2016; Sletten, 2016) have studied the *c.* 80 m thick exposed section in the Corinth Canal and divided it into six tectono-stratigraphic units (Meling, 2016; Sletten, 2016). The lowermost tectono-stratigraphic units, units 1 to 3, represents lacustrine environment and are time correlated to Seismic Unit 1. Tectono-stratigraphic units 4 to 6 are composed of marine deposits and these units are correlated to Seismic Unit 2 and the upper surface of unit 4 is correlated to the basin-wide unconformity subsurface Gulf of Corinth (described below in sub-chapter 3.4.3) (Meling, 2016; Sletten, 2016).

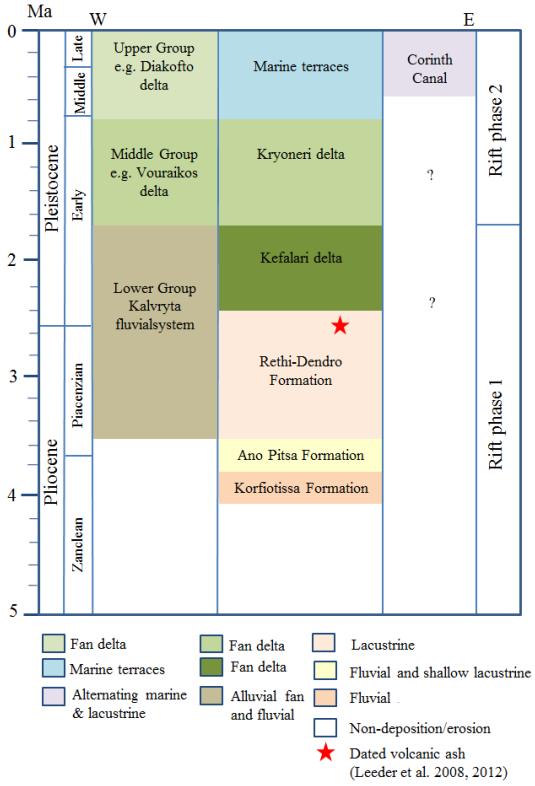

Figure 3.7 Simplified stratigraphic column to illustrate the relative age of the syn-rift successions in the western area near Diakopto, the central area near Xylokastro and the Corinth Canal. Dated volcanic ash at 2.55 Ma in the Rethi-Dendro Formation. Figure drawn based on Collier (1990); Leeder et al. (2008); (2012); Ford et al. (2013); Gawthorpe et al. (2018).

3.4.3 The syn-rift stratigraphy of the Gulf of Corinth

The present Gulf of Corinth has a maximum water depth of approximately 900 m and comprises a 2.5 km thick (at its maximum) syn-rift sedimentary package. The syn-rift sedimentary package is divided into two seismic units, Seismic Unit 1 and Seismic Unit 2, based on their seismic character (Perissoratis et al., 2000; Nixon et al., 2016) . Seismic Unit 1 (SU1) is the deeper sequence aged 2-1.5 to 0.8 Ma and is overlain by Seismic Unit 2 (SU2) aged 0.8 Ma to present (Fig. 3.8) (Nixon et al., 2016; McNeill et al., 2019). The units are separated by a basin-wide unconformity aged 0.78 Ma (McNeill et al., 2019). Seismic Unit 1 is of lower amplitude reflectors compared to SU2 and is largely lacking continuous and coherent reflections. Seismic Unit 2 is well stratified and consist of high-amplitude reflectors and is more continuous and coherent than SU1 (Fig. 3.6) (Bell et al., 2008; Nixon et al., 2016). Previously studies have mapped out and interpreted SU1 to consist of lacustrine deposits and SU2 to consist of alternating marine and lacustrine deposits (Perissoratis et al., 2000; Nixon et al., 2016). The SU2 deposits are interpreted to be related to the Quaternary 100 kyr glacio-eustatic sea-level cycles. During interglacial highstands the Corinth Rift was connected to the Ionian Sea as the Rion Strait sill was flooded. This caused a marine depositional environment in the Corinth Gulf. When the Rion Strait sill worked as a land barrier, the depositional setting was lacustrine (e.g. Perissoratis et al., 2000; Sachpazi et al., 2003; Bell et al., 2008; 2009; Taylor et al., 2011; Nixon et al., 2016). Seismic Unit 1 and Seismic Unit 2 are time equivalent to the Middle Group and Upper Group, respectively. The Lower Group deposits are absent or thin basinward (Rohais et al., 2007b; Leeder et al., 2012; Ford et al., 2013; Nixon et al., 2016).

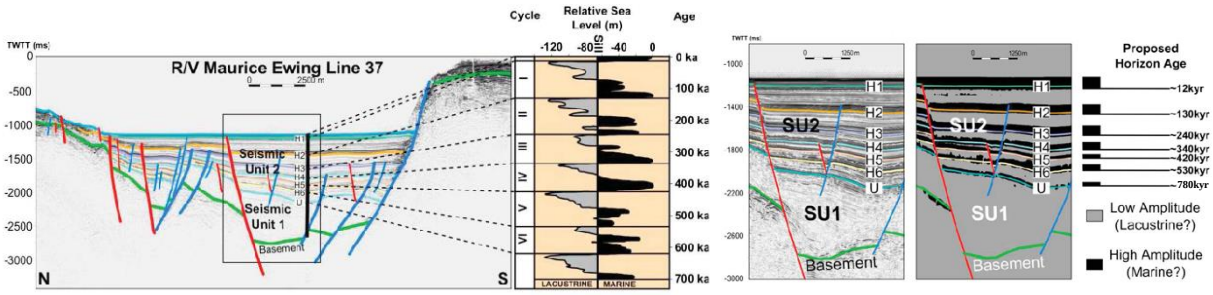

Figure 3.8 a) Seismic profile line 37 illustrating the seismic stratigraphy and correlation of Seismic Unit 2 to relative sea level curve of Bintanja and van de Wal (2008) b) Seismic Units 1 and 2 on conventional seismic reflection profile and on a profile with an amplitude volume attribute to highlight the marine and lacustrine packages. The marine horizons have a proposed horizon age. Modified from Nixon et al. (2016).

4. Data and Methods

4.1 Data and software

The data used for this thesis were gathered in the field at the northern Peloponnese margin by supervisors and coworkers. The data subsea Gulf of Corinth were collected in 2001 by multichannel seismic (MCS) using R/V Maurice Ewing (Zelt et al., 2004; Taylor et al., 2011). The data from the northern Peloponnese margin were compiled in ArcGIS, while the seismic data is interpreted using Petrel. Move Midland Valley has been used to create cross-sections and to perform the structural restoration (Fig. 4.1). The coordinate system used was WGS_1984_UTM_Zone_34N.

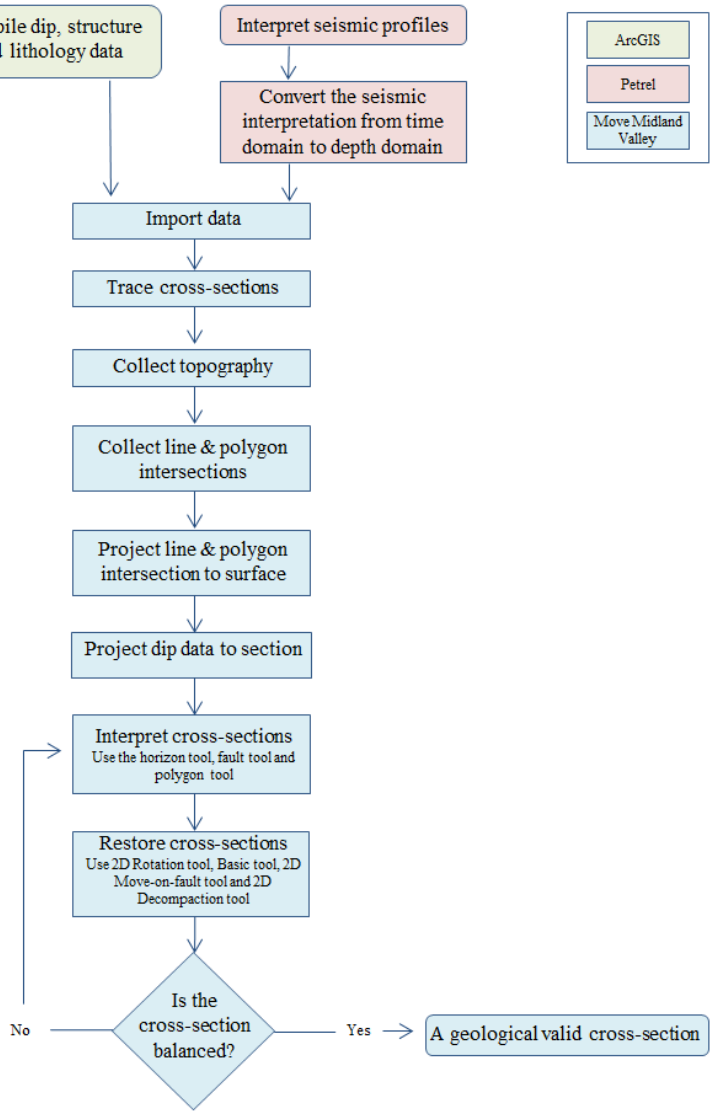

Figure 4.1 Flowchart illustrating the workflow followed from start to finish. Data were first compiled in ArcGIS and Petrel before importing it to Move Midland Valley. Move Midland Valley was utilized to construct cross-sections and perform the restoration process.

4.2 Data analysis

4.2.1 Compilation of the data from the northern Peloponnese margin

The data gathered at the northern Peloponnese margin were compiled in ArcGIS as a geological map showing the different lithological units, the position of fault structures and dip data. The field mapping, digitization and georeferencing were performed by supervisors and coworkers. Digital elevation models (DEM) were also used and contain information about the X, Y, Z values in the area of interest. The geological data from ArcGIS were imported into Move Midland Valley as vector files/shapefiles and rasterfiles. The files imported were: Xyl_Geology.shp; Xyl_Structures.shp; Xyl_dips.shp; Sythas_dip; Area_shifted.

4.2.2 Compilation of the data subsea Gulf of Corinth

The seismic data used in this project are 2-D multichannel seismic reflection data. The data were acquired by R/V Maurice Ewing in the Gulf of Corinth in 2001 using a 20 air-gun array source of 8445 cu. in. recorded by 240 channels along a 6 km streamer and also several tens of stations distributed across Greece (Zelt et al., 2004). From this dataset four seismic lines, L27, L35, L45 and L44 were interpreted using Petrel 2016. L27, L35 and L45 are oriented N-S, and L44 is oriented NW-SE, but the part of L44 oriented N-S is used (Fig. 4.2). The line lengths vary from 1 km to 28 km and the spacing between the lines ranges from 14 km to 40 km. As the seismic lines do not reach the present shoreline there were areas lacking data between the Gulf of Corinth and the northern Peloponnese margin.

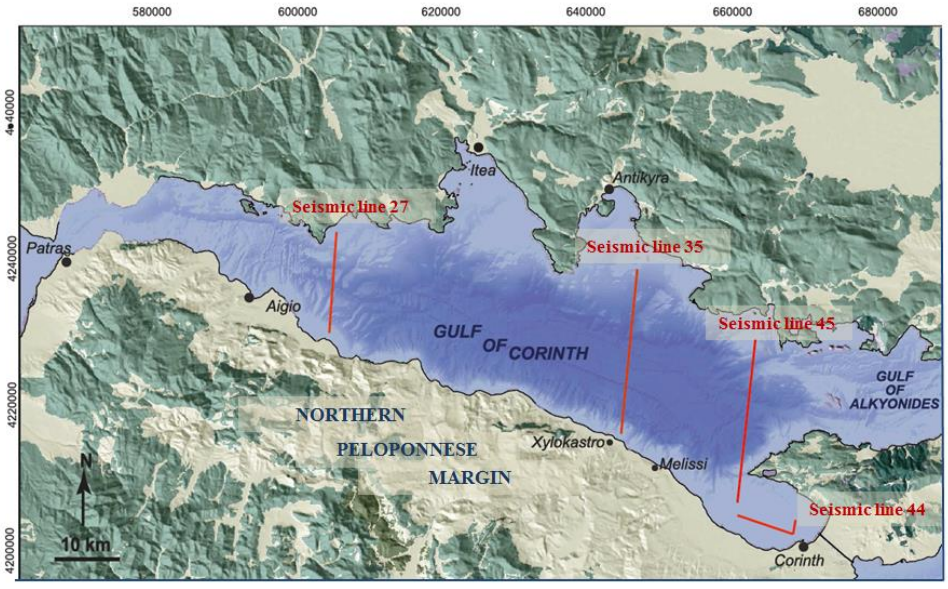

Figure 4.2 The seismic lines of the profiles that were used in this study for the offshore area. Seismic line 27, 35, 44, 45 do not reach shore. Modified from Nixon et al. (2016); Gawthorpe et al. (2018).

The Time Gain Volume attribute has been applied to the seismic lines to emphasize the reflectors deeper in the profile (Sarhan, 2007). The Root Mean Square Amplitude (RMS Amplitude) attribute has been applied on the Time Gain seismic line to better distinguish between reflectors with low and high amplitude. The seismic interpretation of Nixon et al. (2016) has been used with some readjustments. The interpretation method "Guided Autotracking" was used while interpreting as well as the "Interpret Faults" tool.

A velocity model was created in Petrel to convert the seismic profiles from time to depth domain. The different velocity models applied to the seismic dataset were:
From the seabed and down to the basement:

V_s=1.6 km/s + 1.1 km/s/s (McNeill et al., 2019)

From the basement and down:

V_b= 5km/s + 0.25 km/s/s (Taylor et al., 2011)

The water column velocity was set to 1.5 km/s

4.2.3 Cross-section construction

The data compiled in ArcGIS and the seismic data compiled in Petrel were imported to Move Midland Valley. After importing the data, a stratigraphic column was created. In the "Stratigraphy" tool, information such as name, age, thickness and rock properties were filled in for each lithological unit. The interpretation undertaken in Petrel for the three seismic lines was digitized by using the "Create horizon" tool and the "Create fault" tool. To create the cross-sections for the northern Peloponnese margin the same approach was used for all three sections. First, the "Trace" tool was used in Map View to determine the location of the cross-sections (Fig. 4.3 and 4.4). In Section View this trace can be viewed and information can be added. The topography, line and polygon intersections were collected. Dip data was projected to the section with a distance of 4 km. The projection tool "To surface" was utilized to project the line and polygon intersections to the topographic line by choosing the DEM surface as target (Fig. 4.3 and 4.4). The faults that were included in the cross-section construction were the basement cutting faults as these are the most likely major faults that are most important for the tectono-stratigraphic evolution of the Corinth Rift. The faults were projected down as planar faults from their intersect point on the topographic line by using the "Create fault" tool with the "Snap to angle" option toggled on (Appendix I Present day dip angle for active and inactive faults). The horizons were created using the "Create horizon" tool for the first horizon, before using the "Create horizon from template" tool with the first horizon as

template to create the remaining horizons. This tool allows one to vary the thickness of the unit and which horizons that should be active or not, allowing lateral facies variations. For the Corinth Canal the interpretation of Sletten (2016) was used to digitize the Surface 4 as this is the surface correlated with the basin-wide unconformity subsurface Gulf of Corinth (Meling, 2016; Sletten, 2016). The surfaces were mapped in limited extent, both vertically and horizontally so the displacement was assumed constant along the fault trace. The faults in the Corinth Canal section were digitized based on previous work done by Turner et al. (2010) and Sletten (2016).

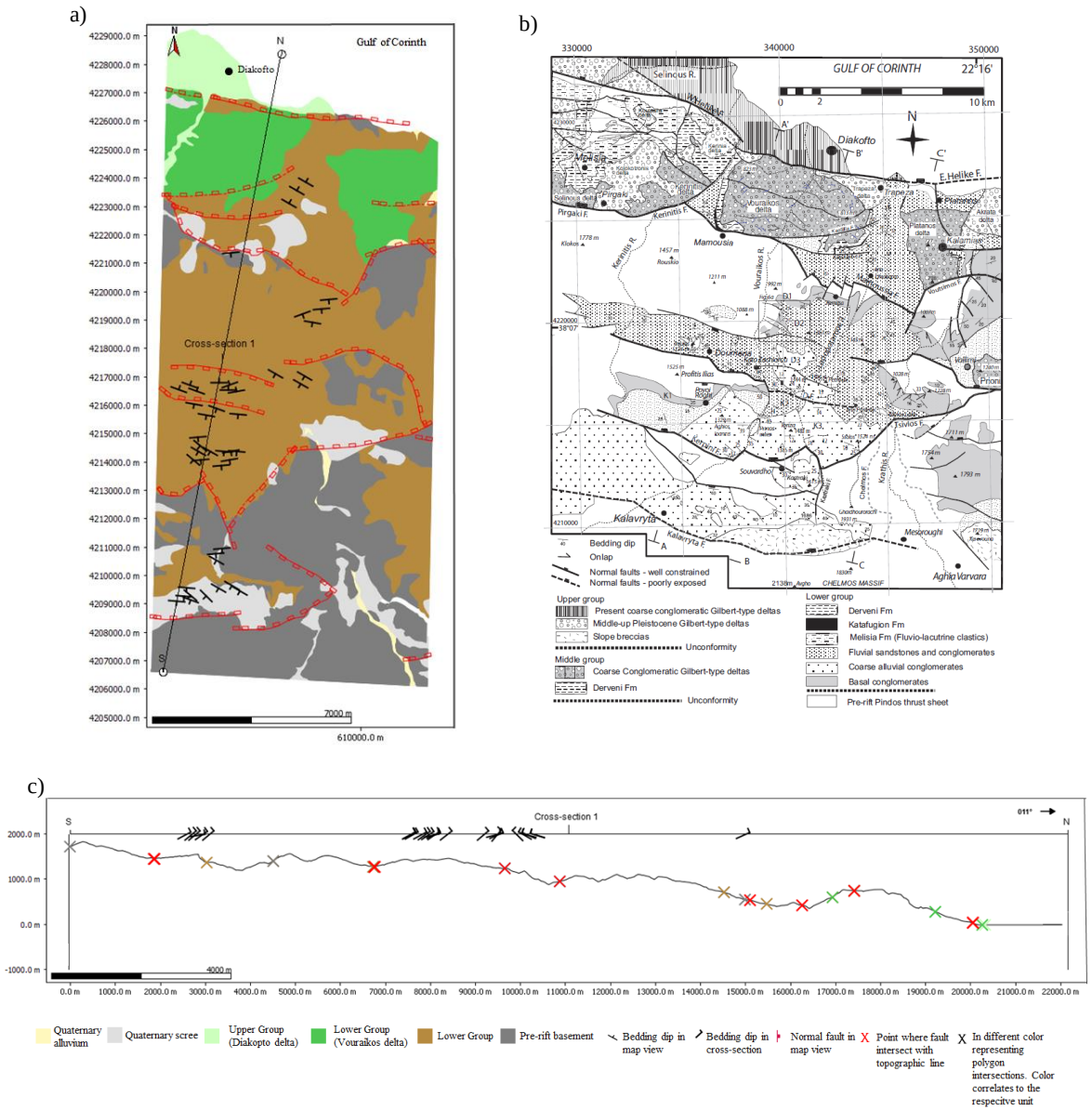

Figure 4.3 a) The geological map imported from ArcGIS to Move including mapped stratigraphic boundaries, dip measurements and the structural data of the area near Diakopto. The trace of the N-S cross-section 1 is indicated in black b) A geological map of the area of interest from Ford et al. (2013) c) The section trace in cross-section view (location in a)) with the existing topography. The line and polygon intersections were projected to the surface and the bedding dip measurements were projected to the section.

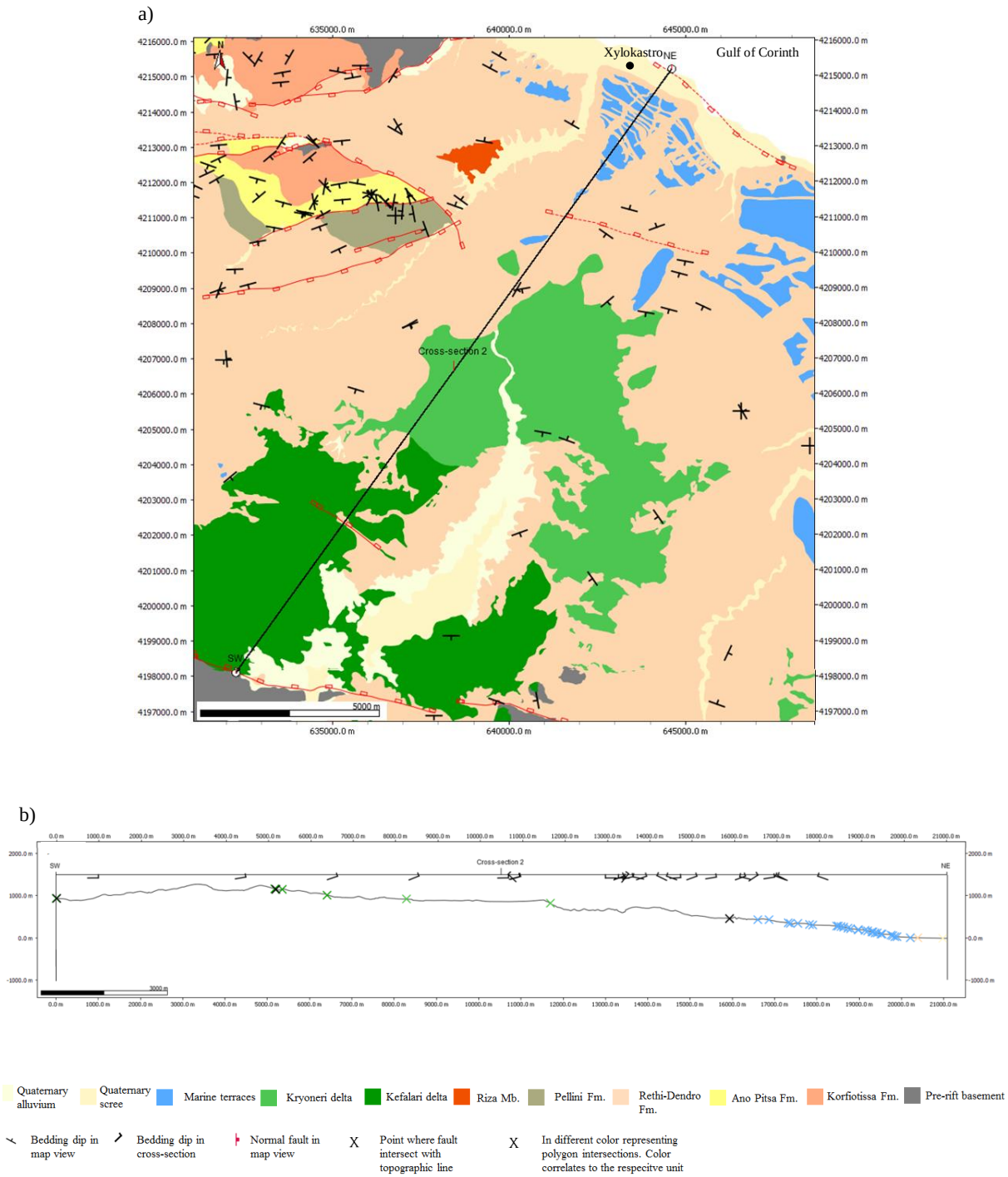

Figure 4.4 a) The geological map imported from ArcGIS to Move including mapped stratigraphic boundaries, dip measurements and the structural data of the area near Xylokastro. The trace of the SW-NE cross-section 2 is indicated in black b) The section trace in cross-section view (location in a)) with the existing topography. The line and polygon intersections were projected to the surface and the bedding dip measurements were projected to the section.

4.2.4 Structural restoration of the cross-sections

The main idea behind the structural restoration is to go back in geological time to strip off one layer at a time and to geologically validate the interpretation (Woodward et al., 1989; Fossen, 2010). A balanced cross-section is a section that can be geometrically restored to its predeformed state and Dahlstrøm (1969) was the first to introduce the concept.

It is important to know the sea-level at time of deposition of the units to be able to move the section to the location relative to the sea-level when the unit was deposited. The syn-rift deposits were most likely deposited in a lake, therefore the only units that could be correlated by using the global sea-level curve were the marine terraces. For the other units the lake-level during deposition was set to 0 m. The depth of deposition of the syn-rift units were estimated and relative to the lake-level set to 0 m (Table 1) (Miller et al., 2005; Gawthorpe et al., 2018).

Table 1. The formations and units with estimated age and correlated to estimated sea-level and water depth at time of deposition. Modified from Armijo et al. (1996); Miller et al. (2005); Ford et al. (2013); Gawthorpe et al. (2018).

Formation/Unit	Age (Ma)	Sea-level estimated (m)	Water depth (m)
Old Corinth marine terrace (MIS 7.5)	0.235 to 0.245	-50	0
Kryoneri delta	1.4 to 0.7	0	0
Vouraikos delta	1.8-1.5 to 0.7-0.5	0	0
Katafugion Fm.	-	0	0
Lower Group	<5 to 1.8-1.5	0	10-30
Kefalari delta	2.2 to 1.8	0	0
Rethi-Dendro Fm.	3.6 to 1.8	0	-500
Ano Pitsa Fm.	3.8 to 3.6	0	10-30
Korfiotissa Fm.	4 to 3.8	0	10-30

The structural restoration was performed in Move Midland Valley. The theory for the restoration assumes that no rock volume was destroyed or created during the deformation process and that the rock volume was only changed by erosion or sediment compaction (Move). It also assumes minimal volume loss attributed to pressure solution and tectonic compaction (Move). Other made assumptions are that brittle faulting was the dominant deformation process and that folding was related to faulting (Move). The tools such as 2D Unfolding, 2D Move-on-Fault and 2D Decompaction were used to perform the restoration process.

a) 2D Unfolding/Rotation

   The 2D Unfolding tool was used to restore a horizon back to its pre-deformed state as all geological layers are assumed deposited horizontal. The simple shear algorithm was applied because it is assumed that there was no layer parallel slip between the beds and it is also typically used for extensional regimes (Move). The basic tool was utilized for the horizons subsea Gulf of Corinth to rotate the dipping layers back to their pre-deformed state and to maintain the topography of the layers beneath.

b) 2D Move-on-fault

   The 2D Move-on-Fault tool was used to restore the displacement along faults. The tool has seven different algorithms: simple shear, fault parallel flow, fault bend fold, detachment fold, fault propagation fold, trishear and elliptical fault flow (Move). The algorithm used in this project was the simple shear algorithm which models the deformation throughout the hangingwall rather than as discrete slip between bedding planes (Move). A fault was selected as active in the simple shear algorithm tool to restore the displacement. All objects in the section were collected as objects to be moved and removal of displacement along the fault was done by joining the uppermost bed that was affected by the faulting.

c) 2D Decompaction

   The 2D Decompaction tool was used to remove the volume loss due to sediment compaction. In the study area the units that are decompacted consists of different lithologies so an average initial porosity, depth coefficient and density was calculated based on Sclater and Christie (1980) and Rougier et al. (2016) (Table 2). For the tectono-stratigraphic units 1 to 3 the default parameters for silt was used (Sclater and Christie, 1980; Sletten, 2016). Sclater and Christie (1980) assumes that the porosity decreases with increasing depth and increase with decreasing depth and this is represented by:

$$f = f_0 (e^{cy})$$

f is the present-day porosity at depth; f_0 is the porosity at the surface; C is the porosity-depth coefficient (km^{-1}); y is the depth (m) (Sclater and Christie, 1980).

The algorithm for the decompaction in Move Midland Valley accounts for mechanical compaction under normally pressured circumstances (Move). Chemical compaction was not encountered as it was assumed that only mechanical compaction has occurred due to lack of information about chemical compaction or diagenetic porosity loss in the area. In the 2D Decompaction tool the top beds were collected as these were considered the load being restored. Further the objects affected by the overlying load were collected as active intermediate objects and the base level was selected. Also, isostasy was accounted for at this step and as sediment facies information provides estimates of depth of deposition this was used as an approximation (Move). The whole section was shifted in vertical position using the basic tool.

Table 2. The % lithology, initial porosity, depth coefficient and density calculated for the formations/units at the northern Peloponnese margin which were used during decompaction. Abbreviations: Lst, Limestone; Cgl, Conglomerate; Sil, Siltstone; Sst, Sandstone; Shl, Shale; Mrl, Marl. Modified from Sclater and Christie (1980); Rougier et al. (2016).

Formation/Unit	% lithology	Initial Porosity	Depth Coefficient (km^{-1})	Density (kg/m^3)
Korfiotissa Fm.	Cgl51;Sil19;Sst30	0.59	0.39	2627.59
Ano Pitsa Fm.	Cgl38;Lst4;Shl42;Sst16	0.55	0.39	2662.32
Rethi-Dendro Fm.	Cgl12;Mrl11;Sst76	0.50	0.31	2622.15
Kefalari delta	Cgl100	0.50	0.30	2600.00
Tectono-strat unit 1 to 3	Sil100	0.56	0.39	2680.00

For the deposits subsurface Gulf of Corinth a compaction curve was used (McNeill et al., 2019). During the IODP Expedition 381 three sites were drilled through 700 m of rock, mostly through Seismic Unit 2 deposits. An extrapolated porosity was used for the deposits deeper down in the succession (Fig. 4.5). This was done by making an exponential trendline as it was assumed that the porosity decreases exponentially with depth (Sclater and Christie, 1980). The equation from the trendline ($y = 0{,}505308e^{-0{,}000475x}$) was used to extrapolate the porosity down to about 3 km depth of deposits (Fig. 4.5).

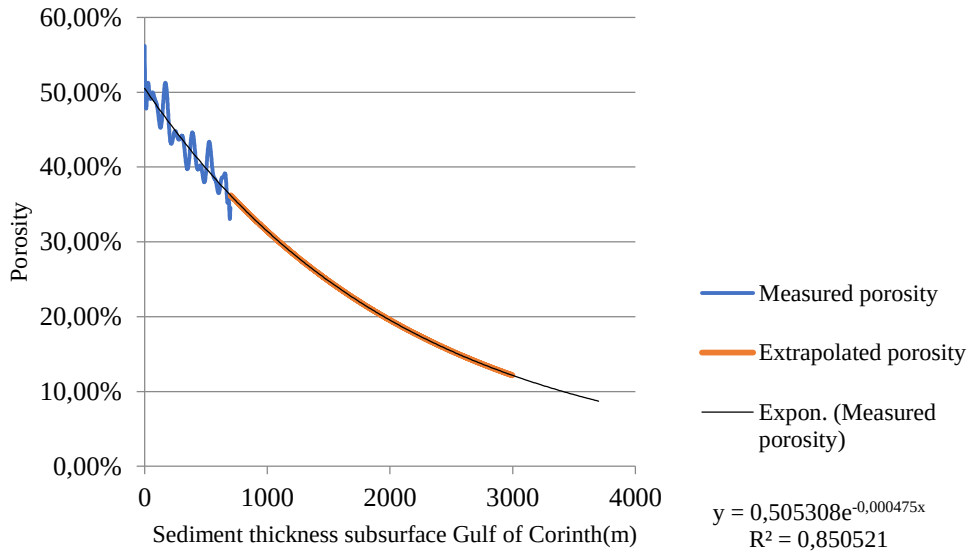

Figure 4.5 Compaction curve showing % decrease in porosity subsurface Gulf of Corinth. The porosity is measured through 700 m of rock and these measurements are used to extrapolate the porosity of the deposits below reaching a thickness of 3 km. The porosity at 0 m sediment thickness subsurface Gulf of Corinth is 56 % and the porosity decreases exponentially to approximately 12 % at 3 km sediment thickness subsurface Gulf of Corinth. Modified from McNeill et al. (2019).

Expansion indices

The thickening of deposits across faults can help determine the development of the faults. By measuring the true stratigraphic thickness of the sedimentary package in the hangingwall and dividing it with the true stratigraphic thickness of the corresponding footwall the expansion indices can be found (e.g. Thorsen, 1963; Cartwright et al., 1998; Jackson and Rotevatn, 2013). If the expansion index is larger than one, most likely more accommodation was created for sediment to be deposited in the hangingwall which indicates syn-sedimentary growth faulting (e.g. Cartwright et al., 1998). An expansion index less than one indicates thinning of hangingwall strata and if the ratio equals one, the fault was either active after deposition of the sedimentary package or the fault was buried or inactive during deposition of the strata.

4.3 Limitations and uncertainties

Both the stratigraphic framework and the structural analysis were limited by the inaccessibility to observe the whole vertical extent of the strata at the northern Peloponnese margin. The data collected by supervisors and coworkers such as dip data were also limited as they were not measured exactly where the cross-sections in this study are located and the lack of dip data is a factor of uncertainties. Additionally, most used data is lacking absolute age and when the rift was lacustrine this creates uncertainty around the lake-level at the time of deposition of strata.

The methods and algorithms used in Move Midland Valley have some limitations and uncertainties which affects the geological modelling. The algorithms used are simplified models of the processes that are active during deformation and that produce the geological structures. A model will most likely be able to be restored using different algorithms which could cause the models to have different interpretations to some extent of the restored section. Another limitation is that Move Midland Valley seems to prefer the layer-cake model which is a simplified description of a geological scenario as it assumes a stack of conformable layers and this makes it difficult to model complex stratigraphy such as delta clinoforms (Move).

5. Present day sections

The evolution of the rift was analyzed by correlating the rift successions at the northern Peloponnese margin to the rift successions subsurface Gulf of Corinth. The cross-sections offer an integrated stratigraphic and structural interpretation of the study area. Cross-section 1 is the section in the western area, cross-section 2 is the section in the central area and cross-section 3 is the section located in the eastern area of the Corinth Rift (Fig. 5.1). Subindex "a" represents present day while every subindex after represents one step in the restoration process. This chapter will further present the cross-sections and the present-day sections will be described first before presenting the main steps in the restoration process going back in time in chapter 6.

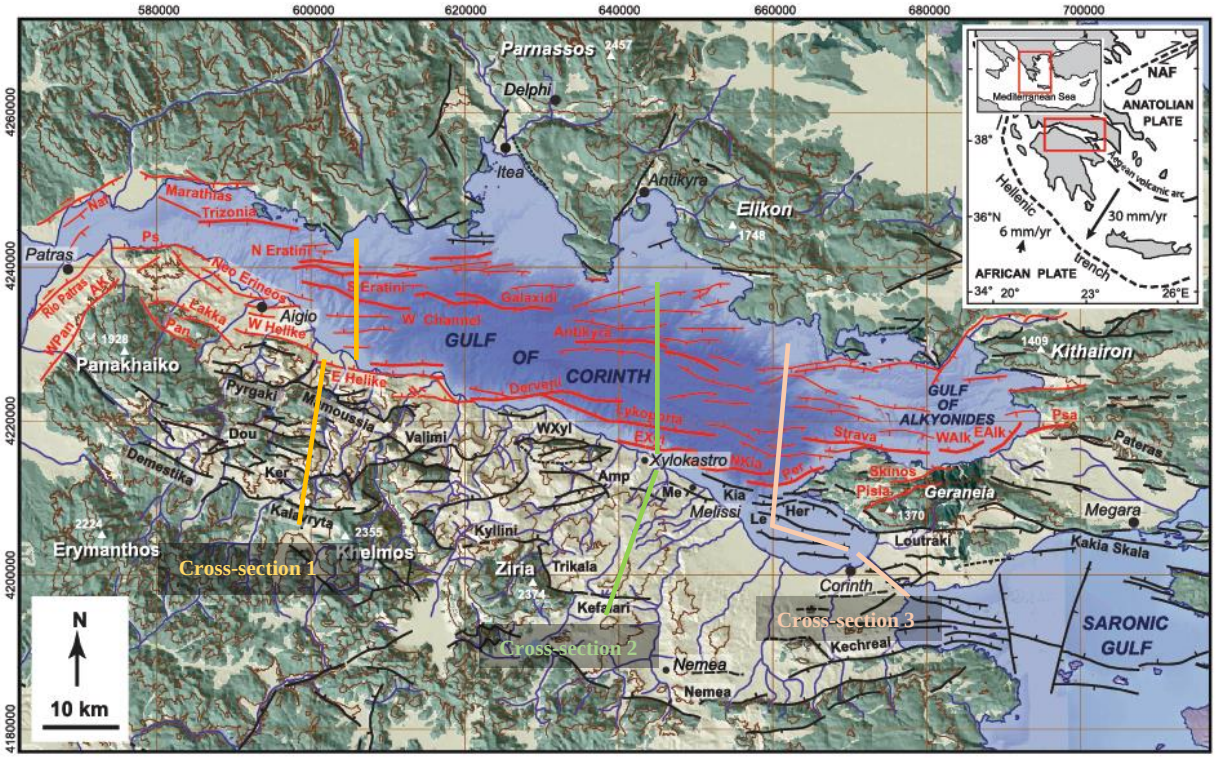

Figure 5.1. The Corinth Rift and the location of the three cross-sections. The oranges lines in the west show the position of cross-section 1, the green lines in the central area show the position of cross-section 2 and the pink lines to the west show the position of cross-section 3. Red faults indicate active faults (active post 0.8 Ma) and inactive faults are indicated in black color. The green color represents the pre-rift Hellenide basement, while the beige color represents the Plio-Pleistocene syn-rift sediments. Inset show the location of the Corinth rift. Abbreviations of fault names: AK, Ano Kastritsi fault; Amp, Amphithea fault; Dou, Doumena fault: EAlk, East Alkynoides fault; EXyl, East Wylokastro fault; Her: Heraion fault; Ker, Kerpini fault; Kia, Kiato fault; Le, Lechion fault; Me, Melissi fault; Naf, Nafpaktos fault; NKia, North Kiato fault; Pan, Panachaikon fault; WXyl, West Xylokastro fault. Modified from Gawthorpe et al. (2018). The faults subsurface Gulf of Corinth are from Nixon et al. (2016) and the faults at the northern Peloponnese margin are from Rohais et al. (2007a); Ford et al. (2013); (2017); Gawthorpe et al. (2018).

5.1 Cross-section 1-a (Present day)

Cross-section 1-a is oriented N-S. The total length of the section is 37.8 km with 21 km length at the northern Peloponnese margin, 15 km length of seismic line 27 and 1.8 km of the section is lacking data.

The majority of the faults in cross-section 1-a dip towards the north and the dip angle range from 15 to 75°. The dip angle for the S-dipping faults range from 55 to 60°. The smallest fault block is about 300 m wide while the largest is about 5 km wide and these were filled with sediment successions. The thickness of the sedimentary packages deposited at the northern Peloponnese margin changes across and within fault blocks. The strata located in the hangingwall of the Kalavryta, Kerpini and Doumena faults developed a wedge geometry and are thickening towards the respective faults. To the north in cross-section 1-a, subsurface Gulf of Corinth, the sediment thickness does not change significantly within the fault blocks and the expansion indices are higher than one for the faults. The maximum heave of the faults ranges from 300 m to 800 m.

Based on these observations the major faults are the currently inactive Kalavryta, Kerpini, Doumena, Mamoussia and West Channel faults and the currently active East Heliki and Diakopto faults. The Kalavryta, Kerpini and Doumena faults were active during deposition of the Lower Group (Fig. 5.2). The N-and S-dipping faults subsurface Gulf of Corinth were approximately of equal activity resulting in a basin with almost symmetrical graben geometry. The Diakopto and West Channel faults were active during the deposition of both seismic units, and the North and South Eratini faults were active during deposition of Seismic Unit 2. The depositional environment in the rift has varied from continental to lacustrine and marine. In summary, there was a northwards shift in fault activity from the northern Peloponnese margin towards the Gulf of Corinth.

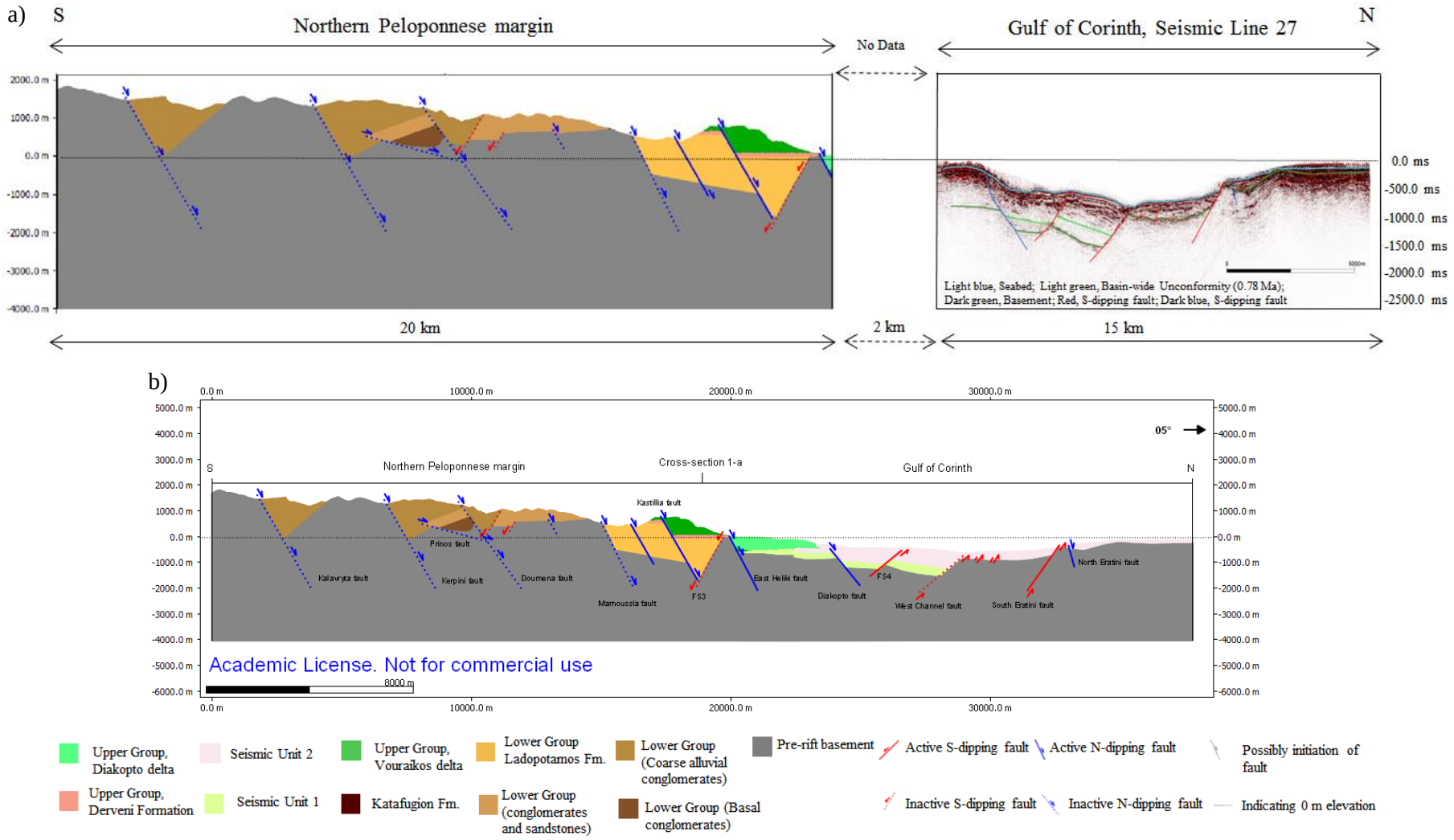

Figure 5.2 a) Cross-section 1 with original orientation of the section onshore and the Seismic line 27 with interpretations. Note that the section at the northern Peloponnese margin is in m vertical extent and the seismic profile is in ms. This is illustrative and not to scale b) Cross-section 1-a, the seismic interpretation was converted to depth domain (m) and correlated to the onshore area. The area lacking data was interpreted to mainly consist of delta deposits. Cross-section 1-a was further restored by four steps described in chapter 6.

5.2 Cross-section 2-a (Present day)

Cross-section 2-a is oriented N-S. The total length of the section is 48 km with 17.5 km length at the northern Peloponnese margin, 29.5 km length subsurface Gulf of Corinth and 0.6 km of the section is lacking data.

The majority of the faults in cross-section 2-a dip towards the north and the dip angle range from 60 to 70°. The dip angle of the S-dipping faults range from 55 to 85°. The maximum heave range from approximately 5 m to 3.2 km. The largest heaves were accumulated by the now inactive faults on land with larger fault blocks (largest 9.8 km wide) than the active faults subsea (smallest 190 m wide) (Fig. 5.3). The thickness of the sedimentary packages deposited to the south of the Melissi fault does not show significant variations across and within fault blocks (Fig. 5.3.a). The strata in fault blocks 1 and 2 dip toward the south and the strata in fault block 3 dip towards the north. Also, the Rethi-Dendro and Ano Pitsa formations thicken towards the Kefalari, FN2 and Melissi faults. The maximum thickness of the Rethi-Dendro Formation is 4 km and it is considerably thicker than the other syn-rift sedimentary packages in the section. To the north in the section the sediment thickness is changing within fault blocks as the strata are south thickening towards the East Xylokastro, FN5 and Lykoporia faults. The expansion indices are also higher than one for the faults offshore.

Based on these observations it can be inferred that the major faults in this area are the currently active East Xylokastro and Lykoporia faults and the currently inactive Kefalari, FN2, FN3, Melissi and East Antikyra faults. The Kefalari, FN2 and Melissi faults were active during deposition of the Kefalari delta, Rethi-Dendro and Ano Pitsa formations and there were also displacement along these faults after deposition of the strata (Fig. 5.3.a). The thickness of the Rethi-Dendro Formation is larger than the other syn-rift successions. This is most likely due to either more accommodation created by faulting, higher sediment supply or a combination of both during the deposition of this formation. The East Xylokastro, FN5 and Lykoporia faults had larger displacement than the S-dipping faults in the Gulf of Corinth and are therefore the controlling faults of the present day basin. The East Xylokastro, FN5, Lykoporia, FN7, FS2, FS3 and East Antikyra faults initiated during deposition of Seismic Unit 1 and continued to accumulate displacement during deposition of Seismic Unit 2. The faults further north in the section initiated after deposition of Seismic Unit 1 and were active during deposition of Seismic Unit 2 (Fig. 5.3.b). In summary, there was a northwards shift in fault activity from the northern Peloponnese margin towards the present Gulf of Corinth.

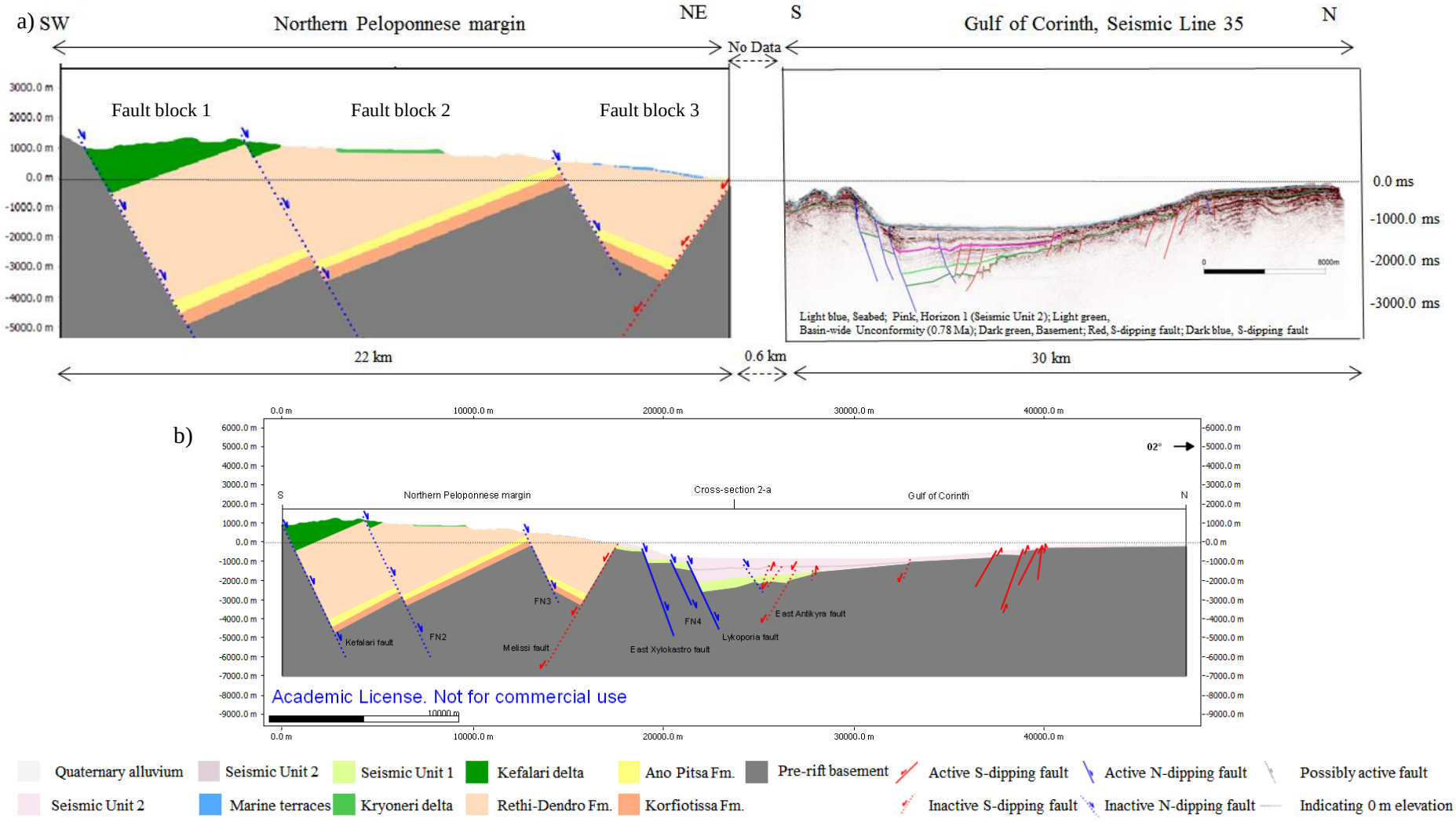

Figure 5.3 a) Cross-section 2 with original orientation of the section onshore and the Seismic line 35 with interpretations. Note that the section at the northern Peloponnese margin is in m vertical extent and the seismic profile is in ms. This is illustrative and not to scale b) Cross-section 2-a, the seismic interpretation was converted to depth domain (m) and correlated to the onshore area. The area lacking data was interpreted to be mainly a continuation of the Seismic Unit 1 and 2 deposits. Cross-section 2-a was further restored by seven steps described in chapter 6.

5.3 Cross-section 3-a (Present day)

Cross-section 3-a is oriented N-S and is 31 km long. The seismic lines 44 and 45 are 1 km long and 25 km long respectively and between these two lines 1 km is lacking data. The section of the excavated Corinth Canal is SE-NW oriented and 6.4 km long. For calculating the N-S extension of cross-section 3, the SE-NW Corinth Canal section was projected to the N-S oriented seismic lines. The length of the N-S projected Corinth Canal was 4 km.

Cross-section 3-a consisted of several north and south dipping faults and the dip angle ranges between 29-80° for the present day subaqueous faults, and in the Corinth Canal the dip angle of the faults ranges from 54-82°. The heave ranges from approximately 50 to 900 m, with the largest heaves of the faults subsurface Gulf of Corinth. The smaller fault blocks are located in the Corinth Canal (smallest 30 m wide), while the largest fault blocks are located in the Gulf of Corinth (largest 5 km wide) (Fig. 5.4). The thickness of Seismic Unit 1 and 2 changes across and within fault blocks and Seismic Unit 1 is north thickening, while Seismic Unit 2 is south thickening. There are two main basins in this section, one accumulated in the hangingwall of the Perachora fault and one in the hangingwall of the Lechaion fault. The expansion indices of the sedimentary packages in the Corinth Canal is higher than one for the tectono-stratigraphic units 4 to 6 and equal one for the tectono-stratigraphic units 1 to 3.

Based on these observations the major faults were the currently active Perachora fault and the currently inactive FN1, Lechaion, Heraion and FS4 faults. The displacement along these faults during deposition of Seismic Unit 1 was larger along the S-dipping faults than the N-dipping faults, and during deposition of Seismic Unit 2 the displacement along the N-dipping faults became larger. This is indicative that the S-dipping faults subsurface Gulf of Corinth were the controlling faults of the basin during deposition of Seismic Unit 1. The N-dipping faults were the controlling faults of the basin during deposition of Seismic Unit 2 until present day (Fig.5.4.b). The faults in the Corinth Canal became active after deposition of the tectono-stratigraphic units 1 to 3 and were active during deposition of the youngest successions (tectono-stratigraphic units 4 to 6). In summary, the faults subsurface Gulf of Corinth have a shift in largest accumulated displacement from the S-dipping faults to the N-dipping faults.

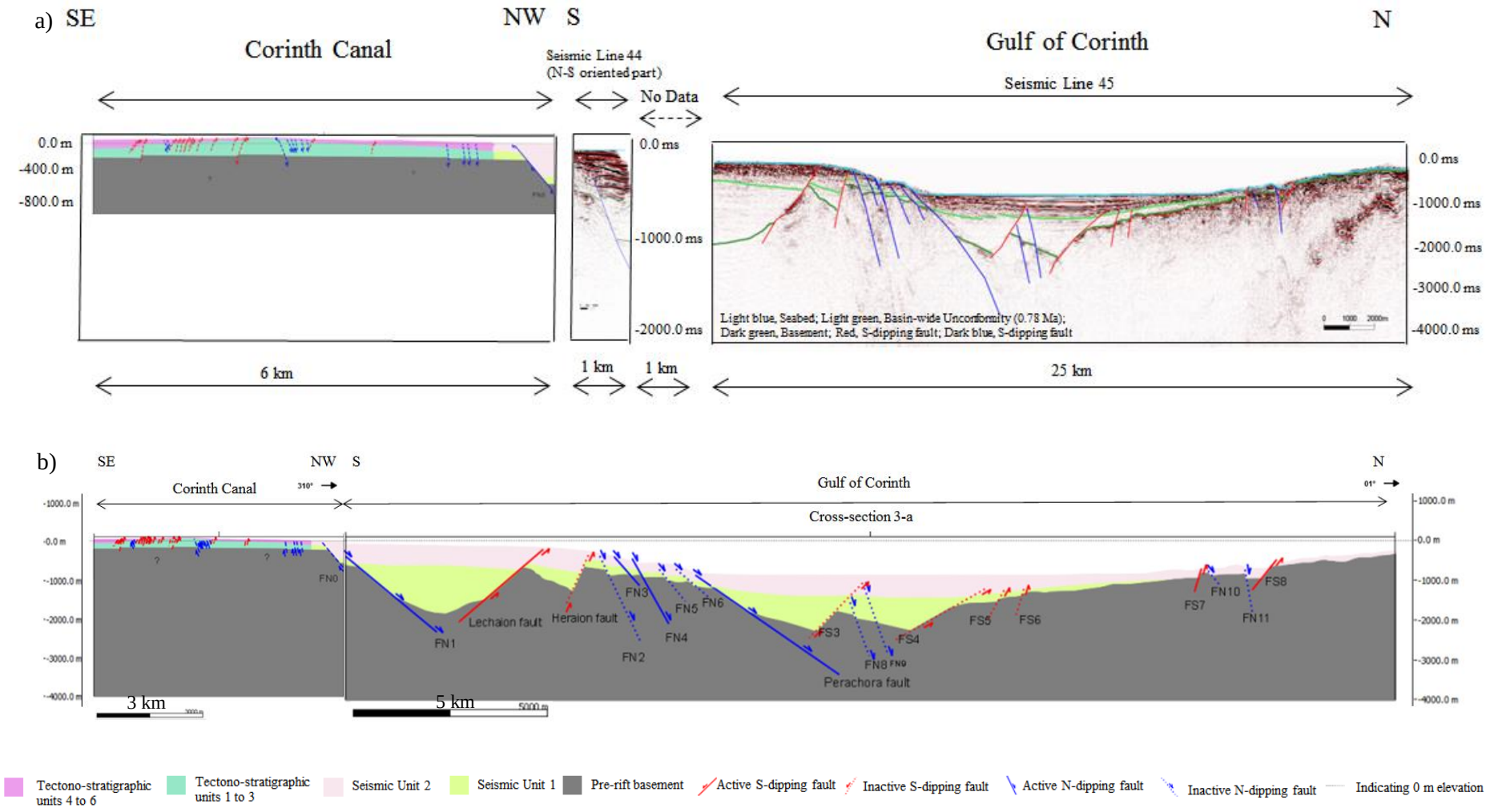

Figure 5.4 a) Cross-section 3 with original orientation of the section onshore and the Seismic lines 44 and 45 with interpretations. Note that the section at the northern Peloponnese margin is in m vertical extent and the seismic profile is in ms. This is illustrative and not to scale b) Cross-section 3-a, the seismic interpretation was converted to depth domain (m) and correlated to the onshore area. This section 3-a was further restored by two steps described in chapter 6. Note the two different scales. The scale (3 km) to the left is for the Corinth Canal section and the scale (5 km) to right is for the Gulf of Corinth section.

6. Restored sections

6.1 Cross-section 1

6.1.1 Cross-section 1-b

Cross-section 1-b was the first step of the restoration process going back in time form 1-a (described in chapter 5) (Fig. 6.1.b). The main differences between section 1-a and 1-b was that the topography of the Lower Group to the south of the Mamoussia fault was restored. The length of 1-b was 36 km and Seismic Unit 2 and the Upper Group deposits were restored. The East Heliki fault had a total heave of 332 m. In the hangingwall of the Mamoussia fault the Vouraikos delta was restored to a maximum thickness of 790 m and the maximum heave along the Kastillia fault was 333 m. The Vouraikos delta and the Derveni Formation truncates the underlying layers and the delta was laterally correlated basinward with Seismic Unit 1. Seismic Unit 1 was thickening towards the West Channel fault, and the Diakopto fault had an expansion index higher than one.

Based on these observations it can be inferred that section 1-b was shorter than section 1-a because the displacement along the East Heliki fault was restored, as well as the displacement along faults active during deposition of Seismic Unit 2. To the north of the active Mamoussia fault the depositional environment was lacustrine and in the footwall of the fault the area was continental. An angular unconformity separates the Vouraikos delta and the Derveni Formation from the Katafugion Formation and the Lower Group. The West Channel and Diakopto faults were active during this stage with larger displacement along the West Channel fault than the Diakopto fault.

6.1.2 Cross-section 1-c and 1-d

Cross-sections 1-c and 1-d were the two next steps in the restoration process after 1-b (Fig. 6.1.c,d). These sections were similar as the main separation was the presence of the Katafugion Formation in section 1-c. The length of the sections are 35 km and Seismic Unit 1 and the Upper Group deposits were restored. The total heave of the Mamoussia, West Channel and Diakopto faults were respectively 600 m, 332 m and 22 m. The Lower Group deposits were thickening towards the Kalavryta, Kerpini, Doumena and FS3 faults.

Based on these observations it can be inferred that the section was shorter than the previous due to displacement along the faults active during deposition of Seismic Unit 1 and the Upper Group. The active faults during this stage were the Kalavryta, Kerpini, Doumena and FS3 faults and the environmental setting was continental. There were no fault activity or deposits of sediments in the area north of the FS3 fault. It is likely that there were some accumulation of sedimentary deposits which were most probably eroded away or not visible in the present day seismic profile due to low resolution (Fig. 6.1.c,d).

6.1.3 Cross-section 1-e

Cross-section 1-e was the last step in the restoration process of cross-section 1. The difference from the previous two sections to this step was that there are no faults and the total length of the section was 32 km. The total heave of the Kalavryta, Kerpini, Doumena and FS3 faults were respectively 660 m, 833 m, 182 m and 788m. The topography of the pre-rift strata was not completely horizontal.

Based on these observations there were no active faults at this stage, and the displacement on the faults active during deposition of the Lower Group were restored resulting in a shorter section with an extension of 6 km from this section to section 1-a. The basement was exposed to erosion previous to the initiation of the faults the pre-rift topography had variating relief indicating that the faulting was induced on pre-existing topography (Fig. 6.1.e).

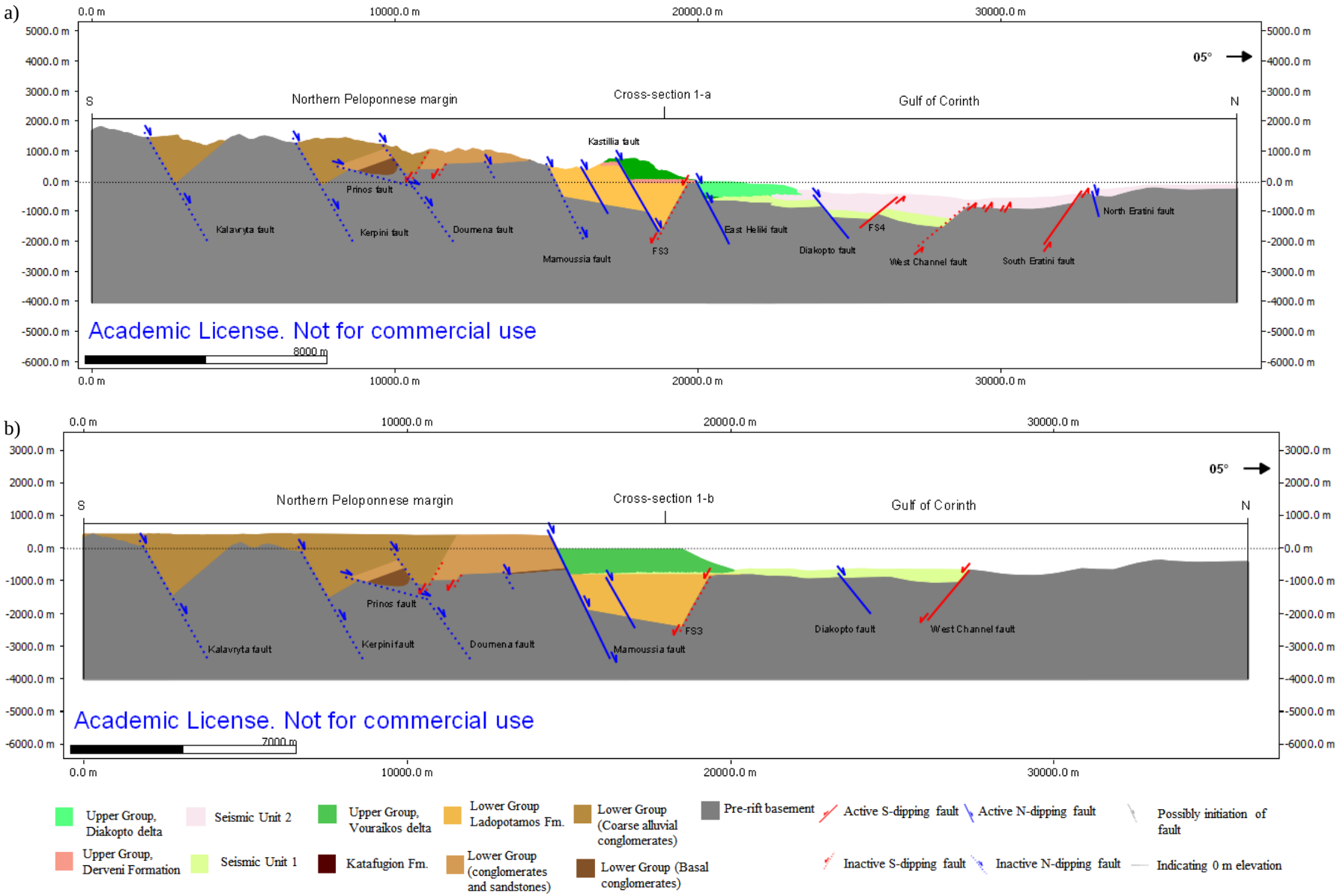
a)
0.0 m
10000.0 m
20000.0 m
30000.0 m
5000.0 m
4000.0 m
3000.0 m
2000.0 m
1000.0 m
0.0 m
-1000.0 m
-2000.0 m
-3000.0 m
-4000.0 m
-5000.0 m
-6000.0 m
05°
S
Northern Peloponnese margin
Cross-section 1-a
Gulf of Corinth
N
Kastillia fault
Prinos fault
Kalavryta fault
Kerpini fault
Doumena fault
Mamoussia fault
FS3
East Heliki fault
FS4
Diakopto fault
West Channel fault
South Eratini fault
North Eratini fault
Academic License. Not for commercial use
8000 m
b)
Northern Peloponnese margin
Cross-section 1-b
Gulf of Corinth
Prinos fault
Kalavryta fault
Kerpini fault
Doumena fault
Mamoussia fault
FS3
Diakopto fault
West Channel fault
Academic License. Not for commercial use
7000 m
Upper Group, Diakopto delta
Seismic Unit 2
Upper Group, Vouraikos delta
Lower Group Ladopotamos Fm.
Lower Group (Coarse alluvial conglomerates)
Pre-rift basement
Active S-dipping fault
Active N-dipping fault
Possibly initiation of fault
Upper Group, Derveni Formation
Seismic Unit 1
Katafugion Fm.
Lower Group (conglomerates and sandstones)
Lower Group (Basal conglomerates)
Inactive S-dipping fault
Inactive N-dipping fault
Indicating 0 m elevation

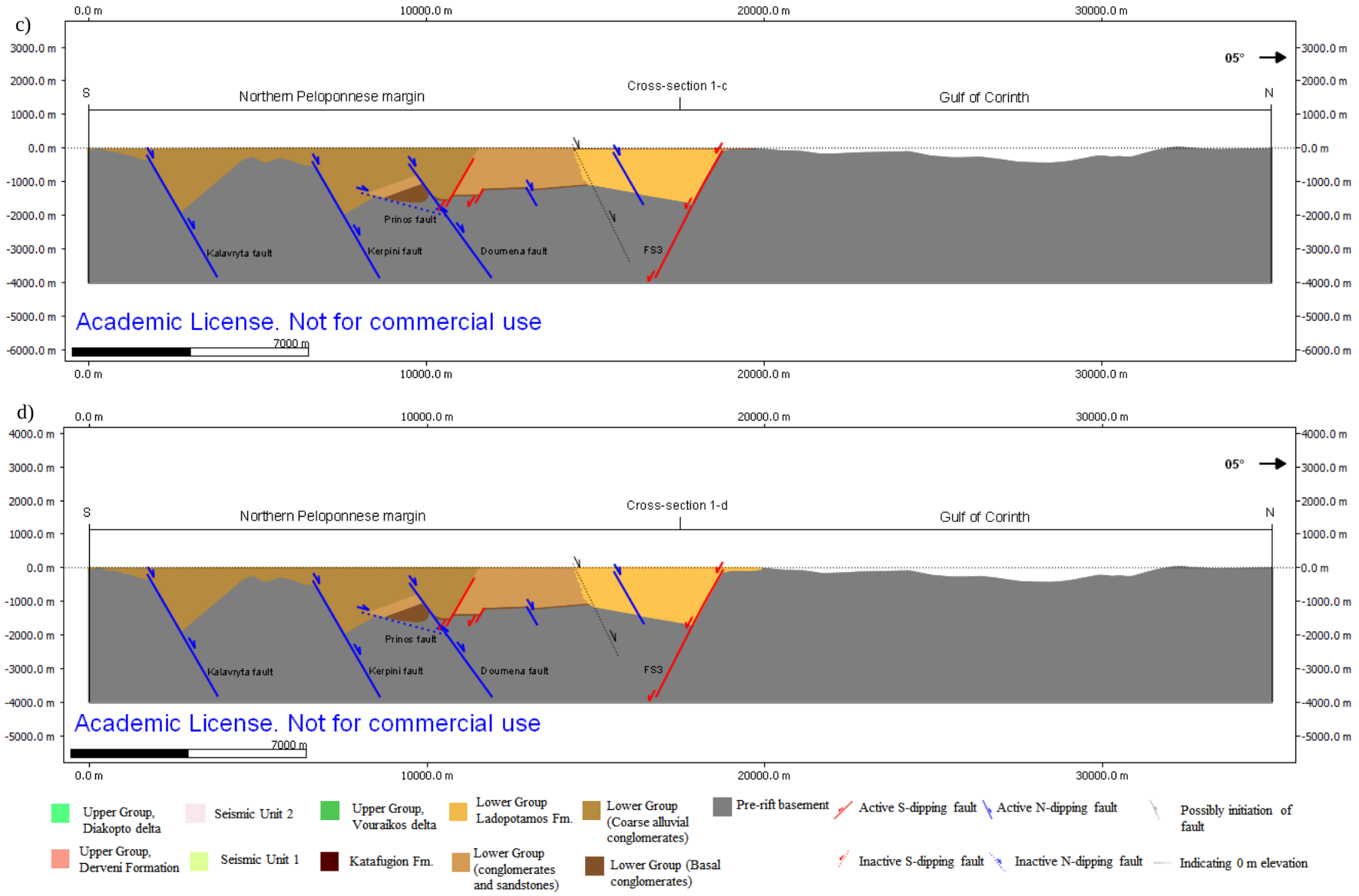
c)
0.0 m
10000.0 m
20000.0 m
30000.0 m
3000.0 m
2000.0 m
1000.0 m
0.0 m
-1000.0 m
-2000.0 m
-3000.0 m
-4000.0 m
-5000.0 m
-6000.0 m
05°
S
Northern Peloponnese margin
Cross-section 1-c
Gulf of Corinth
N
Prinos fault
Kalavryta fault
Kerpini fault
Doumena fault
FS3
Academic License. Not for commercial use
7000 m
d)
4000.0 m
3000.0 m
2000.0 m
1000.0 m
0.0 m
-1000.0 m
-2000.0 m
-3000.0 m
-4000.0 m
-5000.0 m
05°
S
Northern Peloponnese margin
Cross-section 1-d
Gulf of Corinth
N
Prinos fault
Kalavryta fault
Kerpini fault
Doumena fault
FS3
Academic License. Not for commercial use
7000 m
Upper Group, Diakopto delta
Seismic Unit 2
Upper Group, Vouraikos delta
Lower Group Ladopotamos Fm.
Lower Group (Coarse alluvial conglomerates)
Pre-rift basement
Active S-dipping fault
Active N-dipping fault
Possibly initiation of fault
Upper Group, Derveni Formation
Seismic Unit 1
Katafugion Fm.
Lower Group (conglomerates and sandstones)
Lower Group (Basal conglomerates)
Inactive S-dipping fault
Inactive N-dipping fault
Indicating 0 m elevation

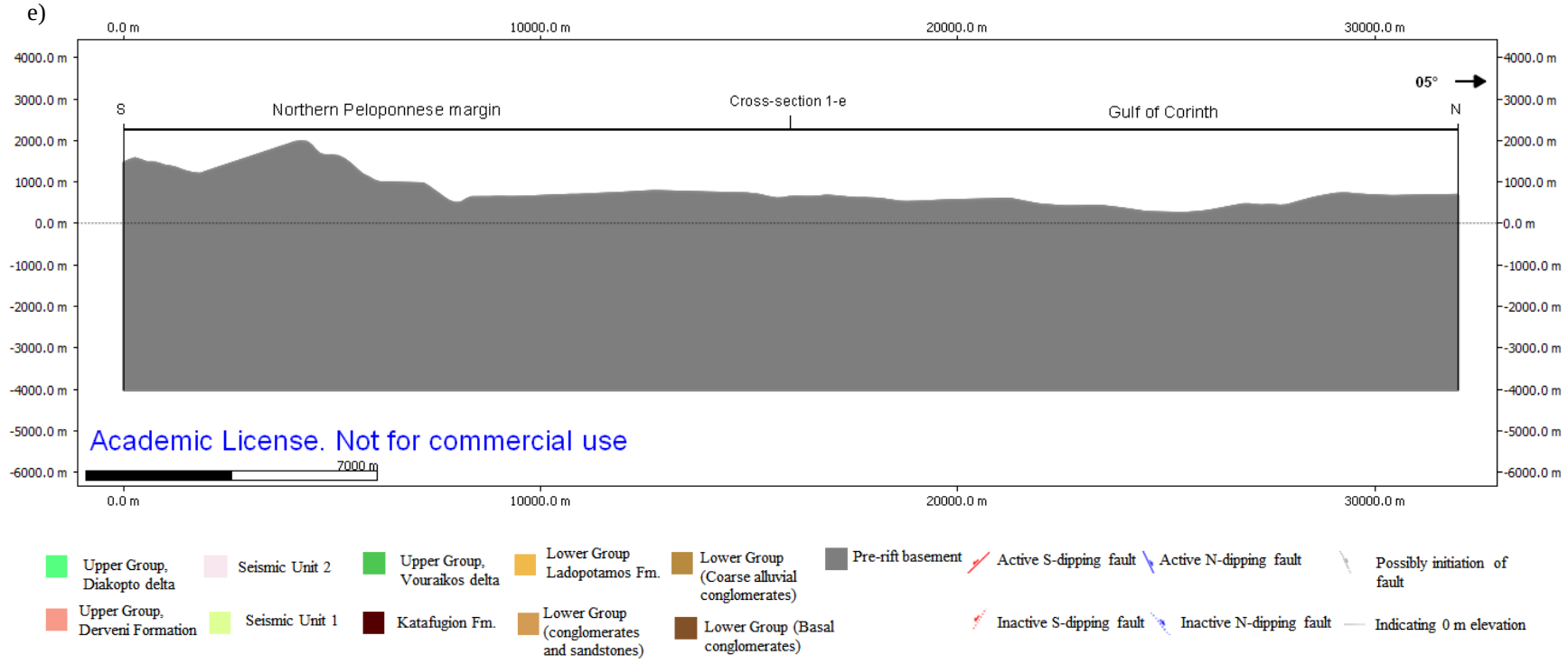

Figure 6.1. a) Cross-section 1-a represents present day. The Diakopto delta was correlated basinward to Seismic Unit 2 b) Cross-section 1-b represents the first step in the restoration process and the Vouraikos delta was restored as well as the topography of the Lower Group south of the Mamoussia fault. The Vouraikos delta was correlated basinward to Seismic Unit 1 The faults interpreted to be active after deposition of Seismic Unit 1 were restored c) Cross-section 1-c represents the second step in the restoration process. The faults active during deposition of Seismic Unit 1 and the Middle Group were restored. There were no deposits below Gulf of Corinth d) Cross-section 1-d is the third step in the restoration process and the Katafugion Formation was restored. There were no deposits below Gulf of Corinth e) Cross-section 1-e is the last step in the restoration process of cross-section 1 and represents the pre-deformed area.

6.2 Cross-section 2

6.2.1 Cross-section 2-b, 2-c

Cross-section 2-b was the first step of the restoration process going back in time form 2-a (described in chapter 5) (Fig. 6.2.b). Cross-section 2-b was 47.5 km long and similar to the previous section (2-a) with only the restored Old Corinth marine terrace that was laterally correlated basinward to horizon 1 as a differentiator. When moving to the next step of the process, one can observe that the main difference between cross-section 2-b and 2-c was that in 2-c the Kryoneri delta was restored and was laterally correlated basinward to Seismic Unit 1. The total length of cross-section 2-c was 47 km and Seismic Unit 1 was overall south thickening towards the N-dipping faults, except where the unit was also thickening towards the East Antikyra fault (Fig. 6.2.c). To the north in the section there are no sedimentary successions on top of the basement.

Based on these observations cross-section 2-b was 0.5 km shorter than section 2-a due to removal of displacement along the faults active after deposition of the Old Corinth marine terrace. Cross-section 2-c is 0.5 km shorter than section 2-b because the displacement along the faults that initiated after deposition of Seismic Unit 1 and during deposition of Seismic Unit 2 was restored. The Kryoneri delta was separated from the Rethi-Dendro Formation by an angular unconformity. The faults that were interpreted as active in these two sections were the faults located to the north of the East Xylokastro fault and the controlling faults of the basin were the S-dipping East Xylokastro, FN2 and Lykoporia faults. During deposition of Seismic Unit 1 the displacement along the S-dipping East Antikyra fault was almost as large as the displacement along the N-dipping Lykoporia fault. The northern part of the section might be a by-pass area for sediments or the strata was not possible to detect on the present day seismic profile.

6.2.2 Cross-section 2-d, 2-e, 2-f, 2-g

Cross-section 2-d was the next step in the restoration process and included in this sub-chapter is also the description of section 2-e, 2-f and 2-g as they are quite similar (Fig. 6.2.d). A similarity for all the four sections was that to the north of the Melissi fault there was not accumulated syn-rift strata and the top basement was approximately 180-900 m above lake-level (0 m). The fault blocks were rotated 20° from section 2-c to 2-d (Fig. 6.2.d). Cross-section 2-d had a total length of 46 km. The maximum thickness of the Kefalari delta was 1.7 km and the top Rethi-Dendro Formation was located 1.7-1.8 km below lake-level (0 m).

Cross-section 2-e differs from the previous 2-d section because the load of the Kefalari delta and the water column were restored (Fig. 6.2.e). The total length of this cross-section was 45.5 km and the heave of the Kefalari and Melissi faults at this stage were 633 m and 604 m, respectively. In cross-section 2-f the load of the Rethi-Dendro Formation was restored (Fig. 6.2.f). The total length of the section was 42 km and the heave of FN3, FN2, Kefalari and Melissi faults were 24 m, 54 m, 2.2 km, 2.3 km, respectively at this stage. In cross-section 2-g the load of the Ano Pitsa Formation was restored (Fig. 6.2.g). The total length of the section was 41.5 km and the heave of the Kefalari and Melissi faults at this stage were 233 m and 209 m, respectively.

Based on these observations it can be inferred that the Kefalari and Melissi faults were active at the same time and accumulated similar amount of displacement creating a symmetric graben geometry. These faults initiated approximately in section 2-g creating accommodation for the Korfiotissa Formation to be deposited and they were approximately active until the faults subsurface Gulf of Corinth initiated. The FN2 and FN3 faults initiated in section 2-e, during deposition of the Rethi-Dendro Formation. From cross-sections 2-g to 2-e there was an deepening upward trend and in section 2-d the Kefalari delta was deposited. The thickness of the delta could indicate that there were more than one delta cycle. Most likely the water depth in section 2-d was not representative of the water depth at this step and it would probably decrease if the Kefalari delta was not as simplified in the restoration process and the pro-delta deposits were included.

6.2.3 Cross-section 2-h

Cross-section 2-h was the last step of the restoration process for cross-section 2. The total length of the section was 41 km and the minimum heave of the Kefalari fault was 450 m and the for the Melissi fault it was 475 m at this stage (Fig. 6.2.h).

Based on these observations the section was shorter than the previous section because displacement along the faults active during deposition of the Korfiotissa Formation was restored and the total extension from this step to cross-section 2-a was 7 km. There was topography with variating relief existing before faulting initiated, suggesting that the Corinth Rift was induced on inherited relief.

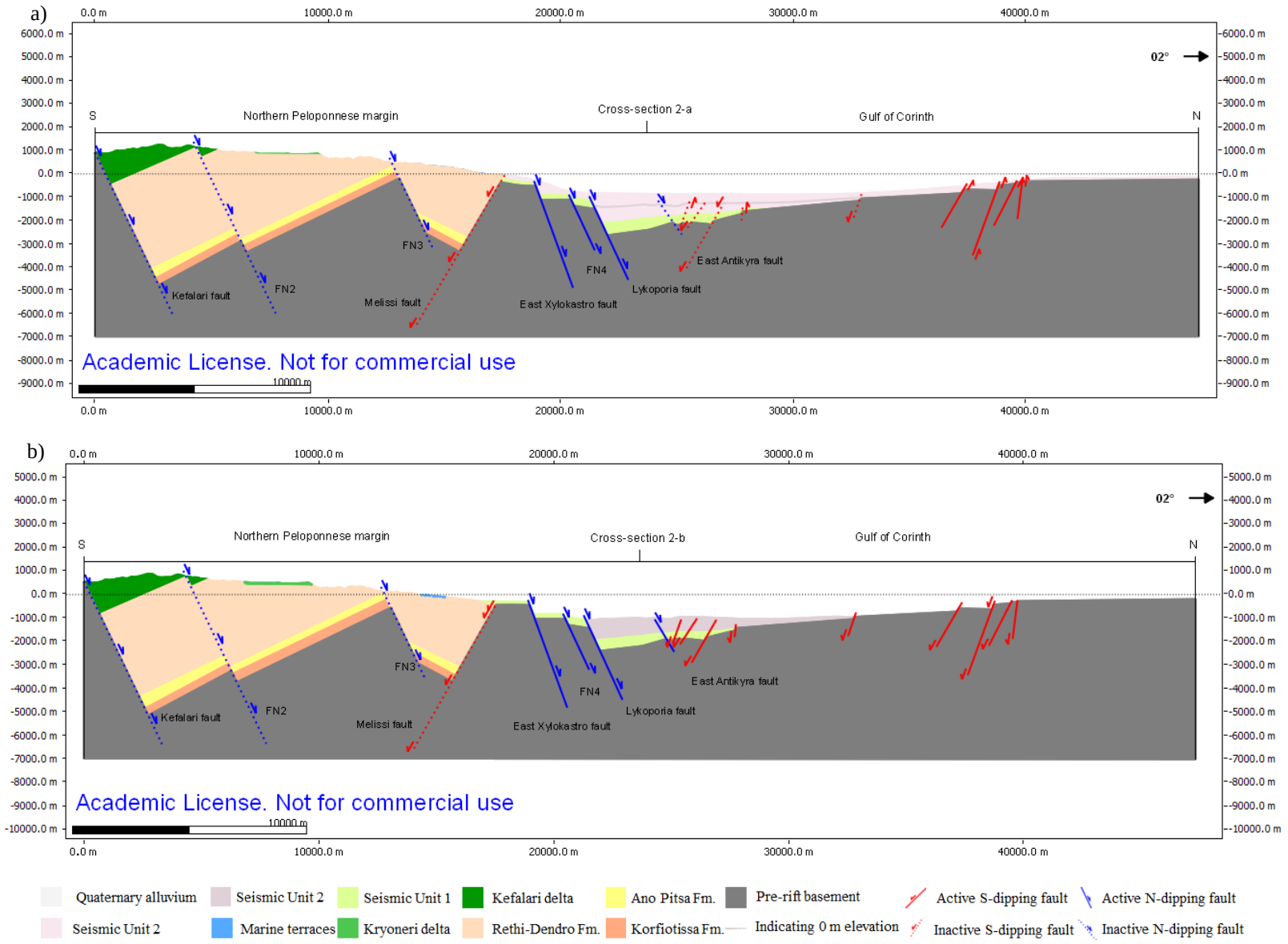
a)
0.0 m
10000.0 m
20000.0 m
30000.0 m
40000.0 m
6000.0 m
5000.0 m
4000.0 m
3000.0 m
2000.0 m
1000.0 m
0.0 m
-1000.0 m
-2000.0 m
-3000.0 m
-4000.0 m
-5000.0 m
-6000.0 m
-7000.0 m
-8000.0 m
-9000.0 m
02°
S
Northern Peloponnese margin
Cross-section 2-a
Gulf of Corinth
N
FN3
FN4
East Antikyra fault
Kefalari fault
FN2
Melissi fault
East Xylokastro fault
Lykoporia fault
Academic License. Not for commercial use
10000 m
b)
5000.0 m
4000.0 m
3000.0 m
2000.0 m
1000.0 m
0.0 m
-1000.0 m
-2000.0 m
-3000.0 m
-4000.0 m
-5000.0 m
-6000.0 m
-7000.0 m
-8000.0 m
-9000.0 m
-10000.0 m
02°
S
Northern Peloponnese margin
Cross-section 2-b
Gulf of Corinth
N
FN3
FN4
East Antikyra fault
Kefalari fault
FN2
Melissi fault
East Xylokastro fault
Lykoporia fault
Academic License. Not for commercial use
10000 m
Quaternary alluvium
Seismic Unit 2
Seismic Unit 2
Seismic Unit 1
Marine terraces
Kryoneri delta
Kefalari delta
Rethi-Dendro Fm.
Ano Pitsa Fm.
Korfiotissa Fm.
Pre-rift basement
Indicating 0 m elevation
Active S-dipping fault
Inactive S-dipping fault
Active N-dipping fault
Inactive N-dipping fault

c)

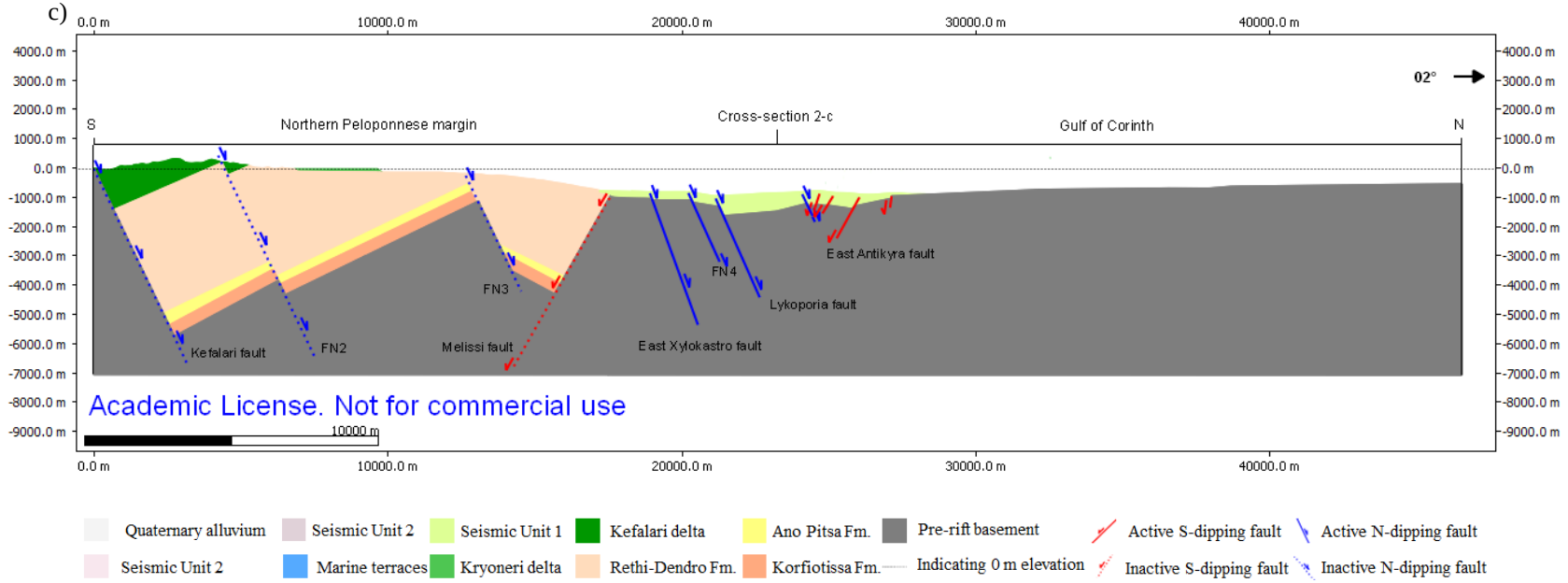
0.0 m
10000.0 m
20000.0 m
30000.0 m
40000.0 m
4000.0 m
3000.0 m
2000.0 m
1000.0 m
0.0 m
-1000.0 m
-2000.0 m
-3000.0 m
-4000.0 m
-5000.0 m
-6000.0 m
-7000.0 m
-8000.0 m
-9000.0 m
02°
S
Northern Peloponnese margin
Cross-section 2-c
Gulf of Corinth
N
Kefalari fault
FN2
Melissi fault
FN3
East Xylokastro fault
FN4
Lykoporia fault
East Antikyra fault
Academic License. Not for commercial use
10000 m
Quaternary alluvium
Seismic Unit 2
Seismic Unit 2
Marine terraces
Seismic Unit 1
Kryoneri delta
Kefalari delta
Rethi-Dendro Fm.
Ano Pitsa Fm.
Korfiotissa Fm.
Pre-rift basement
Indicating 0 m elevation
Active S-dipping fault
Inactive S-dipping fault
Active N-dipping fault
Inactive N-dipping fault

d)

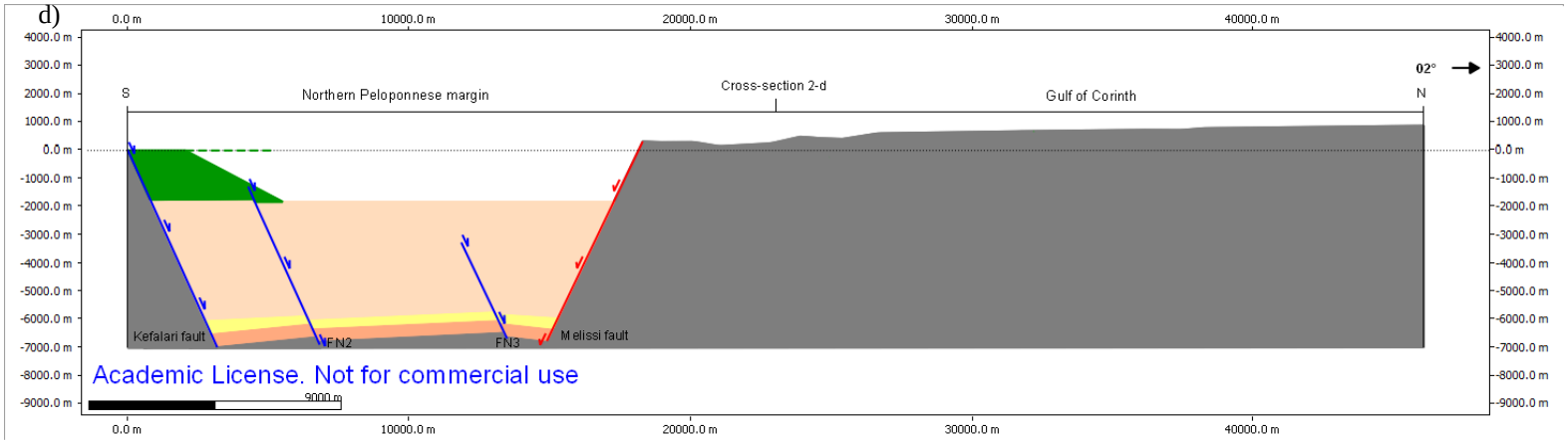
0.0 m
10000.0 m
20000.0 m
30000.0 m
40000.0 m
4000.0 m
3000.0 m
2000.0 m
1000.0 m
0.0 m
-1000.0 m
-2000.0 m
-3000.0 m
-4000.0 m
-5000.0 m
-6000.0 m
-7000.0 m
-8000.0 m
-9000.0 m
S
Northern Peloponnese margin
Cross-section 2-d
Gulf of Corinth
N
02°
Kefalari fault
FN2
FN3
Melissi fault
Academic License. Not for commercial use
9000 m

e)

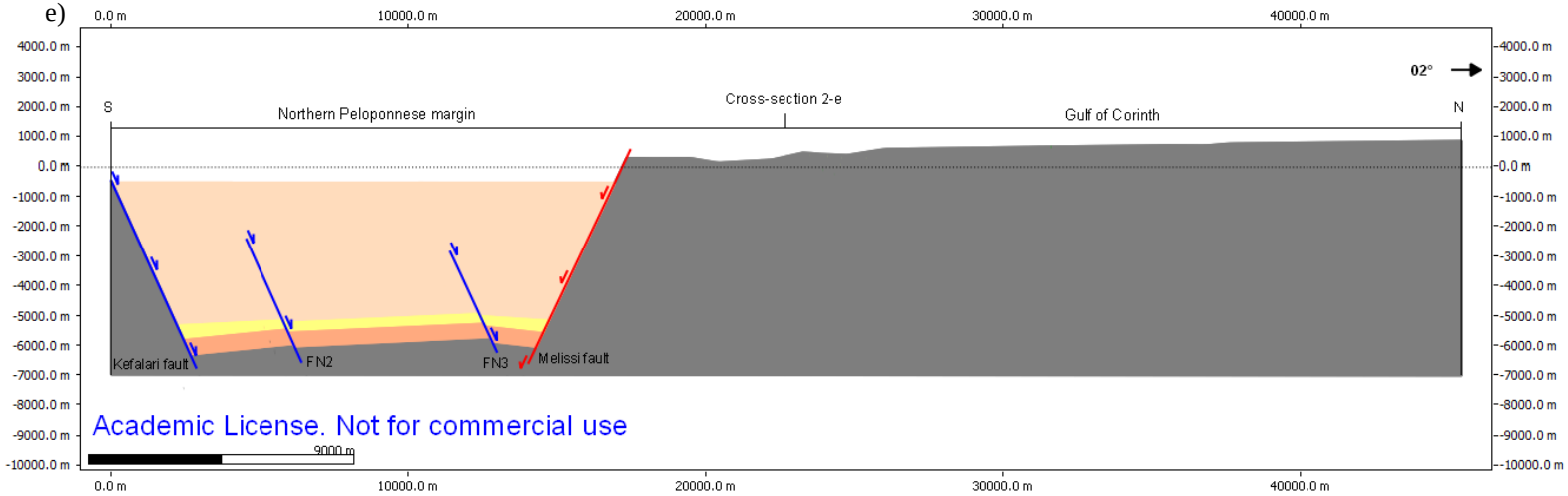
0.0 m
10000.0 m
20000.0 m
30000.0 m
40000.0 m
4000.0 m
3000.0 m
2000.0 m
1000.0 m
0.0 m
-1000.0 m
-2000.0 m
-3000.0 m
-4000.0 m
-5000.0 m
-6000.0 m
-7000.0 m
-8000.0 m
-9000.0 m
-10000.0 m
S
Northern Peloponnese margin
Cross-section 2-e
Gulf of Corinth
N
02°
Kefalari fault
FN2
FN3
Melissi fault
Academic License. Not for commercial use
9000 m

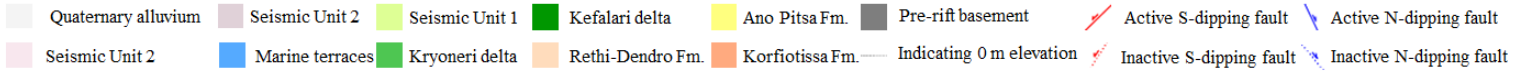
Quaternary alluvium
Seismic Unit 2
Seismic Unit 2
Seismic Unit 1
Kefalari delta
Ano Pitsa Fm.
Pre-rift basement
Active S-dipping fault
Active N-dipping fault
Marine terraces
Kryoneri delta
Rethi-Dendro Fm.
Korfiotissa Fm.
Indicating 0 m elevation
Inactive S-dipping fault
Inactive N-dipping fault

f)

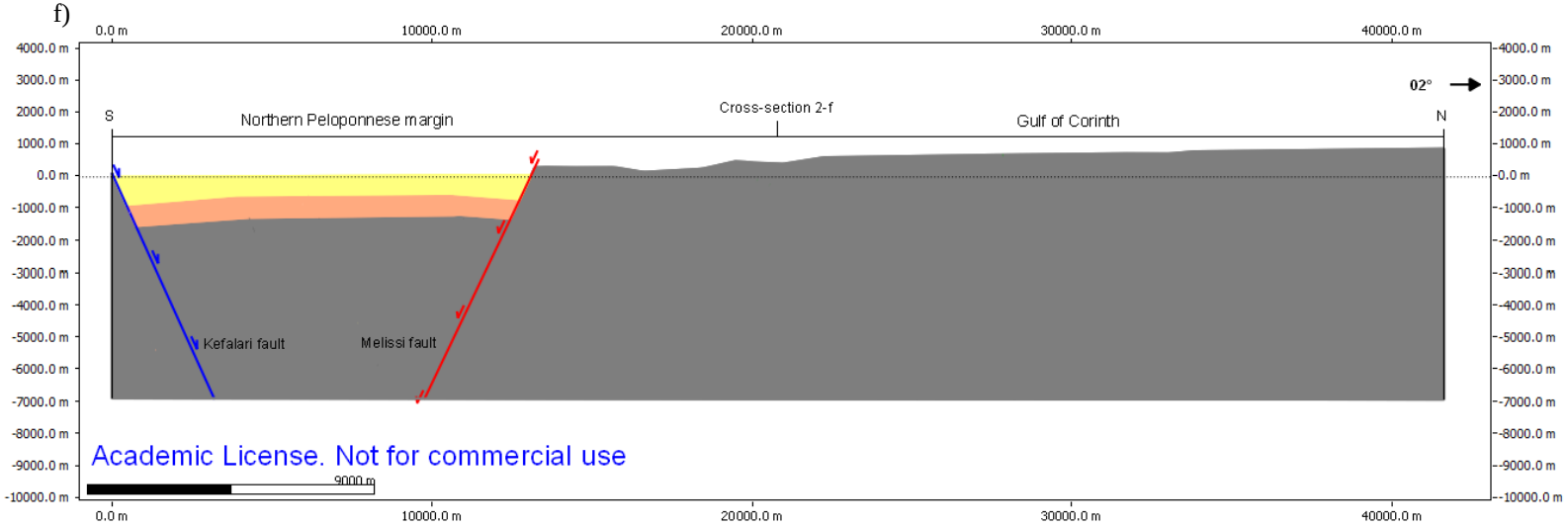
0.0 m
10000.0 m
20000.0 m
30000.0 m
40000.0 m
4000.0 m
3000.0 m
2000.0 m
1000.0 m
0.0 m
-1000.0 m
-2000.0 m
-3000.0 m
-4000.0 m
-5000.0 m
-6000.0 m
-7000.0 m
-8000.0 m
-9000.0 m
-10000.0 m
02°
S
Northern Peloponnese margin
Cross-section 2-f
Gulf of Corinth
N
Kefalari fault
Melissi fault
Academic License. Not for commercial use
9000 m

g)

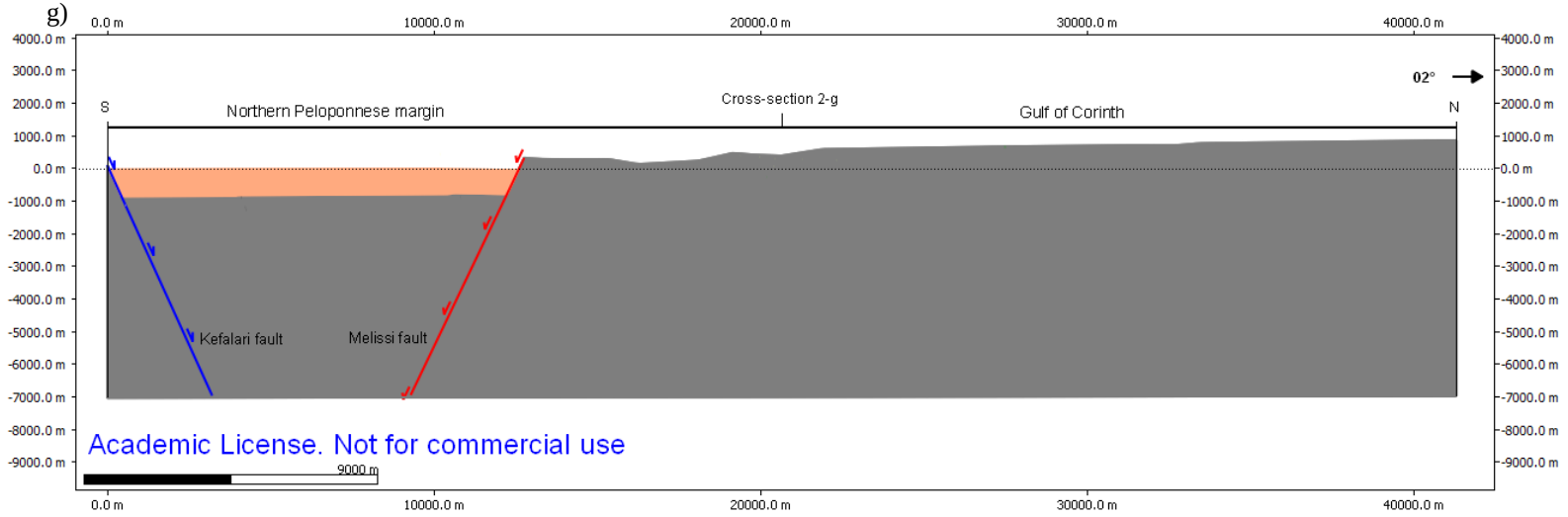
0.0 m
10000.0 m
20000.0 m
30000.0 m
40000.0 m
4000.0 m
3000.0 m
2000.0 m
1000.0 m
0.0 m
-1000.0 m
-2000.0 m
-3000.0 m
-4000.0 m
-5000.0 m
-6000.0 m
-7000.0 m
-8000.0 m
-9000.0 m
02°
S
Northern Peloponnese margin
Cross-section 2-g
Gulf of Corinth
N
Kefalari fault
Melissi fault
Academic License. Not for commercial use
9000 m

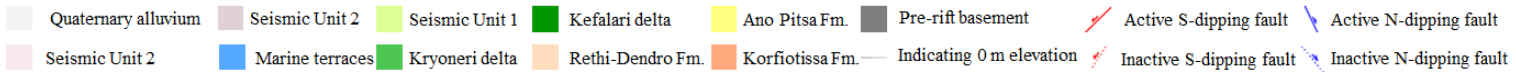
Quaternary alluvium
Seismic Unit 2
Seismic Unit 1
Kefalari delta
Ano Pitsa Fm.
Pre-rift basement
Active S-dipping fault
Active N-dipping fault
Seismic Unit 2
Marine terraces
Kryoneri delta
Rethi-Dendro Fm.
Korfiotissa Fm.
Indicating 0 m elevation
Inactive S-dipping fault
Inactive N-dipping fault

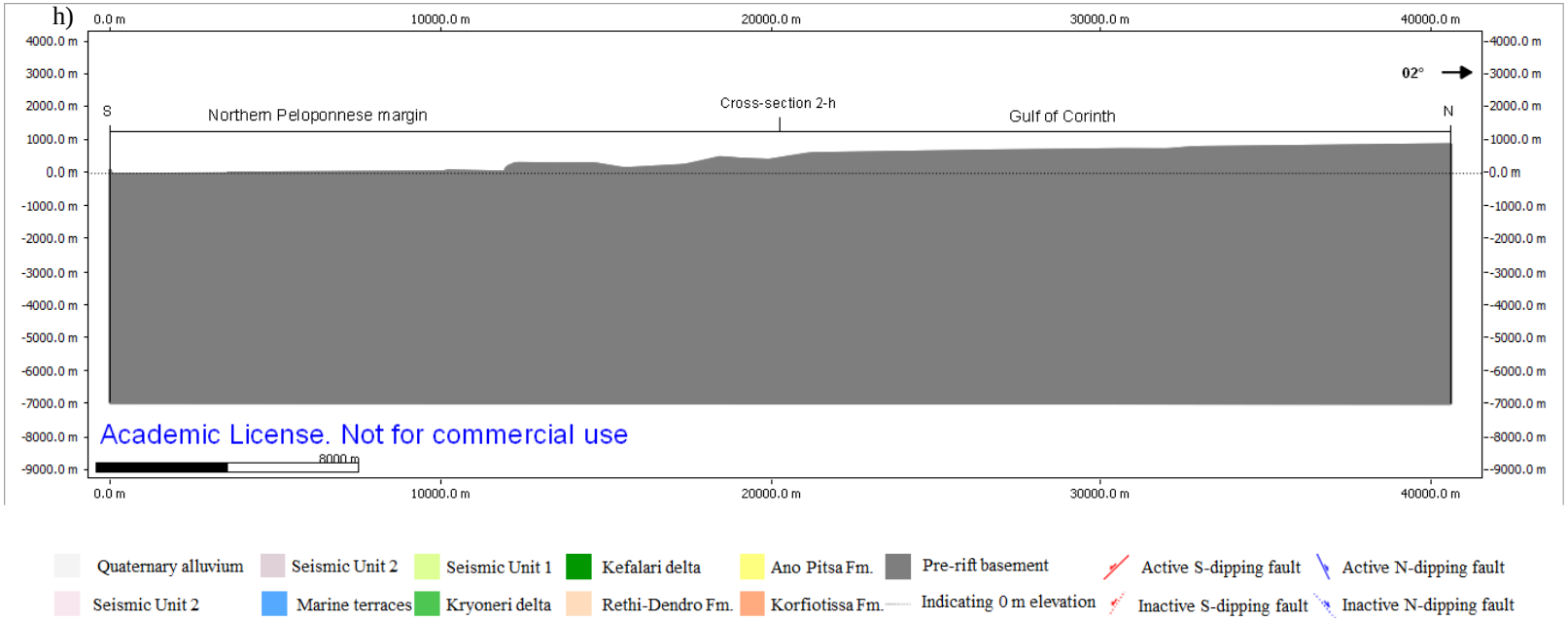

Figure 6.2 a) Cross-section 2-a represents the present day b) Cross-section 2-b is the first step in the restoration process and the Old Corinth marine terrace was correlated to horizon 1 (Seismic Unit 2) c) Cross-section 2-c is the second step in the restoration process. The displacement along the faults that were active after deposition of Seismic Unit 1 were restored and the Kryoneri delta was correlated basinward with Seismic Unit 1 d) Cross-section 2-d is the third step in the restoration process and the displacement along the faults active during deposition of Seismic Unit 1 was restored and the Kefalari delta was restored. There are no deposits below Gulf of Corinth e) Cross-section 2-e is the fourth step in the restoration process. The load of the Kefalari delta was restored and the Rethi-Dendro Fm. was restored to its original dip and position. There were no deposits below Gulf of Corinth f) Cross-section 2-f is the fifth step in the restoration process. The load of the Rethi-Dendro Fm. was restored and the Ano Pitsa Fm. was restored to its original dip and position. There were no deposits below Gulf of Corinth g) Cross-section 2-g is the sixth step in the restoration process and the load of the Ano Pitsa Fm. was restored and the Korfiotissa Fm. was restored to its original dip and position. There were no deposits below Gulf of Corinth h) Cross-section 2-h is the last step in the restoration process of cross-section 2 and represents the pre-deformed state.

6.3 Cross-section 3

6.3.1 Cross-section 3-b

Cross-section 3-b is the first step of the restoration process going back in time from 3-a (described in chapter 4) (Fig. 6.3.b). The main difference between section 3-a and 3-b is that the length of 3-b is 32.5 km and Seismic Unit 2 was restored. The expansion indices were higher than one for the faults subsurface Gulf of Corinth and Seismic Unit 1 thickens towards the S-dipping faults. In the Corinth Canal there are no faults and the tectono-stratigraphic units 4 to 6 were restored (Appendix II Close up of the Corinth Canal).

Based on these observations it could be inferred that section 3-b is shorter than section 3-a because the displacement along the faults active during deposition of Seismic Unit 2 were restored. The faults observed in the section were active during deposition of Seismic Unit 1 and the S-dipping faults were interpreted to have been the controlling faults of the basin subsurface Gulf of Corinth. There were no active faults in the Corinth Canal at this stage and the tectono-stratigraphic units 4 to 6 was not yet deposited and the depositional environment in rift was lacustrine.

6.3.2 Cross-section 3-c

Cross-section 3-c is the last step in the restoration process of cross-section 3 (Fig. 6.3.c). The difference from sections 3-a and 3-b is that the deposits of Seismic Unit 1 were restored and the total length of the section is 32 km. The heave of the faults that were active during deposition of Seismic Unit 1 ranges from 140 to 940 m. The top basement was not completely horizontal.

Based on these observations section 3-c is shorter than the previous section due to removal of the displacement of the faults active during deposition of Seismic Unit 1. There were no active faults during this stage and the variating relief of the basement is suggesting existing topography before the faulting initiated. The total extension from this step to cross-section 3-a is 5 km and this is calculated based on the projection of the Corinth Canal section to the N-S oriented Gulf of Corinth section.

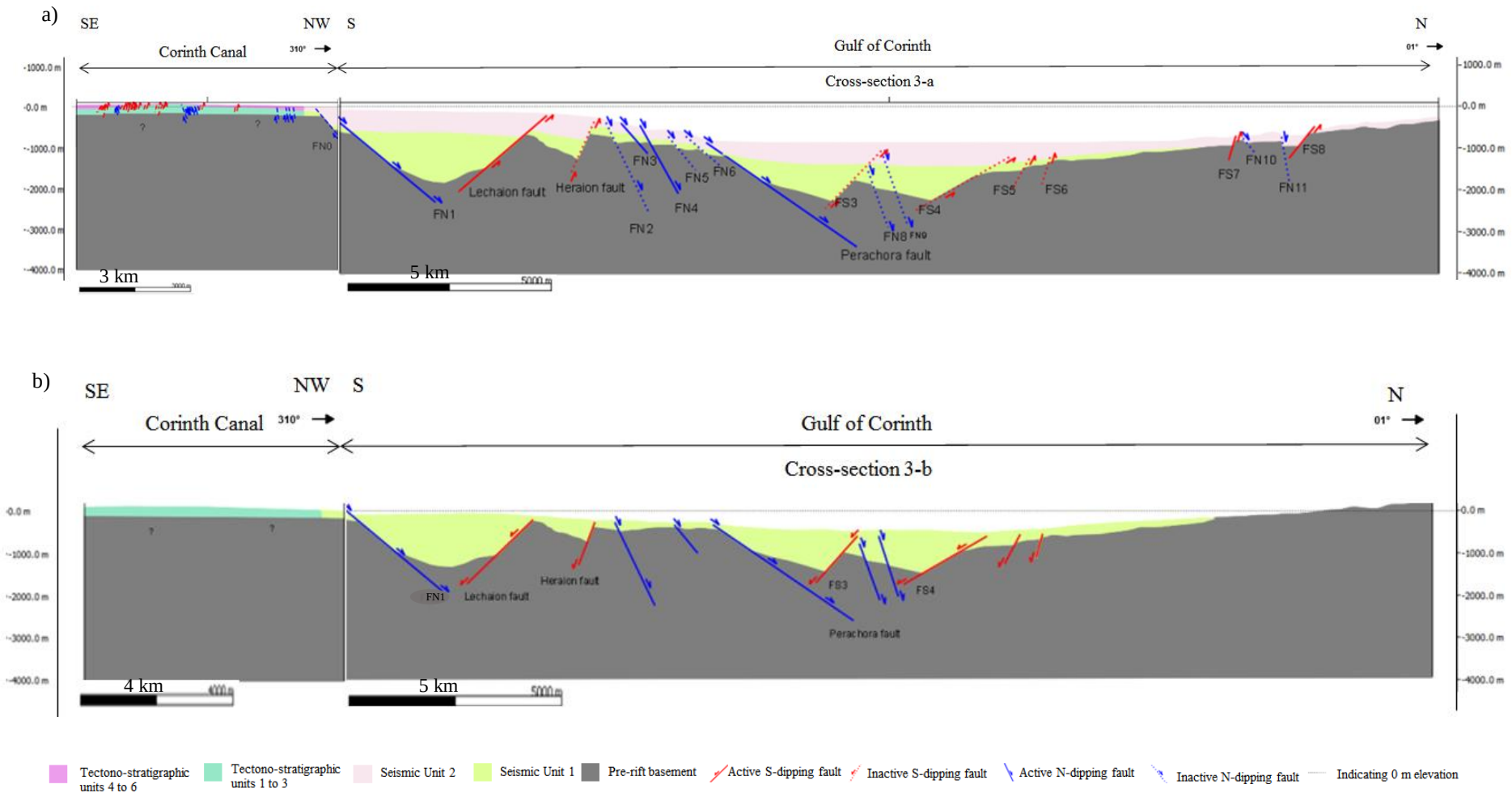
a)
SE
NW
S
N
Corinth Canal
310°
Gulf of Corinth
01°
Cross-section 3-a
FN0
FN1
Lechaion fault
Heraion fault
FN2
FN3
FN4
FN5
FN6
FS3
FS4
FS5
FS6
FN8
FN9
Perachora fault
FS7
FN10
FS8
FN11
3 km
5 km
b)
SE
NW
S
N
Corinth Canal
310°
Gulf of Corinth
01°
Cross-section 3-b
FN1
Lechaion fault
Heraion fault
FS3
FS4
Perachora fault
4 km
5 km
Tectono-stratigraphic units 4 to 6
Tectono-stratigraphic units 1 to 3
Seismic Unit 2
Seismic Unit 1
Pre-rift basement
Active S-dipping fault
Inactive S-dipping fault
Active N-dipping fault
Inactive N-dipping fault
Indicating 0 m elevation

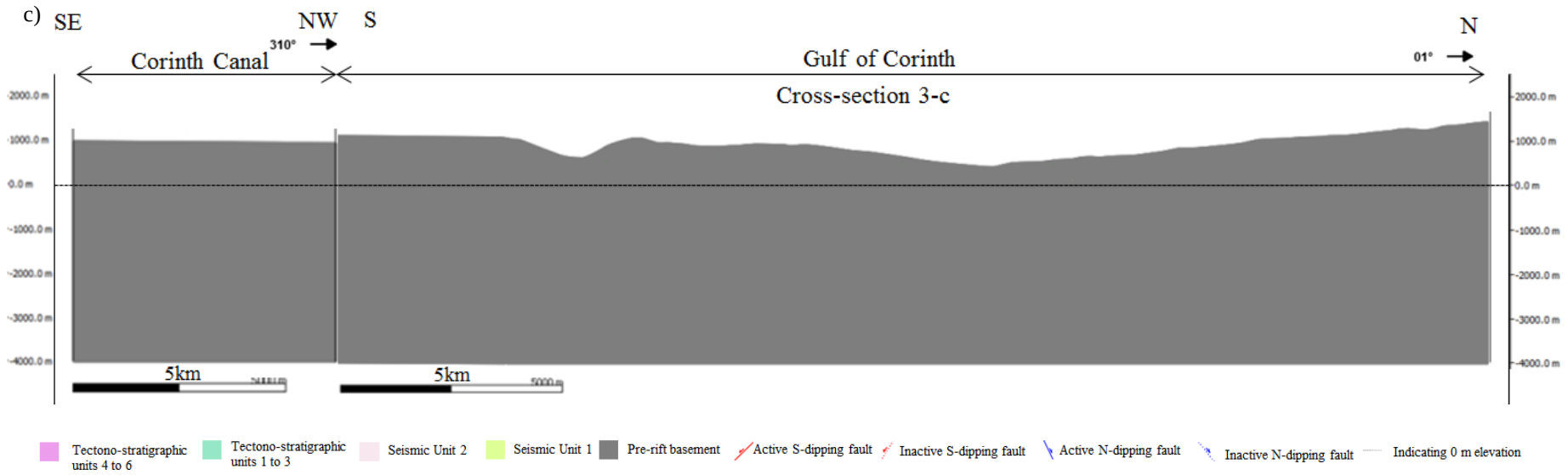

Figure 6.3 a) Cross-section 3-a represents the present day section. The tectono-stratigraphic units 4 to 6 were correlated basinward to Seismic Unit 2 b) Cross-section 3-b is the first step in the restoration process and the load of Seismic Unit 2 as well as tectono-stratigraphic units 4 to 6 were restored. The displacement along the faults active during deposition of these units were also restored. The tectono-stratigraphic units 1 to 3 were correlated basinward to Seismic Unit 1 c) Cross-section 3-c is the last step in the restoration process of cross-section 3 and represent the pre-deformed state. Seismic Unit 1 and tectono-stratigraphic units 1 to 3 were restored, as well as the displacement along the faults active during deposition of Seismic Unit 1.

6.4 Main differences detected between the three cross-sections

The total extension varies along the rift axis. The total extension of cross-section 1 was 6 km, for cross-section 2 it was 7 km and for cross-section 3 the total extension was 5 km (Table 3). The depositional environment also changed along strike and in the western area of the northern Peloponnese margin the rift initially established a continental environment with alluvial and fluvial deposits (Fig. 6.1.c). In the central area the rift basin was dominated by lacustrine deposits. During initiation of faulting the Corinth Rift was overfilled in the western area, and underfilled in the central and eastern areas (Fig.6.1.c, 6.2.d). Later, a northwards shift in fault activity occurred both in the western and central areas (cross-section 1 and 2). Gilbert-type deltas were deposited laterally and continuous basinwards to Seismic Unit 1 (Fig.6.1.b, 6.2.c). The Corinth Rift was at this stage characterized by lacustrine deposits. As faulting continued at the southern margin of the Gulf of Corinth, the northern Peloponnese margin was progressively uplifted (Gawthorpe et al., 2018). In cross-section 1 the East Heliki fault initiated at this stage and in cross-section 2, the activity along the East Xylokastro, FN2 and Lykoporia faults continued (Fig. 6.1.a, 6.2.a,b). There was also a northward shift in activity of the S-dipping faults from the East Antikyra and West Channel faults to the faults on the northern margin of the Gulf of Corinth (Fig. 6.2.b). Present day the N-dipping faults on the southern margin of the Gulf of Corinth are the dominant faults, i.e. the faults with the largest accumulated displacement (Fig. 6.1.a, 6.2.a, 6.3.a). These faults are creating a southern border fault system and an asymmetric graben geometry of the basin in the Gulf of Corinth (Nixon et al., 2016).

Table 3. The total extension for cross-section 1, 2 and 3 derived from the restoration process. Cross-section 2 has the largest extension, of 7 km, compared to cross-section 1 (6 km extension) and cross-section 3 (5 km extension). The extension of the cross-sections were calculated based on the N-S projections of the sections at the northern Peloponnese margin.

Length (km)	Cross-section 1	Cross-section 2	Cross-section 3
Deformed	38	48	31
Pre-deformed	32	41	26
Total extension	6	7	5

7. Discussion

7.1 Correlation of the onshore and offshore area

The integration of the onshore and offshore areas was undertaken using the Move Midland Valley software. The available data was merged to construct three N-S cross-sections (west, central and east). The main limitation for the correlation of these two areas was the lack of data and age constraints. There were no seismic lines available from the onshore area and the offshore seismic lines end 0.5 to 2 km from shore. In addition there was very little offshore core data. The uncertainty of the age was a limitation and better constraint on stratigraphic ages would further improve the correlation of the onshore and offshore areas. The rift, being lacustrine, creates uncertainty around lake-level at the time of deposition of the strata.

The main results from the correlation of the northern Peloponnese margin to the Gulf of Corinth were that different formations and units were laterally and continuous basinward and were time equivalent. The Lower Group does not exist below the Gulf. The Vouraikos delta and the Derveni Formation was laterally correlated with Seismic Unit 1 and the Upper Group, Diakopto delta, was laterally correlated with Seismic Unit 2 (Fig.6.1.b,c). This agrees with previous research (Ford et al., 2013; 2017). The Kefalari delta and the older syn-rift successions in the central area were restricted to the northern Peloponnese margin. The Kryoneri delta was correlated to Seismic Unit 1 and the marine terraces were correlated to the marine stages in Seismic Unit 2 (Fig.6.2.b,c) (Gawthorpe et al., 2018). In the Corinth Canal the lacustrine deposits below surface S4 were correlated with Seismic Unit 1 and the marine deposits above S4 were correlated with Seismic Unit 2 (Fig.6.3.a,b) (Meling, 2016; Sletten, 2016).

This integration contributes to knowledge and better understanding of the Corinth Rift as it provides a possible model of the rift evolution. The proposed tectono-stratigraphic evolution based on the results of the integration of the onshore and offshore areas is discussed below and compared to previous research (e.g. Ford et al., 2013; 2017; Nixon et al., 2016; Gawthorpe et al., 2017; 2018).

7.2 Tectono-stratigraphic evolution of the Corinth Rift

The tectono-stratigraphic evolution presented in this thesis is the result of the structural and stratigraphic analysis described in chapters 5 and 6. The temporal evolution has been divided into three main syn-rift stages, syn-rift stage 1, 2 and 3, based on main events detected in the restoration process. The three stages are discussed below.

7.2.1 Syn-rift stage 1

During syn-rift stage 1 the first sign of fault displacement was observed in the cross-sections and both N- and S-dipping faults were active and the basin acquired a graben geometry. The syn-rift stage 1 corresponds to cross-sections 1-c, 1-d, 2-d, 2-e, 2-f and 2-g (Fig. 6.1.c,d and Fig. 2.d,e,f,g). From the restoration process no record of the syn-rift stage 1 was present in the Corinth Canal. The area before the rift initiation is shown by cross-sections 1-e, 2-h and 3-c, and represents the state of the sections pre-rifting (Fig. 6.1.e, Fig. 6.2.h and Fig.3.c). The length of these sections was respectively 32 km, 41 km and 26 km.

During syn-rift stage 1 the fault displacement initiated on the northern Peloponnese margin and major faults such as the Kalavryta, Kerpini, Doumena and FS3 faults were the first to initiate in the western area. In the central area, shown by cross-section 2-d, 2-e, 2-f, 2-g, the Kefalari and Melissi faults were the first to initiate and the two faults had similar displacement creating a graben geometry of the rift basin (Fig. 6.2.g). Later in syn-rift stage 1, the FN2 and FN3 faults became active in the central area (cross-section 2-d, 2-e) and the Kefalari and Melissi faults were still active in the late stage of syn-rift stage 1. This was interpreted as the fault blocks rotated approximately 20° before the activity decreased and there was a change in fault activity towards the initiation of syn-rift stage 2. The successions deposited during syn-rift stage 1 are the oldest syn-rift sequences in the rift evolution with an overall estimated age of approximately 5-1.8 Ma (Ford et al., 2013; 2017; Gawthorpe et al., 2017; 2018). These deposits are characterized by the alluvial to fluvial Lower Group to the west and the Korfiotissa Formation, Ano Pitsa Formation, Rethi-Dendro Formation and the Kefalari delta in the central area of the northern Peloponnese margin (Fig.7.1) (Ford et al., 2013; 2017; Gawthorpe et al., 2017; 2018). These deposits suggest what type of environment occurred in the rift at the time of syn-rift stage 1. In the western area rivers with high sediment supply were the dominant sedimentary systems (Ford et al., 2013; 2017) and to the north of the Lower Group in cross-section 1-c and 1-d the basement was below lake-level (0

m) and most likely there would have existed a shallow lacustrine environment here (Fig.7.1). There was no evidence of sediments deposited at this area during syn-rift stage 1. If there was deposition of sediments in this area at this stage, they were not preserved or not possible to detect on the present day seismic profiles due to low resolution (Bell et al., 2008; Ford et al., 2013; Nixon et al., 2016). The rivers that deposited the Lower Group were flowing towards the east and therefore the rivers did not reach the northern part of cross-sections 1-c and 1-d to deposit sedimentary successions corresponding to the Lower Group (Fig.7.1.a,b) (Rohais et al., 2007b; Ford et al., 2013; Gawthorpe et al., 2018). At approximately the same time in the central area sediments were deposited in a deep lacustrine environment, which is characterized as the Rethi-Dendro Formation. The Kefalari delta was also deposited at the end of this stage (Fig.7.1.a,c) (Gawthorpe et al., 2017; 2018). It was detected from the restoration process that the Kefalari delta was 1.7 km thick. From previous research it is stated that the deltas at the northern Peloponnese margin prograded into waters of 300-600 m depth (Gawthorpe et al., 2017; 2018) and the current level of exposure of the Kefalari delta does not allow to identification of internal units within it. Based the previous, it was interpreted that the 1.7 km Kefalari delta succession was composed of more than only one delta cycle.

Based on the results from the restoration process combined with previous research (Ford et al., 2013; 2017; Nixon et al., 2016; Gawthorpe et al., 2017; 2018) the syn-rift stage 1 experienced deepening of the rift basin in the central area (Fig.7.1.a,c). There was not detected faulting activity and sedimentary successions in the eastern area at this stage. Previous research (e.g. Nixon et al., 2016; Gawthorpe et al., 2018) have proposed that the N-dipping Nemea and Kechreai faults and the S-dipping Lecahion fault was the border faults of the rift system and that the environment of the rift basin was lacustrine (Collier, 1990; Collier and Dart, 1991; Nixon et al., 2016; Gawthorpe et al., 2018). In the late syn-rift stage 1 there was a transgression in the western area in cross-section 1-c and the Katafugion Formation was deposited. This transgression is not well constrained due to an erosional event following the transgression that is currently described as a conundrum (e.g. Ford et al., 2013; 2017; Gawthorpe et al., 2017; 2018). The rift experienced deepening of the basin in the east and central areas in the earlier stages and this is consistent with previous interpretations of the early rift being closed to the west (Ford et al., 2013; 2017).

The syn-rift stage 1 was compared to rift phase 1 (age 5.0-3.6 Ma to 2.2-1.8 Ma) defined by Gawthorpe et al. (2018) as they both have in common that the faulting initiated at the northern Peloponnese margin with fault blocks 3-8 km wide and the geometry of the rift was similar to a graben structure (Fig.7.1) (Gawthorpe et al., 2018). The Lower Group in the western area (age 5 Ma to 1.8 Ma), as defined by Ford et al. (2013), does have some similarities with syn-rift stage 1 as these were the first syn-rift successions and time equivalent with the earliest syn-rift deposits in the central area (Ford et al., 2013). Based on the age estimates of rift phase 1 and the Lower Group, syn-rift stage 1 has an approximate age of 5 to 2.2-1.8 Ma.

a)

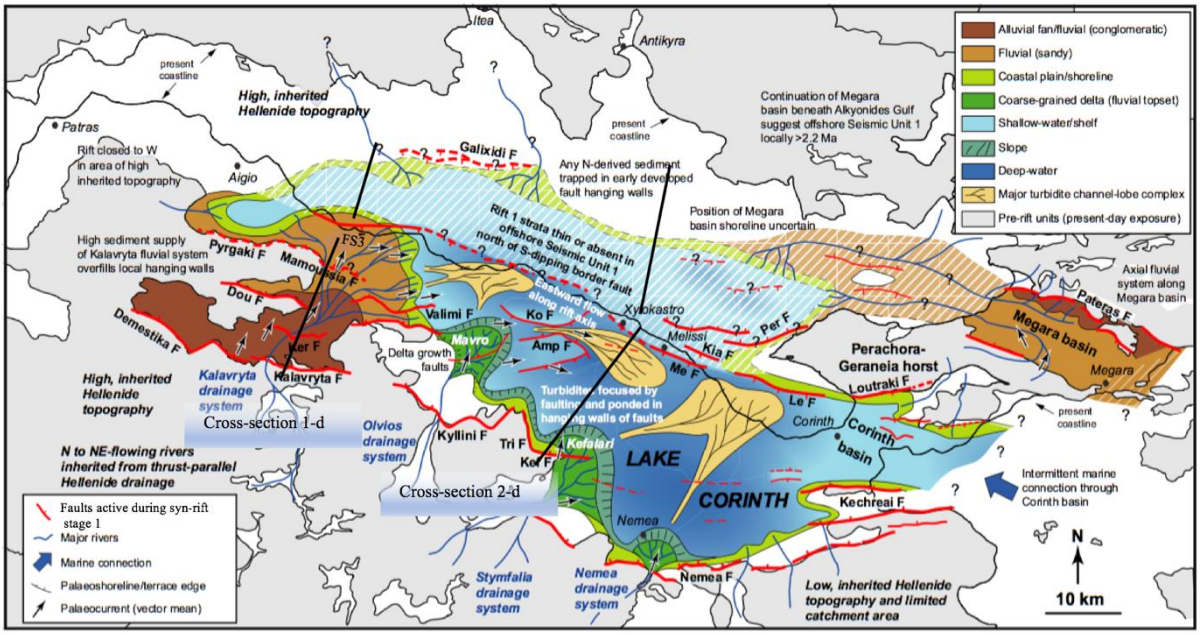

b)

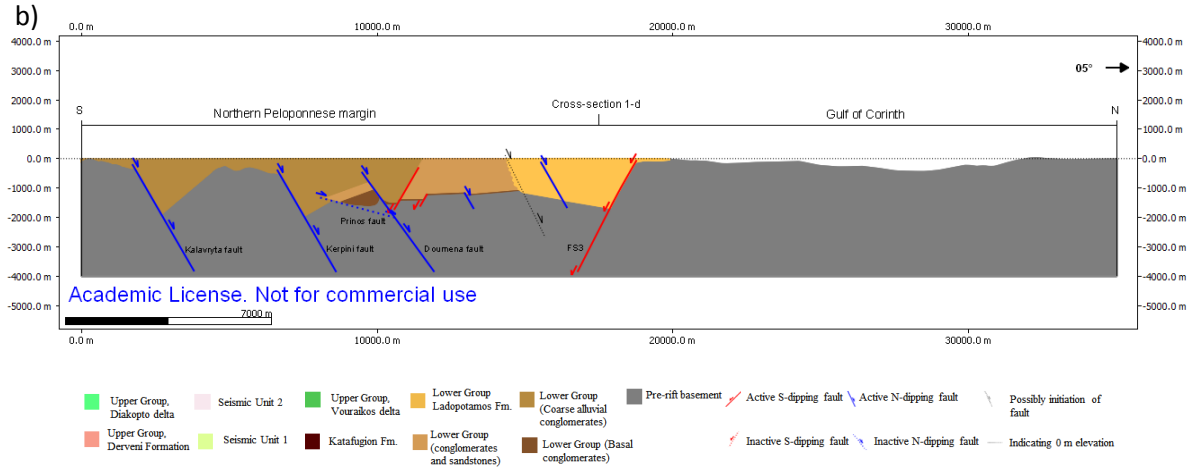

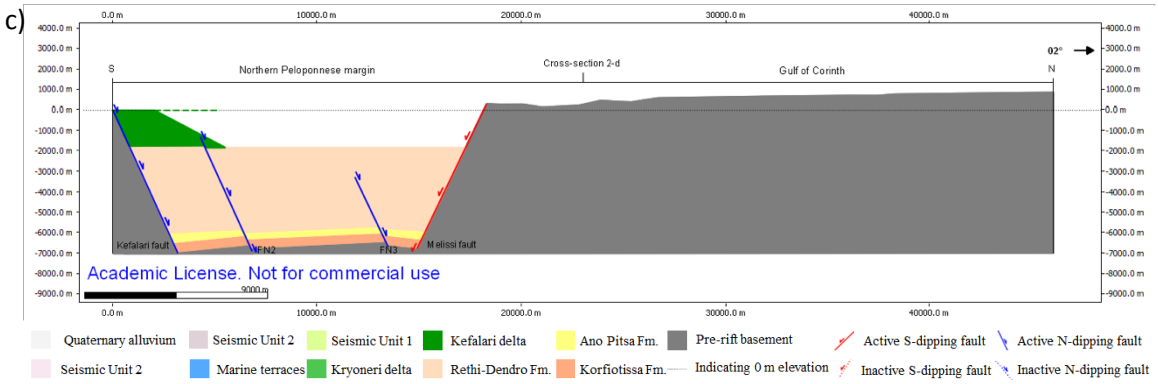

Figure 7.1. a) Palaeographic map of syn-rift stage 1 (approximately 5 to 2.2-1.8 Ma) modified from Gawthorpe et al. (2018). Cross-sections 1-d and 2-d are marked by black N-S lines b) Cross-section 1-d (syn-rift stage 1) corresponds well with the palaeographic map by Gawthorpe et al. (2018). From the restoration process it was detected that there were no syn-rift strata in the Gulf of Corinth at this stage c) Cross-section 2-d (syn-rift stage 1) corresponds well with the palaeographic map by Gawthorpe et al. (2018). From the restoration process it was observed that there were no syn-rift deposits in the Gulf of Corinth. The Kefalari delta also most likely consists of more than one delta cycle.

7.2.2 Syn-rift stage 2

Syn-rift stage 2 is represented by a shift in fault activity towards the north. The faults that were active during syn-rift stage 1 were inactive or defined to little activity at this stage. The syn-rift stage 2 is represented by cross-sections 1-b, 2-c and 3-b. In the western area the fault activity migrated 13 km from the N-dipping Kalavryta fault to the Mamoussia fault, and 9 km from the S-dipping FS3 fault to the West Channel fault. The same characteristics of the initiation of syn-rift stage 2 could be seen in the central area, where fault activity migrated approximately 19 km from the N-dipping Kefalari fault to the East Xylokastro fault and 10 km from the S-dipping Melissi fault to the East Antikyra fault (Fig.7.6). Previous studies have also documented a northwards shift in fault activity with an estimate of 15-30 km (e.g. Armijo et al., 1996; Goldsworthy and Jackson, 2001; Rohais et al., 2007a; Bell et al., 2008; Ford et al., 2013; 2017; Gawthorpe et al., 2018). In the eastern area fault activity was also present in the Gulf of Corinth, but from this study there was no record of fault activity at the northern Peloponnese margin at this stage (cross-section 3-b, Fig.7.4.a,d). In the central and western area the delta deposits were preserved indicating the position of the palaeo-shoreline. The location of the palaeo-shoreline in the eastern area was not possible to determine based on cross-section 3.

The Vouraikos delta deposited in the western area and the Kryoneri delta deposited in the central part were both coarse-grained Gilbert-type deltas, but the vertical thickness of the two deltas were significantly different (Fig. 7.2) (Ford et al., 2013; Gawthorpe et al., 2017; 2018). An explanation for this thickness variation is that the Vouraikos delta was deposited in the hangingwall of the Mamoussia fault (cross-section 1-b Fig.7.4.b), while the Kryoneri delta

was deposited in the footwall of the East Xylokastro fault (cross-section 2-c Fig.7.4.c). The hangingwall of the Mamoussia fault was subsiding creating accommodation for the delta, while the footwall of the East Xylokastro fault was progressively uplifted decreasing the accommodation. This has also been documented by previous researchers (Ford et al., 2013; 2017; Gawthorpe et al., 2017; 2018) and a staircase pattern of the Kryoneri delta deposits located at three different elevations was recognized by Gawthorpe et al. (2017, 2018) which correlates to the progressive uplift of the footwall of the East Xylokastro fault (Fig.7.3) (Gawthorpe et al., 2017; 2018). This downstepping geometry of the delta was not detected in cross-section 2-c and it was interpreted that the Kryoneri delta deposits at the two other elevations did not build as far out to the west during deposition. The deposits could also be eroded and therefore not currently existing.

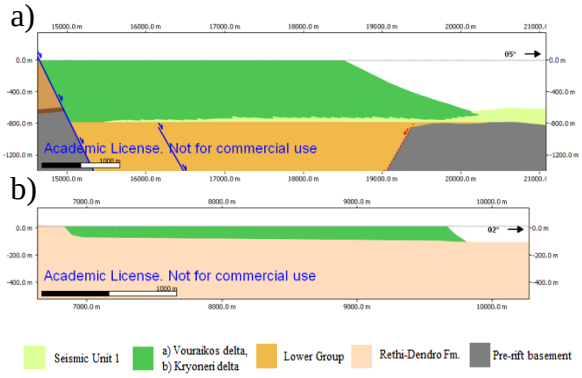

Fig. 7.2 a) Close up of the Vouraikos delta from cross-section 1-b b) Close up of the Kryoneri delta from cross-section 2-c. Notice the thickness variation between the two deltas correlated to be time equivalent.

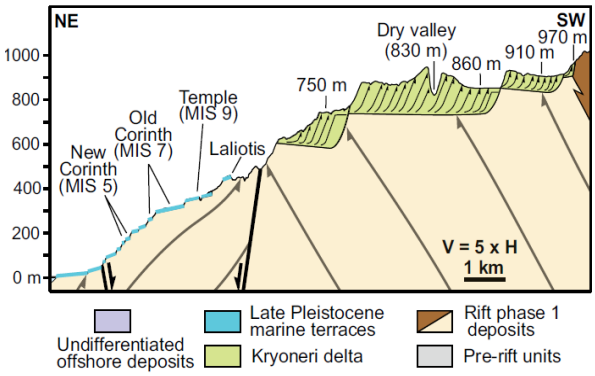

Figure 7.3 Cross-section of the Kryoneri delta progressively downstepping towards the northeast. This cross-section was located to the east of cross-section 2. Modified from Gawthorpe et al. (2017).

Based on the results from the restoration process combined with previous research (Ford et al., 2013; 2017; Gawthorpe et al., 2017; 2018) the syn-rift stage 2 was characterized by a 9-19 km northwards shift of fault activity. Syn-rift stage 2 was compared to the early rift phase 2 (age 2.2-1.8 Ma to present) defined by Gawthorpe et al. (2018) as early rift phase 2 was also characterized by a northwards shift in fault activity with progressive uplift of the northern Peloponnese margin (Fig.7.4.a). The Middle Group (age 2.5-1.8 to 0.7-0.45 Ma) in the western area defined by Ford et al. (2013) also have some similarities with syn-rift stage 2 as these deposits were corresponding to the activity of the Mamoussia fault in the western area. Also, the Middle Group were time equivalent to the Kryoneri delta deposited in the central area (Ford et al., 2013). Based on the age estimates of rift phase 2 and the Middle Group, syn-rift stage 2 has an approximate age of 2.2-1.8 to 0.7 Ma.

a)

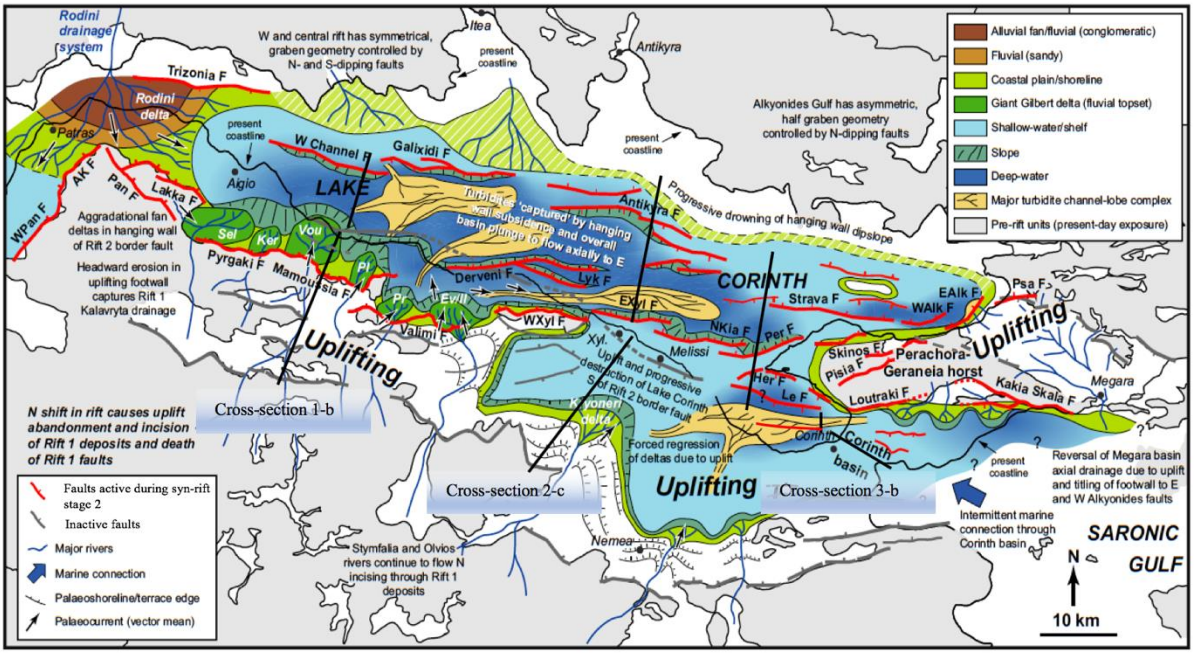
Rodini drainage system
W and central rift has symmetrical, graben geometry controlled by N- and S-dipping faults
Itea
present coastline
Antikyra
Alkyonides Gulf has asymmetric, half graben geometry controlled by N-dipping faults
Trizonia F
Rodini delta
Patras
present coastline
W Channel F
Galixidi F
Aigio
LAKE
AK F
Pan F
Lakka F
WPan F
Aggradational fan deltas in hanging wall of Rift 2 border fault
Sel
Ker
Vou
Pyrgaki F
Mamoussia F
Pl
Headward erosion in uplifting footwall captures Rift 1 Kalavryta drainage
Tithorea valley 'captured' by hanging wall subsidence and overall basin plunge to flow axially to E
Antikyra F
Progressive drowning of hanging wall dipslope
Derveni F
Lyk F
CORINTH
Strava F
EAlk F
WAlk F
Psa F
Uplifting
Ewll
Exyl F
WXyl F
Valimi F
NKla F
Per F
Melissi
Xyl.
Uplift and progressive destruction of Lake Corinth S border fault
Skinos F
Pisia F
Perachora-Geraneia horst
Loutraki F
Her F
Le F
Kakia Skala F
Megara
Kryoneri delta
Forced regression of deltas due to uplift
Corinth
Corinth basin
present coastline
Reversal of Megara basin axial drainage due to uplift and tilting of footwall to E and W Alkyonides faults
Cross-section 1-b
Cross-section 2-c
Uplifting
Cross-section 3-b
N shift in rift causes uplift abandonment and incision of Rift 1 deposits and death of Rift 1 faults
Faults active during syn-rift stage 2
Inactive faults
Major rivers
Marine connection
Palaeoshoreline/terrace edge
Palaeocurrent (vector mean)
Intermittent marine connection through Corinth basin
Nemea
Stymfalia and Olvios rivers continue to flow N incising through Rift 1 deposits
SARONIC GULF
N
10 km
Alluvial fan/fluvial (conglomeratic)
Fluvial (sandy)
Coastal plain/shoreline
Giant Gilbert delta (fluvial topset)
Shallow-water shelf
Slope
Deep-water
Major turbidite channel-lobe complex
Pre-rift units (present-day exposure)

b)

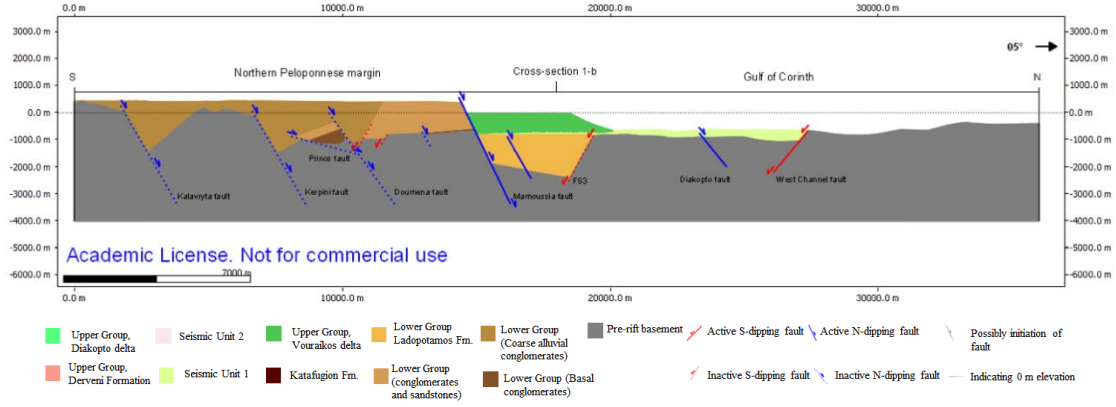
Northern Peloponnese margin
Cross-section 1-b
Gulf of Corinth
S
N
05°
Kalavryta fault
Pirnos fault
Kerpini fault
Doumena fault
FS3
Mamoussia fault
Diakopto fault
West Channel fault
Academic License. Not for commercial use
Upper Group, Diakopto delta
Upper Group, Derveni Formation
Seismic Unit 2
Seismic Unit 1
Upper Group, Vouraikos delta
Katafugion Fm.
Lower Group Ladopotamos Fm.
Lower Group (conglomerates and sandstones)
Lower Group (Coarse alluvial conglomerates)
Lower Group (Basal conglomerates)
Pre-rift basement
Active S-dipping fault
Active N-dipping fault
Inactive S-dipping fault
Inactive N-dipping fault
Possibly initiation of fault
Indicating 0 m elevation

c)

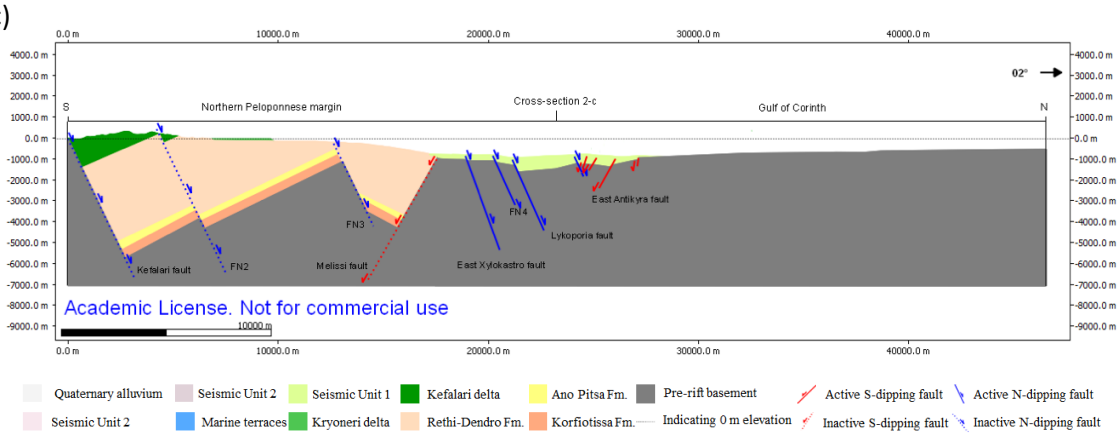
Northern Peloponnese margin
Cross-section 2-c
Gulf of Corinth
S
N
02°
Kefalari fault
FN2
Melissi fault
FN3
FN4
East Xylokastro fault
Lykoporia fault
East Antikyra fault
Academic License. Not for commercial use
Quaternary alluvium
Seismic Unit 2
Seismic Unit 1
Marine terraces
Kefalari delta
Kryoneri delta
Ano Pitsa Fm.
Rethi-Dendro Fm.
Korfiotissa Fm.
Pre-rift basement
Indicating 0 m elevation
Active S-dipping fault
Inactive S-dipping fault
Active N-dipping fault
Inactive N-dipping fault

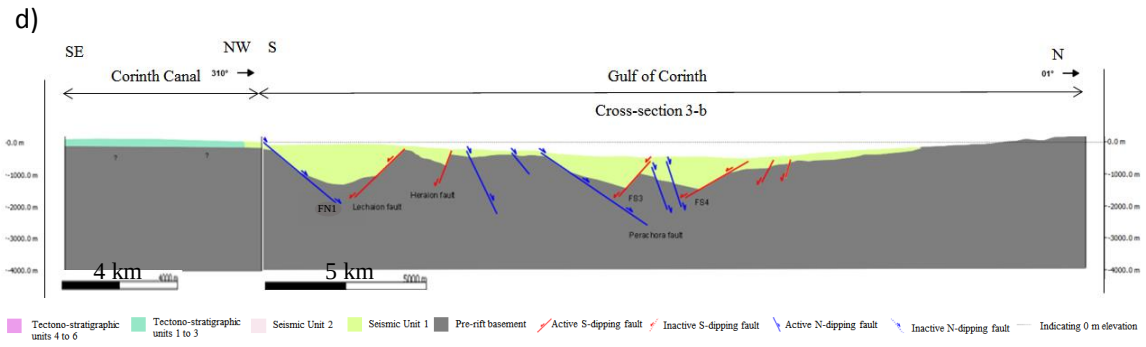

Figure 7.4. a) Palaeographic map of syn-rift stage 2 (approximately 2.2-1.8 to 0.7 Ma) modified from Gawthorpe et al. (2018). The S-dipping FS3 fault in the western area (cross-section 1) was buried below the Vouraikos delta. The N-dipping FN1 fault in the Lechaion Gulf was interpreted to be active at this stage. Cross-sections 1-b, 2-c and 3-b are marked by black N-S lines b) Cross-section 1-b (syn-rift stage 2) corresponds well with the palaeographic map by Gawthorpe et al. (2018) and the inactive, buried S-dipping FN3 fault was added to the map (a)). From the restoration process the Vouraikos delta was correlated to Seismic Unit 1 c) Cross-section 2-c (syn-rift stage 2) corresponds well with the palaeographic map by Gawthorpe et al. (2018). From the restoration process it was observed that the Kryoneri delta was laterally correlated basinward to Seismic Unit 1 d) Cross-section 3-b also corresponds well with the palaeographic map by Gawthorpe et al. (2018). The N-dipping FN1 fault in the Lechaion Gulf was interpreted to be active at this stage and therefore added to the map a).

7.2.3 Syn-rift stage 3

Syn-rift stage 3 is the last stage of the rift evolution and was characterized by a shift in the palaeo-shoreline towards the north (Fig.7.5). Cross-sections 1-a, 2-a, 2-b and 3-a are those that illustrate the Corinth Rift at this stage. The northwards shift of the palaeo-shoreline was supported by the observation of marine terraces at different elevations, with the elevation decreasing towards the north in cross-section 2-b (Fig.7.4.c). The marine terraces were deposited at sea-level, but because of the progressive uplift of the southern rift flank these were present day found at progressively lower elevations as they young (Armijo et al., 1996). In previous studies (Collier, 1990; Armijo et al., 1996) the marine terraces have been correlated to marine isotope stages and dated. The Old Corinth marine terrace (dated 235 ka (+40,-30) by U/Th dating) was in this study correlated to the horizon in Seismic Unit 2 with a proposed age of 240 ka (Armijo et al., 1996; Nixon et al., 2016, and references therein).

The Mamoussia and the West Channel faults were inactive at this stage, while the East Heliki fault was active and created accommodation for the present day Diakopto delta to be deposited (Fig.7.5.b, Fig.7.6). In section 2-b the East Antikyra fault was still active before decreasing in activity in section 2-a. In cross-section 3-a the currently active Perachora fault was the controlling fault of the Corinth basin and in the Corinth Canal the section was characterized by several N-and S-dipping faults (Fig.7.5.c). In the Corinth Canal marine deposits can be found *c.* 80 m above sea-level, interpreted to be related to the uplift of the footwall of the N-dipping FN0 fault (Collier, 1990).

The main characteristics of syn-rift stage 3 was that the major N-dipping faults on the southern margin had larger displacement than the S-dipping faults on the northern margin of the Gulf of Corinth (Fig.7.5). The currently active N-dipping East Heliki, Lykoporia, East Xylokastro and Perachora faults were by, Nixon et al. (2016), interpreted to control one single depocenter subsurface Gulf of Corinth forming an asymmetric rift geometry. In the Lechaion Gulf the S-dipping Heraion fault was controlling a smaller depocenter (Fig.7.5.a) (Nixon et al., 2016). Based on the stratigraphy of the rift during syn-rift stage 3, the environment in the rift was alternating between lacustrine and marine conditions (Nixon et al., 2016). These alternations in the environmental setting have been correlated to the 100 kyr glacio-eustatic cycles, and during interglacial highstands the environment was marine (Perissoratis et al., 2000; Bell et al., 2009; Taylor et al., 2011; Nixon et al., 2016).

The extension measured from syn-rift stage 1 to 3 varies for the three cross-sections. The largest extension was calculated in the central part (7 km) and the least extension was in the eastern area (5 km). The value for the central part and western area (6 km) were similar to the values of previous studies (Bell et al., 2011; Ford et al., 2013). There is uncertainty to these extension values as most of the faults included in this thesis were basement cutting faults, and therefore this was most likely an underestimation of the extension as also smaller faults would accommodate extension. Additionally, the basin is wider in the eastern area compared to the western area, suggesting the amount of extension would have been greater in the east (Armijo et al., 1996). The interpreted underestimation of the extension in the east is interpreted to be due to exclusion of the larger border faults of syn-rift stage 1 in cross-section 3.

The syn-rift stage 3 was compared to the late rift phase 2 (age 2.2-1.8 Ma to present) defined by Gawthorpe et al. (2018) as the rift developed a dominant southern border fault system with progressive uplift of the northern Peloponnese margin (Fig. 7.5.a) (Nixon et al., 2016; Gawthorpe et al., 2018). The Upper Group (0.7 Ma to present) in the western area defined by Ford et al. (2013), also has some similarities with syn-rift stage 3 as these deposits were interpreted to be deposited during initiation of the East Heliki fault to present day, also the Upper Group was time equivalent to the late syn-rift deposits in the central area (Ford et al., 2013). Based on the age estimates of rift phase 2 and the Upper Group, syn-rift stage 3 has an approximate age of 0.7 Ma to present.

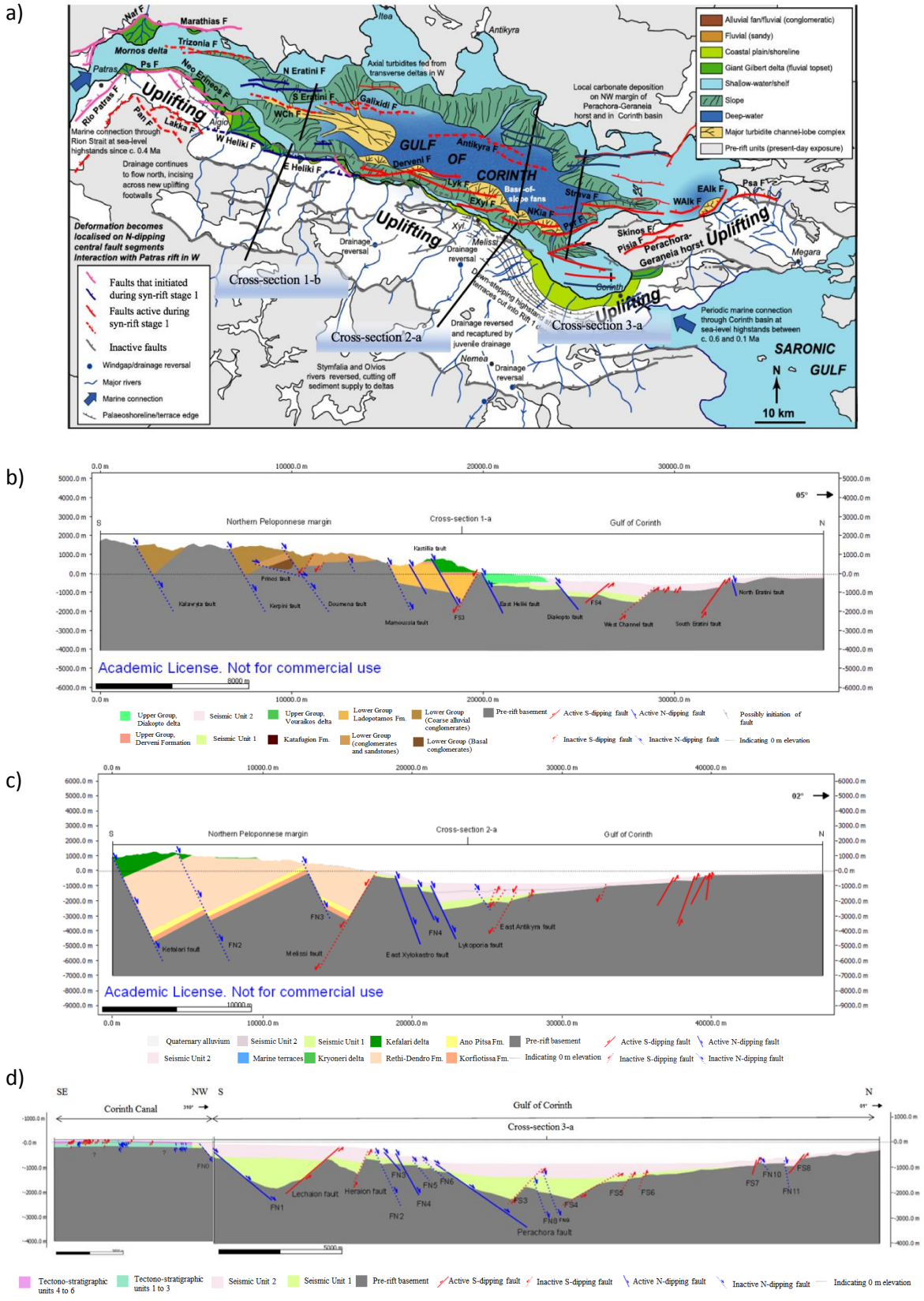

Figure 7.5. a) Palaeographic map of syn-rift stage 3 (approximately 0.7 Ma to present) modified from Gawthorpe et al. (2018). Cross-sections 1-a, 2-a and 3-a are marked by black N-S lines b) Cross-section 1-a (syn-rift stage 3) corresponds well with the palaeographic map by Gawthorpe et al. (2018). The hidden inactive FS3 fault was added to the map (a)) c) Cross-section 2-a (syn-rift stage 3) corresponds well with the palaeographic map by Gawthorpe et al. (2018). The active S-dipping faults north of the East Anitkyra fault was added to the map (a)) d) Cross-section 3-a also corresponds well with the palaeographic map by Gawthorpe et al. (2018). The interpreted active Heraion fault and the two N-dipping faults (FN0 and FN1) was added to the map (a)).

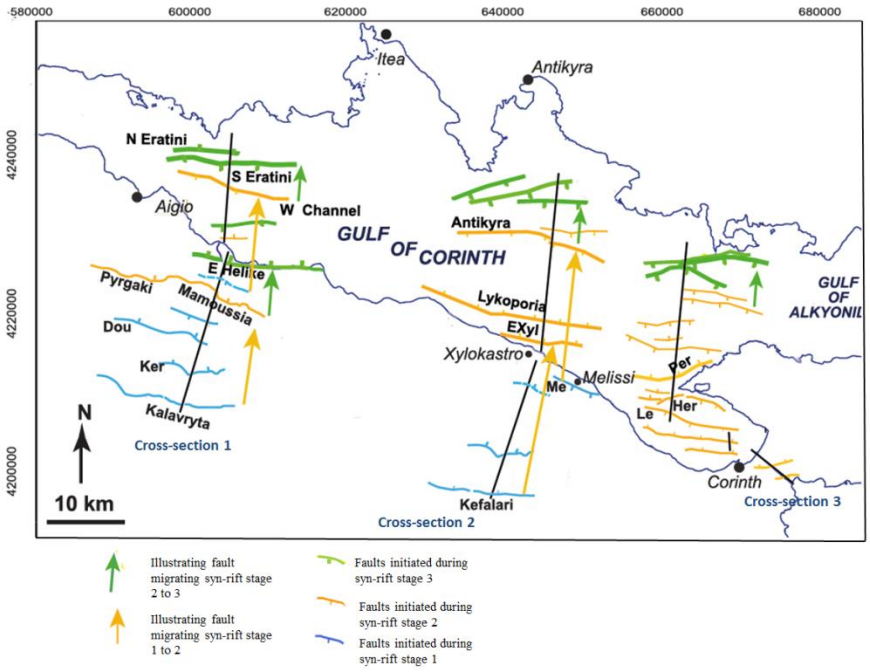

Figure 7.6. Syn-rift stage 1 was characterized by the initiation of the faults on the northern Peloponnese margin indicated in blue. These faults are currently inactive. The shift towards syn-rift stage 2 was marked by the northwards migration of fault activity indicated by orange arrow. The orange faults initiated during syn-rift stage 2 and the faults indicated in blue became inactive. The shift towards syn-rift stage 3 was marked by a fault migration. In the western area there was a shift in fault activity for both the N- and S-dipping faults indicated in a green arrow. The Mamoussia fault and the West Channel faults were inactive at this stage. In the central and eastern area a northwards shift in fault activity was detected for the S-dipping faults on the northern Gulf of Corinth margin (indicated in green arrows). The faults indicated in orange on the southern margin in the central and eastern area interpreted to be active during this stage. Modified from Nixon et al. (2016); Ford et al. (2017); Gawthorpe et al. (2018).

7.3 Controlling factors and driving mechanisms

This sub-chapter will discuss the controlling factors and driving mechanisms for the different syn-rift stages and compare the rift evolution to other rift systems. The evolution of the Corinth Rift is complex and several controlling factors and mechanisms have been part of the development of the rift structure. The Corinth Rift has inherited relief which has not been clearly documented in other rift systems and the late Jurassic rifting of the northern North Sea suggests pre-existing flat topography as faulting initiated on the flat Brent delta (Cowie et al., 2005). The inherited relief played a large part of the Corinth Rift evolution and similarly, it also played an important role for the East African rift system. An example is the Malawi rift that was cutting the pre-existing drainage system and caused the drainage into the rift to be asymmetric (Crossley, 1984; Gawthorpe et al., 2018). This is similar to what can be seen in the early rifting in the Corinth area as the major rivers flowing in the western area of the northern Peloponnese margin deposited the Lower Group and caused the rift to be overfilled, while in the central area the basin was underfilled (Ford et al., 2013). This also makes the Corinth Rift differ from other rift systems as it is thought that in the early rift stages the basin

is overfilled and in later stages the basin becomes underfilled along the rift axis, but for the Corinth Rift this changes along strike (e.g. Ravnås and Steel, 1998; Gawthorpe et al., 2018). The largest shift in northwards migration of fault activity occurred from syn-rift stage 1 to syn-rift stage 2 (Fig.7.6). The northwards migration of the faulting most likely happened due to processes active in the lower crust and earlier research state that it could have been driven by lithospheric cooling and strengthening during rifting (Manatschal and Bernoulli, 1999). Another explanation for the northwards fault migration is that it was controlled by lower crustal flow and the amount of migration that occurred was a function of crustal viscosity and composition, strain softening and initial thermal structure (Brune et al., 2014; Nixon et al., 2016). The fault migration seen in the Corinth Rift could have been caused by these processes in combination with the dynamics that are linked to the underlying subducting plate (e.g. Tiberi et al., 2000; Le Pourhiet et al., 2003; Leeder et al., 2003; Nixon et al., 2016). The main difference between other rifts that experience fault migration and the Corinth Rift, is that studies of the Gulf of Suez and the northern North Sea show that these rifts experience rift narrowing as the faulting migrates towards the rift axis (Gawthorpe et al., 2003; Cowie et al., 2005). In the Corinth Rift both the southern and northern margins were migrating and no noticeably narrowing have occurred (Nixon et al., 2016). This can suggest that the Corinth Rift has low temperatures and a strong lithospheric rheology as rift narrowing models often correspond with thinning of the lithosphere causing increased geothermal gradients and/or strain softening due to inherited weaknesses (Buck, 1991; Brun et al., 1999; Behn et al., 2002; Huismans and Beaumont, 2007).

Through evolution the Corinth Rift has formed an overall asymmetric geometry as strain was located on fewer, larger faults in syn-rift stage 3, which also has been suggested by previous studies (Ford et al., 2013; Nixon et al., 2016; Gawthorpe et al., 2018). This have also be seen in other rifts systems and an example is the East African rift (Nixon et al. 2016, and references therein). The N-dipping faults on the southern margin of the Gulf of Corinth have developed a border fault system in the Gulf of Corinth (Nixon et al., 2016). A linkage of faults through the evolution of the rift development is common in most rift systems as the deformation gets localized (e.g. Ebinger, 1989; Schlische, 1993; Gawthorpe et al., 2003; Walsh et al., 2003; Cowie et al., 2005; Soliva and Schultz, 2008).

The evolution of rift systems are complex and the development of different rifts vary. It is therefore important to study different rift systems to establish the relationship between them

to look at similarities and differences to further get a better understanding of how the systems evolve. The Corinth Rift is a very good analogue to study rifting and the interpretation of the rift evolution show both similarities and dissimilarities with other rifts systems.

8. Conclusions and further work

8.1 Conclusions

The purpose of this study was to improve the understanding of the tectono-stratigraphic evolution of the Corinth Rift by integrating the northern Peloponnese margin with the Gulf of Corinth. The main conclusions from this study were:

- The total extension changes along strike and the total extension in the west (cross-section 1) was 6 km, in the central area (cross-section 2) it was 7 km and in the eastern part (cross-section 3) the total extension was 5 km.
- From the reconstruction from the cross-sections it was detected that the top of the basement was not completely horizontal and the interpretation of this was that the Corinth Rift has inherited relief. In the basin there were areas in the early stages of evolution that was overfilled and underfilled along the rift axis.
- There was a shift in fault activity from the faults at the northern Peloponnese margin towards the Gulf of Corinth. This accounts for a northwards migration of 9-13 km in the western area, 10-19 km in the central area. In the eastern most area this northwards migration could not be calculated because the border fault lies outside the study area.
- The rift has acquired its present day asymmetric geometry through time as the N-dipping faults became the dominant faults and the S-dipping faults on the northern margin became less active.
- Based on main changes in variations of structure and sedimentary style through time detected in the restoration of the three cross-sections the evolution of the rift was divided into 3 syn-rift stages:
    - Syn-rift stage 1 (approximately 5 to 2.2-1.8 Ma) represents the rift initiation and this stage was restricted to the northern Peloponnese area. There was no accumulation of sedimentary deposits in the Gulf of Corinth area.
    - Syn-rift stage 2 (approximately 2.2-1.8 to 0.7 Ma) represents a 9-19 km northwards shift in fault activity. The Vouraikos and Kryoneri deltas correlated basinward to Seismic Unit 1. In the Corinth Canal the tectono-stratigraphic units 1 to 3 were also correlated to Seismic Unit 1.

- Syn-rift stage 3 (age estimated 0.7 Ma to present) represents a northwards shift in palaeo-shoreline. This was due to a northwards shift in fault activity detected in cross-section 1 and progressive uplift of the northern Peloponnese margin in cross-section 2 due to activity of the N-dipping faults. The rift developed an asymmetrical geometry because the N-dipping faults on the southern margin of the Gulf of Corinth became the dominant faults as activity along the S-dipping faults on the northern margin decreased. The present day Diakopto delta, the marine terraces and the tectono-stratigraphic units 4 to 6 were correlated to Seismic Unit 2.

8.2 Further work and limitations

In order to make a more accurate reconstruction of this area one advantage would be to include more data from onshore fieldwork, especially in the eastern area. This combined with several cross-sections along-strike and accurate dip measurements across the sections would improve the restoration. Also, seismic surveying would be helpful to determine what defines the subsurface for the areas lacking exposure of the vertical extent on land of the northern Peloponnese margin. In combination with this, measurement of porosity of the rocks could be undertaken with e.g. boreholes on land so that more exact compaction parameters could be used in the 2D Decompaction step. A 3D digital model of the Corinth Rift would also be helpful for better understanding of the rift evolution.

As a result of using the Move Midland Valley software for the construction and restoration of the area a model of the present-day setting was presented. It is important to know that there were different algorithms in Move Midland Valley that could have been used for different geological settings. Therefore most likely a model could be restored using different algorithms other than the ones chosen to be used in this project and that might produce different interpretations to some extent. The previous, combined with that the software works best with simple geological models with simple geometries, the restored models do not necessarily represent the exact pre-deformed geometry or the path followed by the structural evolution. The model does show a more accurate picture of the deformation history than a non-balanced cross-section as the balanced section is a model that fulfills a number of constraints (Woodward et al., 1989).

Reference list

ALLEN, P. A. & ALLEN, J. R. 2013. *Basin Analysis: Principles and Application to Petroleum Play Assessment*, 3rd ed. West Sussex, UK, Wiley-Blackwell, 632.

ARMIJO, R., MEYER, B., KING, G. C. P., RIGO, A. & PAPANASTASSIOU, D. 1996. Quarternary evolution of the Corinth Rift and its implications for the Late Cenozoic evolution of the Aegean. *Geophys. J. Int,* 126**,** 11-53.

ARMIJO, R., MEYER, B., HUBERT, A. & BARKA, A. 1999. Westward propagatgion of the North Anatolian fault into the northern Aegean: Timing and kinematics. *Geology,* 27**,** 267-270.

AVALLONE, A., BRIOLE, P., AGATZA-BALODIMOU, A. M., BILLIRIS, H., CHARADE, O., MITSAKAKI, C., NERCESSIAN, A., PAPAZISSI, K., PARADISSIS, D. & VEIS, G. 2004. Analysis of eleven years of deformation measured by GPS in the Corinth Rift Laboratory area. *Comptes Rendus Geoscience,* 336**,** 301-311.

BEHN, M. D., LIN, J. & ZUBER, M. T. 2002. A continuum mechanics model for normal faulting using a strain-rate softening rheology: implications for thermal and rheological controls on continental and oceanic rifting. *Earth and Planetary Science Letters,* 202**,** 725-740.

BELL, R. E., MCNEILL, L. C., BULL, J. M. & HENSTOCK, T. J. 2008. Evolution of the offshore western Gulf of Corinth. *Geological Society of America Bulletin,* 120**,** 156-178.

BELL, R. E., MCNEILL, L. C., BULL, J. M., HENSTOCK, T. J., COLLIER, R. E. L. & LEEDER, M. R. 2009. Fault architecture, basin structure and evolution of the Gulf of Corinth Rift, central Greece. *Basin Research,* 21**,** 824-855.

BELL, R. E., MCNEILL, L. C., HENSTOCK, T. & BULL, J. M. 2011. Comparing extension on multiple time and depth scales in the Corinth rift, central Greece. *Geophys. J. Int,* 186**,** 463-470.

BERNARD, P., LYON-CAEN, H., BRIOLE, P., DESCHAMPS, A., BOUDIN, F., MAKROPOULOS, K., PAPADIMITRIOU, P., LEMEILLE, F., PATAU, G., BILLIRIS, H., PARADISSIS, D., PAPAZISSI, K., CASTARÈDE, H., CHARADE, O., NERCESSIAN, A., AVALLONE, A., PACCHIANI, F., ZAHRADNIK, J., SACKS, S. & LINDE, A. 2006. Seismicity, deformation and seismic hazard in the western rift of Corinth: New insights from the Corinth Rift Laboratory (CRL). *Tectonophysics,* 426**,** 7-30.

BILLIRIS, H., PARADISSIS, D., VEIS, G., ENGLAND, P., FEATHERSTONE, W., PARSONS, B., CROSS, P., RANDS, P., RAYSON, M., SELLERS, P., ASHKENAZI, V., DAVISON, M., JACKSON, J. & N., A. 1991. Geodetic determination of tectonic deformation in central Greece from 1900 to 1988. *Nature,* 350**,** 124-129.

BINTANJA, R. & VAN DE WAL, R. S. W. 2008. North American ice-sheet dynamics and the onset of 100,000-year glacial cycles. *Nature,* 454**,** 869-872.

BOTT, M. H. P. 1995. Mechanisms of Rifting: Geodynamic Modeling of Continental Rift Systems *In:* Olsen, K. H. (ed.) *Continental Rifts: Evolution, Structure, Tectonics.* Amsterdam: Elsevier Science B.V. 27-41

BRUN, J. P., WHITE, R. S., HARDMAN, R. F. P., WATTS, A. B. & WHITMARSH, R. B. 1999. Narrow rifts versus wide rifts: inferences for the mechanics of rifting from laboratory experiments. *Philosophical Transactions of the Royal Society of London. Series A: Mathematical, Physical and Engineering Sciences,* 357**,** 695-712.

BRUNE, S., HEINE, C., PEREZ-GUSSINYE, M. & SOBOLEV, S. V. 2014. Rift migration explains continental margin asymmetry and crustal hyper-extension. *Nature Communications,* 5**,** 1-4.

BUCK, W. R. 1991. Modes of continental lithospheric extension. *Journal of Geophysical Research,* 96**,** 161-178.

CARTWRIGHT, J., BOUROULLEC, R., JAMES, D. & JOHNSON, H. 1998. Polycyclic motion history of some Gulf Coast growth faults from high-resolution displacement analysis. *Geology,* 26**,** 819-822.

CHARALAMPAKIS, M., LYKOUSIS, V., SAKELLARIOU, D., PAPATHEODOROU, G. & FERENTINOS, G. 2014. The tectono-sedimentary evolution of the Lechaion Gulf, the south eastern branch of the Corinth graben, Greece. *Marine Geology,* 351**,** 58-75.

CLARKE, P. J., DAVIES, R. R., ENGLAND, P. C., PARSONS, B. E., BILLIRIS, H., PARADISSIS, D., VEIS, G., DENYS, P. H., CROSS, P. A., ASHKENAZI, V. & BINGLEY, R. 1997. Geodetic estimate of seismic hazard in the Gulf of Korinthos. *Geophysical Research Letters,* 24**,** 1303-1306.

COLLIER, R. E. L. 1990. Eustatic and tectonic controls upon Quarternary coastal sedimentation in the Corinth Basin, Greece. *Geological Society,* 147**,** 301-314.

COLLIER, R. E. L. & DART, C. J. 1991. Neogene to Quaternary rifting, sedimentation and uplift in the Corinth Basin, Greece. *Journal of the Geological Society, London,* 148**,** 1049-1065.

COWIE, P. A., GUPTA, S. & DAWERS, N. H. 2000. Implications of fault array evolution for synrift depocentre development: insights from numerical fault growth model. *Basin Research,* 12**,** 241-261.

COWIE, P. A., UNDERHILL, J., BEHN, M., LIN, J. & GILL, C. 2005. Spatio-temporal evolution of strain accumulation derived from multi-scale observations of Late Jurassic rifting in the northern North Sea: A critical test of models for lithospheric extension. *Earth and Planetary Science Letters,* 234**,** 401-419.

COWIE, P. A., ATTAL, M., TUCKER, G. E., WHITTAKER, A. C., NAYLOR, M., GANAS, A. & ROBERTS, G. P. 2006. Investigating the surface process response to fault interaction and linkage using a numerical modelling approach. *Basin Research,* 18**,** 231-266.

CROSSLEY, R. 1984. Controls of sedimentation in the Malawi rift valley, central Africa. *Sedimentary Geology,* 40**,** 33-50.

DAHLSTRØM, C. D. A. 1969. Balanced cross-sections. *Canadian Journal of Earth Sciences,* 6**,** 743-757.

DEMOULIN, A., BECKERS, A. & HUBERT-FERRARI, A. 2015. Patterns of Quaternary uplift of the Corinth rift southern border (N Peloponnese, Greece) revealed by fluvial landscape morphometry. *Geomorphology,* 246**,** 188-204.

DOUTSOS, T., KONTOPOULOS, N. & POULIMENOS, G. 1988. The Corinth-Patras rift as the initial stage of continental fragmentation behind an active island arc (Greece). *Basin Research,* 1**,** 177-190.

DOUTSOS, T. & PIPER, D. J. W. 1990. Listric faulting, sedimentation, and morphological evolution of the Quaternary eastern Corinth rift, Greece: First stages of continental rifting. *Geological Society of America Bulletin,* 102**,** 812-829.

DOUTSOS, T. & POULIMENOS, G. 1992. Geometry and kinematics of active faults and their seismotectonic significance in the western Corinth-Patras rift (Greece). *Journal of Structural Geology,* 14**,** 689-699.

EBINGER, C. J. 1989. Geometric and Kinematic development of border faults and accommodation zones, Kivu-Rusizi Rift, Africa. *Tectonics,* 8**,** 117-133.

FORD, M., ROHAIS, S., WILLIAMS, E. A., BOURLANGE, S., JOUSSELIN, D., BACKERT, N. & MALARTRE, F. 2013. Tectono-sedimentary evolution of the western Corinth rift (Central Greece). *Basin Research,* 25**,** 3-25.

FORD, M., HEMELSDAËL, R., MANCINI, M. & PALYVOS, N. 2017. Rift migration and lateral propagation: evolution of normal faults and sediment-routing systems of the western Corinth rift (Greece). *Geological Society, London, Special Publications,* 439**,** 131-168.

FOSSEN, H. 2010. *Structural Geology*, 3rd ed. New York, USA, Cambridge University Press, 463.

GAWTHORPE, R. L. & LEEDER, M. R. 2000. Tectono-sedimentary evolution of active extensional basins. *Basin Research,* 12**,** 195-218.

GAWTHORPE, R. L., JACKSON, C. A.-L., YOUNG, M. J., SHARP, I. R., MOUSTAFA, A. R. & LEPPARD, C. W. 2003. Normal fault growth, displacement localisation and the evolution of normal fault populations: the Hammam Faraun fault block, Suez rift, Egypt. *Journal of Structural Geology,* 25**,** 883-895.

GAWTHORPE, R. L., ANDREWS, J. E., COLLIER, R. E. L., FORD, M., HENSTRA, G. A., KRANIS, H., LEEDER, M. R., MURAVCHIK, M. & SKOURTSOS, E. 2017. Building up or out? Disparate sequence architectures along an active rift margin—Corinth rift, Greece. *Geology,* 45**,** 1111-1114.

GAWTHORPE, R. L., LEEDER, M. R., KRANIS, H., SKOURTSOS, E., ANDREWS, J. E., HENSTRA, G. A., MACK, G. H., MURAVCHIK, M., TURNER, J. A. & STAMATAKIS, M. 2018. Tectono-sedimentary evolution of the Plio-Pleistocene Corinth rift, Greece. *Basin Research,* 30**,** 448-479.

GIBBARD, P. & COHEN, K. M. 2008. The global chronostratigraphic correlation table for the last 2.7 million years. *Episodes,* 31**,** 243-247.

GOLDSWORTHY, M. & JACKSON, J. 2001. Migration of activity within normal fault systems: examples from the Quaternary of mainland Greece. *Journal of Structural Geology,* 23**,** 489-506.

HUISMANS, R. S. & BEAUMONT, C. 2007. Roles of lithospheric strain softening and heterogeneity in determining the geometry of rifts and continental margins. *Geological Society, London, Special Publications,* 282**,** 111-138.

JACKSON, C. A.-L. & ROTEVATN, A. 2013. 3D seismic analysis of the structure and evolution of a salt-influenced normal fault zone: a test of competing fault growth models. *Journal of Structural Geology,* 54**,** 215-234.

JOLIVET, L., DANIEL, J. M., TRUFFERT, C. & GOFFÉ, B. 1994. Exhumation of deep crustal metamorphic rocks and crustal extension in arc and back-arc regions. *Lithos,* 33**,** 3-30.

JOLIVET, L. 2001. A comparison of geodetic and finite strain pattern in the Aegean, geodynamic implications. *Earth and Planetary Science Letters,* 187**,** 95-104.

JOLIVET, L., FACCENNA, C., HUET, B., LABROUSSE, L., LE POURHIET, L., LACOMBE, O., LECOMTE, E., BUROV, E., DENÈLE, Y., BRUN, J.-P., PHILIPPON, M., PAUL, A., SALAÜN, G., KARABULUT, H., PIROMALLO, C., MONIÉ, P., GUEYDAN, F., OKAY, A. I., OBERHÄNSLI, R., POURTEAU, A., AUGIER, R., GADENNE, L. & DRIUSSI, O. 2013. Aegean tectonics: Strain localisation, slab tearing and trench retreat. *Tectonophysics,* 597-598**,** 1-33.

KEAREY, P., KLEPEIS, K. A. & VINE, F. J. 2009. *Global Tectonics*, 3rd ed. Hoboken, USA, Wiley-Blackwell, 469.

KERAUDREN, B. & SOREL, D. 1987. The terraces of Corinth (Greece) - A detailed record of eustatic sea-level variations during the last 500 000 years. *Marine Geology,* 77**,** 99-107.

LAMBOTTE, S., LYON-CAEN, H., BERNARD, P., DESCHAMPS, A., PATAU, G., NERCESSIAN, A., PACCHIANI, F., BOUROUIS, S., DRILLEAU, M. & ADAMOVA, P. 2014. Reassessment of the rifting process in the Western Corinth Rift from relocated seismicity. *Geophysical Journal International,* 197**,** 1822-1844.

LE PICHON, X. & ANGELIER, J. 1979. The hellenic arc and trench system: A key to the neotectonic evolution of the eastern mediterranean area. *Tectonophysics,* 60**,** 1-42.

LE PICHON, X. & ANGELIER, J. 1981. The Aegean Sea. *Philosophical Transactions of the Royal Society of London,* A300**,** 357-372.

LE POURHIET, L., BUROV, E. & MORETTI, I. 2003. Initial crustal thickness geometry controls on the extension in a back arc domain: Case of the Gulf of Corinth. *Tectonics,* 22**,** 1-9.

LEEDER, M. R., MCNEILL, L. C., LL COLLIER, R. E., PORTMAN, C., ROWE, P. J., ANDREWS, J. E. & GAWTHORPE, R. L. 2003. Corinth rift margin uplift: New evidence from Late Quaternary marine shorelines. *Geophysical Research Letters,* 30**,** 1-4.

LEEDER, M. R., MACK, G. H., BRASIER, A. T., PARRISH, R. R., MCINTOSH, W. C., ANDREWS, J. E. & DUERMEIJER, C. E. 2008. Late-Pliocene timing of Corinth (Greece) rift-margin fault migration. *Earth and Planetary Science Letters,* 274**,** 132-141.

LEEDER, M. R., MARK, D. F., GAWTHORPE, R. L., KRANIS, H., LOVELESS, S., PEDENTCHOUK, N., SKOURTSOS, E., TURNER, J., ANDREWS, J. E. & STAMATAKIS, M. 2012. A "Great Deepening": Chronology of rift climax, Corinth rift, Greece. *Geology,* 40**,** 999-1002.

MANATSCHAL, G. & BERNOULLI, D. 1999. Architecture and tectonic evolution of nonvolcanic margins: Present-day Galicia and ancient Adria. *Tectonics,* 18**,** 1099-1119.

MCKENZIE, D. P. 1978. Active tectonics of the Alpine-Himalayan belt: the Aegean Sea and surrounding regions. *Geophysical Journal of the Royal Astronomical Society,* 55**,** 217-254.

MCNEILL, L. C., SHILLINGTON, D. J., CARTER, G. D. O., EVEREST, J. D., GAWTHORPE, R. L., MILLER, C., PHILLIPS, M. P., COLLIER, R. E. L., CVETKOSKA, A., DE GELDER, G., DIZ, P., DOAN, M.-L., FORD, M., GERAGA, M., GILLESPIE, J., HEMELSDAËL, R., HERRERO-BERVERA, E., ISMAIEL, M., JANIKIAN, L., KOULI, K., LE BER, E., LI, S., NIXON, C. W., OFLAZ, S. A., OMALE, A. P., PANAGIOTOPOULOS, D., PECHLIVANIDOU, S., SAUER, S., SEGUIN, J., SERGIOU, S., ZAKAROVA, N. V. & GREEN, S. 2019. High-resolution record reveals climate-driven environmental and sedimentary changes in an active rift. *Scientific Reports* 9**,** 1-11.

MELING, V. S. 2016. Sedimentology and Sequence Stratigraphy of the Corinth Canal, Central Greece. *University of Bergen. MSc thesis (unpublished)*.

MILLER, K. G., KOMINZ, M. A., BROWNING, J. V., WRIGHT, J. D., MOUNTAIN, G. S., KATZ, M. E., SUGARMAN, P. J., CRAMER, B. S., CHRISTIE-BLICK, N. & PEKAR, S. F. 2005. The Phanerozoic Record of Global Sea-Level Change. *Science,* 310**,** 1293-1298.

MOVE MIDLAND VALLEY 2018.2 2018. Midland Valley Exploration Ltd.

NIXON, C. W., MCNEILL, L. C., BULL, J. M., BELL, R. E., GAWTHORPE, R. L., HENSTOCK, T. J., CHRISTODOULOU, D., FORD, M., TAYLOR, B., SAKELLARIOU, D., FERENTINOS, G., PAPATHEODOROU, G., LEEDER, M. R., COLLIER, R. E. L. I., GOODLIFFE, A. M.,

SACHPAZI, M. & KRANIS, H. 2016. Rapid spatiotemporal variations in rift structure during development of the Corinth Rift, central Greece. *Tectonics,* 35**,** 1225-1248.

ORI, G. G. 1989. Geologic history of the extensional basin of the Gulf of Corinth (?Miocene-Pleistocene), Greece. *Geology,* 17**,** 918-921.

PERISSORATIS, C., PIPER, D. J. W. & LYKOUSIS, V. 2000. Alternating marine and lacustrine sedimentation during late Quaternary in the Gulf of Corinth rift basin, central Greece. *Marine Geology,* 167**,** 391- 411.

PIRAZZOLI, P. A., STIROS, S., FONTUGNE, M. & ARNOLD, M. 2004. Holocene and Quarternary uplift in the central part of the southern coast of the Corinth Gulf (Greece). *Marine Geology,* 212**,** 35-44.

POSTMA, G. & ROEP, R. B. 1985. Resedimented conglomerates in the bottomsets of Gilbert-type gravel deltas. *Journal of Sedimentary Petrology,* 55**,** 874-885.

RAVNÅS, R. & STEEL, R. J. 1998. Architecture of Marine Rift-Basin Successions. *AAPG Bulletin,* 82 110-146.

RIGO, A., LYON-CAEN, H., ARMIJO, R., DESCHAMPS, A., HATZFELD, D., MAKROPOULOS, K., PAPADIMITRIOU, P. & KASSARAS, I. 1996. A microseismic study in the western part of the Gulf of Corinth (Greece): implications for large-scale normal faulting mechanisms. *Geophys. J. Int,* 126**,** 663-688.

ROBERTS, G. P. 1996. Noncharacteristic normal faulting surface ruptures from the Gulf of Corinth, Greece. *Journal of Geophysical Research: Solid Earth,* 101**,** 25255-25267.

ROBERTS, G. P. & MICHETTI, A. M. 2004. Spatial and temporal variations in growth rates along active normal fault systems: an example from The Lazio–Abruzzo Apennines, central Italy. *Journal of Structural Geology,* 26**,** 339-376.

ROHAIS, S., ESCHARD, R., FORD, M., GUILLOCHEAU, F. & MORETTI, I. 2007a. Stratigraphic architecture of the Plio-Pleistocene infill of the Corinth Rift: Implications for its structural evolution. *Tectonophysics,* 440**,** 5-28.

ROHAIS, S., JOANNIN, S., COLIN, J. P., SUC, J. P., GUILLOCHEAU, F. & ESCHARD, R. 2007b. Age and environmental evolution of the syn-rift fill of the southern coast of the gulf of Corinth (Akrata-Derveni region, Greece). *Bull. Soc. géol. Fr.,* 178**,** 231-243.

ROUGIER, G., FORD, M., CHRISTOPHOUL, F. & BADER, A.-G. 2016. Stratigraphic and tectonic studies in the central Aquitaine Basin, northern Pyrenees: Constraints on the subsidence and deformation history of a retro-foreland basin. *Comptes Rendus Geoscience,* 348**,** 224-235.

SACHPAZI, M., CLÉMENT, C., LAIGLE, M., HIRN, A. & ROUSSOS, N. 2003. Rift structure, evolution, and earthquakes in the Gulf of Corinth, from reflection seismic images. *Earth and Planetary Science Letters,* 216**,** 243-257.

SARHAN, M. A. 2007. The efficiency of seismic attributes to differentiate between massive and non-massive carbonate successions for hydrocarbon exploration activity. *NRIAG Journal of Astronomy and Geophysics* 6**,** 311-325.

SCHLISCHE, R. W. 1993. Anatomy and Evolution of the Triassic-Jurassic Continental Rift System, Eastern North America *Tectonics,* 12**,** 1026-1042.

SCLATER, J. G. & CHRISTIE, P. A. F. 1980. Continental stretching: An explanation of the Post-Mid-Cretaceous subsidence of the central North Sea Basin. *Journal of Geophysical Research: Solid Earth,* 85**,** 3711-3739.

SENGÖR, A. M. C. & BURKE, K. 1978. Relative timing of rifting and volcanism on Earth and its tectonic implications. *Geophysical Research Letters,* 5**,** 419-421.

SKOURTSOS, E. & KRANIS, H. 2009. Structure and evolution of the western Corinth Rift, through new field data from the Northern Peloponnesus. *Geological Society, London, Special Publications,* 321**,** 119-138.

SLETTEN, S. H. 2016. Normal fault growth and fault zone architecture of normal faults exposed in the Corinth Canal, central Greece. *University of Bergen. MSc thesis (unpublished)*.

SOLIVA, R. & SCHULTZ, R. A. 2008. Distributed and localized faulting in extensional settings: Insight from the North Ethiopian Rift-Afar transition area. *Tectonics,* 27**,** 1-19.

TAYLOR, B., WEISS, J. R., GOODLIFFE, A. M., SACHPAZI, M., LAIGLE, M. & HIRN, A. 2011. The structures, stratigraphy and evolution of the Gulf of Corinth rift, Greece. *Geophysical Journal International,* 185**,** 1189-1219.

THORSEN, C. E. 1963. Age of Growth Faulting in Southeast Lousiana. *Gulf Coast Association of Geological Societies Transactions,* 13**,** 103-110.

TIBERI, C., LYON-CAEN, H., HATZFELD, D., ACHAUER, U., KARAGIANNI, E., KIRATZI, A., LOUVARI, E., PANAGIOTOPOULOS, D., KASSARAS, I., KAVIRIS, G., MAKROPOULOS, K. & PAPADIMITRIOU, P. 2000. Crustal and upper mantle stucture beneath the Corinth rift (Greece) from a teleseismic tomography study. *Journal of Geophysical Research,* 105**,** 28,159-28,179.

TURNER, J. A., LEEDER, M. R., ANDREWS, J. E., ROWE, P. J., VAN CALSTEREN, P. & THOMAS, L. 2010. Testing rival tectonic uplift models for the Lechaion Gulf in the Gulf of Corinth rift. *Journal of the Geological Society,* 167**,** 1237-1250.

WALSH, J. J., CHILDS, C., IMBER, J., MANZOCCHI, T., WATTERSON, J. & NELL, P. A. R. 2003. Strain localisation and population changes during fault system growth within the Inner Moray Firth, Northern North Sea. *Journal of Structural Geology,* 25**,** 307-315.

WOODWARD, N. B., BOYER, S. E. & SUPPE, J. 1989. *Balanced Geological Cross-Sections: An Essential Technique in Geological Research and Exploration*, Short Course in Geology, vol. 6. Washington, D.C., American Geophysical Union,

ZELT, B., TAYLOR, B., WEISS, J. R., GOODLIFFE, A. M., SACHPAZI, M. & HIRN, A. 2004. Streamer tomography velocity models for the Gulf of Corinth and Gulf of Itea, Greece. *Geophys. J. Int.,* 159**,** 333-346.

ZIEGLER, P. A. 1992. Geodynamics of rifting and implications for hydrocarbon habitat. *Tectonophysics,* 215**,** 221-253.

Appendix I *Present day dip angle for active and inactive faults*

		Fault	Present day dip angle (degrees)
West	Northern Peloponnese margin	FN1 Kalavryta Fault	60
		FN2 Kerpini Fault	60
		FN3 Prinos Fault	15
		FN4 Doumena Fault	60
		FN5 Mamoussia Fault	64
		FN6 Katafugion Fault	60
		FN7 Kastillia Fault	60
		FN10 East Heliki Fault	62
		FS1	60
		FS2	60
		FS3	60
	Subsurface Gulf of Corinth	FN1 Diakopto Fault	50
		FN2 North Eratini Fault	75
		FS1	40
		FS2 West Channel Fault	40
		FS3	55
		FS4	60
		FS5 South Eratini Fault	55
Central	Northern Peloponnese margin	FN1 Kefalari Fault	60
		FN2	60
		FN3	60
		FS1 Melissi Fault	60
	Subsurface Gulf of Corinth	FN1 East Xylokastro	70
		Fault	65
		FN2	65
		FN3 LYK	55
		FN4	70
		FS1	55
		FS2	60
		FS3 WAN/EAN	85
		FS4	72
		FS5	60
		FS6	70
		FS7	63
		FS8	83
		FS9	
East	Northern Peloponnese margin	FN1	77
		FN2	70
		FN3	82
		FN4	82
		FN5	75
		FN6	75

		Fault	Present day dip angle (degrees)
East	Northern Peloponnese margin	FN7	78
		FN8	70
		FN9	61
		FN10	68
		FN11	67
		FN12	69
		FN13	56
		FS1	80
		FS2	72
		FS3	60
		FS4	70
		FS5	75
		FS6	71
		FS7	75
		FS8	74
		FS9	78
		FS10	74
		FS11	80
		FS12	78
		FS13	64
		FS14	56
		FS15	80
		FS16	54
		FS17	54
	Subsurface Gulf of Corinth	FN1	64
		FN2	48
		FN3	60
		FN4	50
		FN5	40
		FN6 PER Fault	34
		FN7	70
		FN8	70
		FN9	50
		FN10	80
		FS1 Lechaion Fault	40
		FS2 Heraion Fault	65
		FS3	45
		FS4	29
		FS5	60
		FS6	73
		FS7	73
		FS8 Vroma Fault	50

Appendix II *Close up of the Corinth Canal*

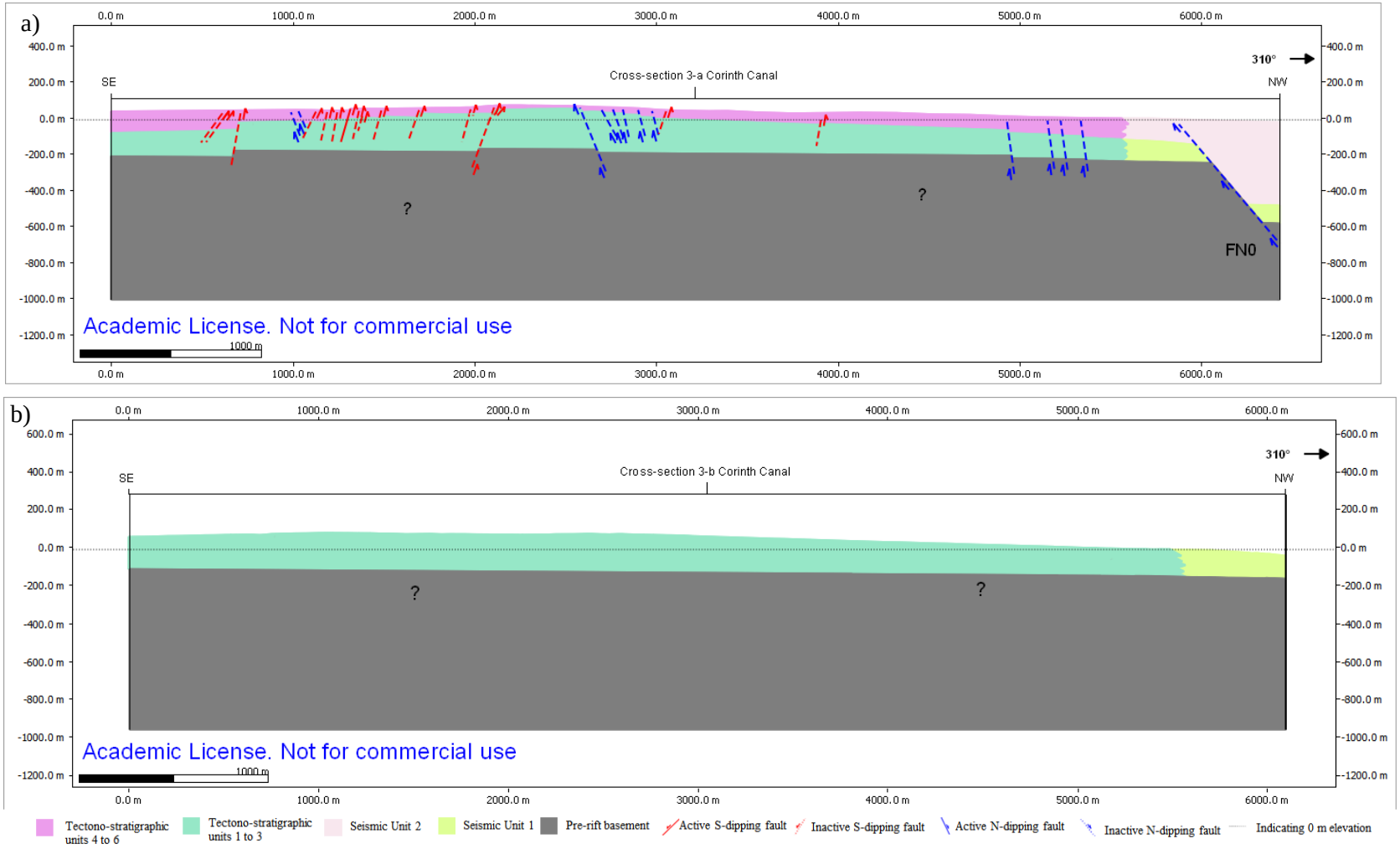

Appendix II a) The present day section with the connection to the Lechaion Gulf to the northwest b) The first step in the restoration process. The tectono-stratigraphic units 3 to 6 was restored and the tectono-stratigraphic units 1 to 3 were laterally and continuous to Seismic Unit 1.